МІНІСТЕРСТВО ОСВІТИ ТА НАУКИ УКРАЇНИ

НАЦІОНАЛЬНИЙ ТЕХНІЧНИЙ УНІВЕРСИТЕТ
«ХАРКІВСЬКИЙ ПОЛІТЕХНІЧНИЙ ІНСТИТУТ»

Ministry of Education & Science of Ukraine
National Technical University
«Kharkiv Polytechnic Institute»

РІЗАННЯ ТА ІНСТРУМЕНТИ в технологічних системах

CUTTING & TOOLS IN TECHNOLOGICAL SYSTEM

Міжнародний науково-технічний збірник
International Scientific-Technical Collection

Заснований у 1966 р. М. Ф. Семко
Found by M. F. Semko in 1966

ВИПУСК № 98
Edition № 98

Харків НТУ «ХПІ» – 2023 – Kharkiv NTU «KhPI»

ББК 34.63
УДК 621.91

Державне видання
Свідоцтво Державного комітету телебачення і радіомовлення України
КВ № 7840 від 8 вересня 2003 року
Друкується за рішенням Вченої Ради НТУ "ХПІ",
протокол № 5 від 02 червня 2023 р.

У збірнику представлені наукові статті, в яких розглядаються актуальні питання в області механічної обробки різних сучасних матеріалів із застосуванням високопродуктивних технологій, нових методик, вимірювальних приладів для контролю якості оброблених поверхонь і високоефективних різальних інструментів. Розглядаються аспекти оптимізації та математичного моделювання на різних етапах технологічного процесу.

Для інженерів і наукових співробітників, що працюють в області технології машинобудування, різання матеріалів, проектування різальних інструментів в технологічних системах.

Науковий збірник «Різання та інструменти в технологічних системах» включений в Перелік фахових видань України категорії «Б», наказ МОН України від 17.03.2020 р., №409

Р34 Резание и инструменты в технологических системах: Междунар. науч.- техн. сб. – Харьков: НТУ «ХПИ», 2023. – Вып. 98. – 128 с.

Адреса редакційної колегії: вул. Кирпичова, 2, Харків, 61002, Національний технічний університет «Харківський політехнічний інститут», кафедра «Інтегровані технології машинобудування» ім. М.Ф. Семка, тел. +38 (057) 706-41-43.

ББК 34.63
Матеріали відтворені з авторських оригіналів
НТУ «ХПІ», 2023

UDC 620.179.118 **doi: 10.20998/2078-7405.2023.98.01**

J. Zaghal, M. Benke, Miskolc, Hungary

DETERMINATION OF RELIABLE AREA SIZES FOR 3*D* ROUGHNESS MEASUREMENT

Abstract. *Surface roughness characterization plays an important role in the qualification of machined surfaces. As a result of the development of high resolution 3D scanning techniques, researchers and technologists have more possibilities to analyze surface topography in a more detailed way. The purpose of this study is determining the minimal measurement area size of surfaces hard machined by single-point and abrasive tools. Some important height parameters were analyzed: S_a, S_q, S_p, S_v, S_{sk} and S_{ku}. It was found that the minimum area sizes vary for the different roughness parameters, however, in several cases minimization is possible, depending on the purpose of the surface analytics.*
Keywords: *hard turning; grinding; polishing; 3D surface topography.*

1. INTRODUCTION

In the automotive industry, surface topography characterization and surface qualification have great importance. Not only the machined parts have to fulfill the quality requirements but also with the appearance of new materials the technologists have to improve the machining procedures and circumstances [1]. 2*D* surface measurement has been widely applied in the last several decades; however, mainly in technology development the application of 3*D* is increasingly widespread. 3*D* surface analysis provides more detailed and more exact information about the surfaces, which has a great importance e.g. in tribological characteristics of contact surfaces or fatigue characteristics [2].

The selection of measurement area size is an unsolvable problem in 3*D* surface topography analysis. There is no exact method that ensures the scanned area results in reliable parameter values or analytics [3]. At the same time, 3*D* surface scanning is a time-consuming and therefore relatively expensive process. This means that the designation of a minimum surface that produces reliable results is important [4].

There are many studies that prove that the unification of measurement and evaluation area is still not solved. Grzesik et al. [5] applied a 2.5 × 2.5 mm area size for hard turning. For the same machining technology studies for 0.8 × 0.8 [6] and 0.5 × 0.5 mm [7] area sizes can also be found. Similarly, for grinding 0.5 × 0.5 mm [7] and 2.5 × 2.5 mm [8] areas can be found. At the same time, not only squared areas are applied for measurement, but also rectangular ones for griding (e.g. [9, 10]. Squared 1.75 × 1.75 [11] and also rectangular 1.9 × 2.5 mm [12] areas were applied in polishing experiments. There is relatively high diversity in burnishing [5, 13], milling [14, 15] and in other technologies [16, 17] too.

Analyzing the different surface areas and the reliability of the measurements based on descriptive statistical methods seems a promising process for minimizing the scanned area size [18]. Molnar and Szabo suggested a simple method for determining this minimum in the case of different roughness parameters for hard turning and grinding [19].

In this paper this method is applied for the same two technologies but with different material and technological data. Additionally, the minimization method is applied for a polished surface.

In 3*D* surface topography characterization, some important surface height parameters were analyzed. The arithmetical (S_a) and root mean square height (S_q) are the first choices for judging the 'smoothness' of a surface. The 2*D* counterpart of the S_a parameter is widely applied in machining technology in part drawings and in academic studies, too. The 3*D* parameter S_a is widely used in scientific studies, e.g. for comparing theoretical and real roughness values [20] and analyzing the effects of technological parameters [21] or the effects of the cutting tool path on the topography features [22]. The maximum peak height (S_p), the maximum pit height (S_v), the kurtosis (S_{ku}) and the skewness (S_{sk}) parameters are determining parameters for the characterization of tribological behavior [23], including wear resistance [24, 25], fatigue strength or fluid-retention ability [26, 27].

2. APPLIED METHODS

In the experiments three surfaces were analyzed. One was hard turned, the other was ground after hard turning and the third was polished after hard turning.

The hard turning was carried out on a CNC lathe type Optiturn S600. The applied insert was CNGA 120408 TA4. The cutting parameters were: cutting speed (v_c): 120 m/min; feed rate (f): 0.1 mm/rev; depth-of-cut (a_p): 0.2 mm. For grinding a CNC mantle grinder type Studer S31 was used. The grinding wheel speed (v_T) was 25 m/s, the workpiece rpm (n_W) was 600 1/min, the feed rate (f) was 700 mm/min, and the removed allowance (Z) was 0.005 mm. The diameter of the corundum wheel was 400 mm, and the grain size was 80 μm. For the polishing, a manual grinder type Bernardo DS200-400 was used. The polishing speed was 2850 1/min, the paste used was Diastar (diamond grit 5.5–8 μm).

The machined surfaces were external cylindrical surfaces with 50 mm diameter and 25 mm length, the material grade was AISI 4140, with hardness 53–54 HRC.

For the roughness measurement, a 3*D* roughness tester type AltiSurf 520 was used. The measured area was 1.75 × 1.75 mm, the side length of the evaluated area were 1.5 mm. The cutoff was 0.25 mm. The resolution of the optical sensor (type CL2) was 1 μm in x and y directions and 0.012 μm in z direction. The scanning speed was 1000 μm/s. For analyzing the different area sizes the highest area was

scanned and smaller areas were then extracted from it. The difference in the side length of two consecutive areas was 0.1 mm. 14 areas were analyzed (side lengths from 0.2 to 1.5 mm). In this study an evaluation area was accepted as minimal if its roughness value does not exceed ±5% of a previously designated reference value.

3. RESULTS AND DISCUSSION

In Fig. 1 the analyzed surfaces are demonstrated. It can be observed that the ground surface (Fig 1b) is random, because the feed marks of the roughing (hard turning) are entirely removed by choosing a minimum allowance [28], and in the case of the polished surface (Fig. 1c) the feed marks of the previous (roughing) machining procedure can still be observed. The reason for this difference between the two abrasive finishing procedures is that in the case of grinding the size of the removed allowance is larger, while the manual polishing only improved some roughness parameter values.

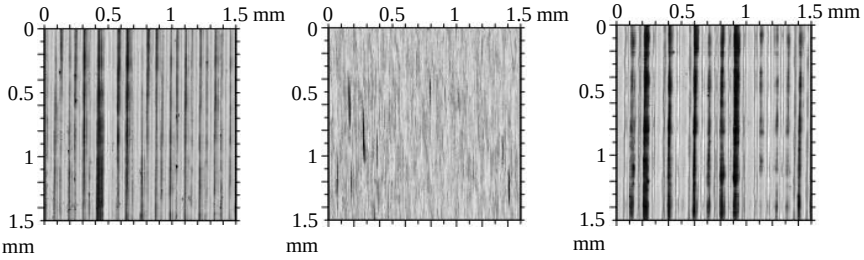

Figure 1 – Topography of the hard turned (a), ground (b) and the polished (c) surfaces

The 2*D* and 3*D* roughness parameter values were compared, from which it can be observed that there are relatively high differences between the corresponding values (Table 1). The 2*D* measurements were carried out at 1.25 mm evaluation length, and the 3*D* ones at 1.5 × 1.5 mm area.

The 3*D* parameters are considered reliable because the magnitude of the measured points is larger. In the case of hard turning and polishing the S_q and S_a parameters are 3.03–4.2% higher than their 2*D* counterparts. In the case of grinding the 3*D* values are lower by 4.67–7.03%. Concerning the S_p and S_v parameters, relatively high fluctuations were observed in the data: the 3*D* values are 4.83–18.42% higher that the R_p and R_v values obtained in the three analyzed machining technology. The skewness and kurtosis values are also fluctuating: the differences for hard turning, grinding and polishing (3*D* compared to the 2*D*

parameter) are 0.44%, 8.85%, and -26.23%, respectively. These values for the kurtosis parameter are 2.28%, 14.04%, and 2.51%.

Table 1 – Comparison of the 2*D* and 3*D* roughness parameters

Roughness parameter	Hard turning		Grinding		Polishing	
	2*D*	3*D*	2*D*	3*D*	2*D*	3*D*
R_q / S_q	0.4738	0.4904	0.4094	0.3903	0.2216	0.2309
R_a / S_a	0.3597	0.3706	0.3298	0.3066	0.1919	0.1976
R_p / S_p	1.4114	1.5377	0.8183	0.8578	0.4416	0.4783
R_v / S_v	0.8179	0.8623	1.168	1.2926	0.3474	0.4114
R_{sk} / S_{sk}	1.0926	1.0974	-0.5243	-0.5707	0.3569	0.2633
R_{ku} / S_{ku}	3.8495	3.9373	2.9867	3.4060	1.9107	1.9586

In Figs. 2–7 the analyzed roughness values are plotted as a function of the evaluation area. The S_q and S_a values of the hard turned surface are similar when the side lengths of the evaluation area are between 0.6 and 1.5 mm, while on lower areas a deviation can be observed in the data (Fig. 2a). Concerning the S_p and S_v values for the same surface, low deviation of the values can be observed between 0.8 and 1.5 mm side lengths (Fig. 2b). Below this range the values show deviation, and between 0.2 and 0.5 mm side lengths: an increase and a decrease can be observed in the S_v and S_p data, respectively.

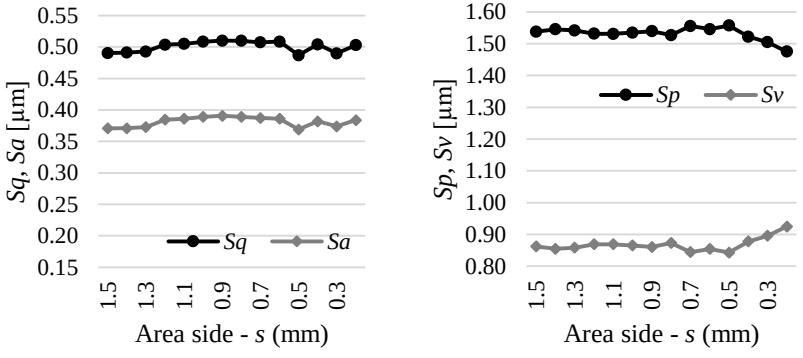

Figure 2 – S_q and S_a parameters (a) and S_p and S_v parameters (b) as a function of the area size for hard turned surface

In the case of the ground surface the S_q and Sa data are relatively stable between 0.7 and 1.5 mm side lengths; however, both data are increasing slightly (Fig. 3a). Below these area sizes the parameters decrease and at the smallest analyzed area an outlying value is observed. Concerning the S_p and S_v values of the ground surface, both are stable at all area sizes (Fig. 3b).

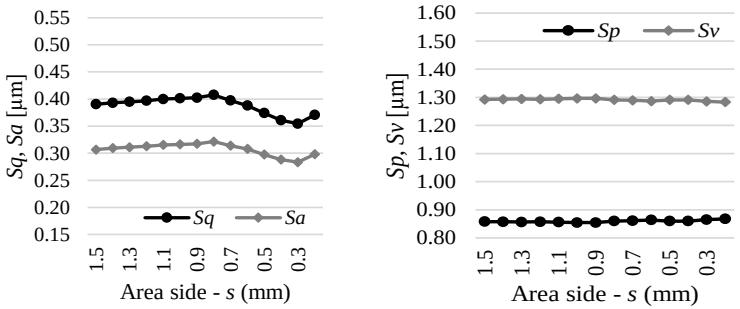

Figure 3 – The S_q and S_a parameters (a) and the S_p and S_v parameters (b) in function of the area size for ground surface

For the S_q and S_a values stable data were obtained between 1.1 and 1.5 mm side lengths (Fig. 4a). Below this area the values were decreased and between 0.2 and 0.6 mm increasing deviations were observed. The S_p and S_v values of the polished surface are not stable on the whole range (Fig. 4b). By decreasing the evaluation area, first a decrease, then an increase can be observed in the S_p values. Between 0.4 and 1 mm side lengths the values decrease again, and below this range a deviation is observed. The reason for the relatively high deviation is that the polishing was preceded by hard turning, and the height distribution is influenced by both the hard turning and the abrasive machining.

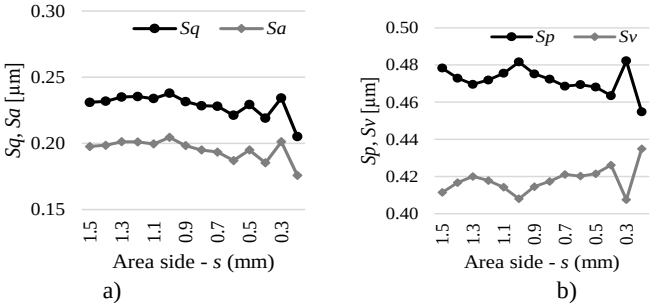

Figure 4 – S_q and S_a parameters (a) and the S_p and S_v parameters (b) as a function of the area size for polished surface

This phenomenon draws the attention that the S_a parameter, which indicates improvement of the polished surface compared to the hard turned and ground ones, is not enough to characterize the surface in a detailed manner. The tendencies of the S_v values are the opposite of those of the S_p values. The reason for this is that the maximum height (S_z), which is the sum of S_p and S_v, is constant at all the analyzed area sizes. This is valid for all three analyzed surfaces. The S_z values for the hard turned, ground and polished surface at 1.5 × 1.5 mm evaluation area are 2.40, 2.15, and 0.89, respectively.

The skewness (S_{sk}) and the kurtosis (S_{ku}) are the higher moments of the height distribution of a surface. They are determinant parameters from the tribological point of view; however, they are sensitive to extreme peaks and valleys, and behave differently when cutting procedures are compared. This can be observed in the S_{ku} values of the hard turned surface (Fig. 5). The topography is periodic, and due to the characteristics of hard machining the distribution of sharp peaks varies throughout the analyzed area. At large areas (1.3–1.5) its values are high, but on smaller are sizes first a decrease, then an increase, and between 0.2 and 0.5 mm side lengths a relatively high deviation can be observed. In contrast, the S_{sk} values are relatively stable; the highest values were obtained between area sizes 1.3 × 1.3 and 1.5 × 1.5 mm.

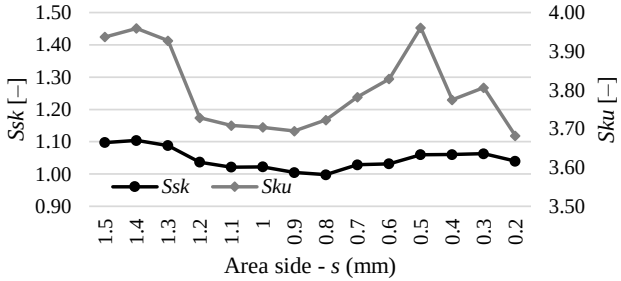

Figure 5 – S_{sk} and S_{ku} parameters as a function of the area size for hard turned surface

Analyzing the ground surface, where height distribution is random, the S_{ku} and S_{sk} values are relatively stable between 0.8 and 1.5 mm side lengths (Fig. 6). Below this range a decrease is obtained in the S_{ku} and an increase in the S_{sk} values.

The S_{sk} parameter of the polished surface show a considerable decrease between side lengths 0.4 and 1.5 mm, while the S_{ku} parameter shows a considerable deviation between 0.2 and 1.1 mm (Fig. 7). The reason for the relatively high deviation is the above-mentioned complexity of the topography (polishing after hard turning).

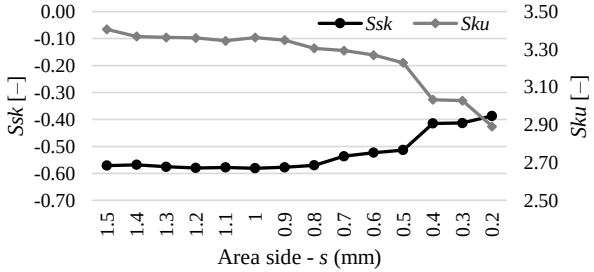

Figure 6 – S_{sk} and S_{ku} parameters as a function of the area size for ground surface

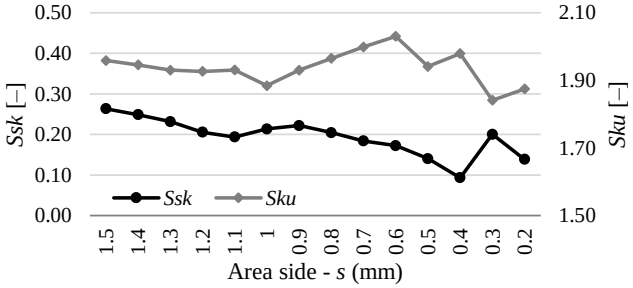

Figure 7 – S_{sk} and S_{ku} parameters as a function of the area size for polished surface

Applying the evaluation area minimization method, the parameter values obtained at the highest evaluation area (basis value) were considered reliable and a ±5% difference range was designated. The minimum area was the smallest at which a parameter value does not exceed this limit. In Table 2 the basis value, the ±5% limit (acceptance range), the first not acceptable value, and the acceptable roughness value and the corresponding area size are summarized. For the hard turned surface, the S_q, S_p and S_v parameter values at relatively small areas (0.2–0.3 mm side length) are similar to those obtained at 1.5 × 1.5 mm. The S_{sk} and S_{ku} parameters can be considered reliable at 1.3 × 1.3 mm or larger areas. A ground surface is random, i.e. the height distribution is closer to normal and the feed marks do not influence the topography as much as in the case of hard turning. The S_p and S_v values can be evaluated reliably at 0.2 mm side length areas, while the minimum area for S_q and S_a mean height parameters is 0.5 × 0.5 mm. In the case of the S_{sk} and S_{ku} parameters the minimum area is lower than that of hard turning: 0.6–0.8 mm side length. Similar area sizes were obtained for polishing in the cases of S_q, S_a,

S_p and S_v. The minimum side length of the area for S_q and S_a is 0.5–0.7 mm and for S_p and S_v 0.2–0.3 mm. The S_{sk} and S_{ku} parameters, however, cannot be compared well to those of the other two procedures. The minimum side length for the S_{sk} is 1.5 mm and for the S_{ku} is 0.4 mm.

Table 2 – Determination of the minimal area size

Roughness parameter	Roughness value at 1.5 × 1.5 mm	Acceptance range (± 5%)		Rejected value	Accepted value	Accepted area (mm^2)
Hard turning						
S_q	0.490	0.466	0.515	–	0.503	0.2×0.2
S_a	0.371	0.352	0.389	0.391	0.389	1×1
S_p	1.538	1.461	1.615	–	1.475	0.2×0.2
S_v	0.862	0.819	0.905	0.925	0.896	0.3×0.3
S_{sk}	1.097	1.043	1.152	1.037	1.088	1.3×1.3
S_{ku}	3.937	3.740	4.134	3.728	3.928	1.3×1.3
Grinding						
S_q	0.390	0.371	0.410	0.361	0.374	0.5×0.5
S_a	0.307	0.291	0.322	0.288	0.298	0.5×0.5
S_p	0.858	0.815	0.901	–	0.867	0.2×0.2
S_v	1.293	1.228	1.357	–	1.283	0.2×0.2
S_{sk}	-0.571	-0.542	-0.599	-0.536	-0.570	0.8×0.8
S_{ku}	3.406	3.236	3.576	3.229	3.270	0.6×0.6
Polishing						
S_q	0.231	0.219	0.242	0.219	0.229	0.5×0.5
S_a	0.198	0.188	0.207	0.187	0.193	0.7×0.7
S_p	0.478	0.454	0.502	–	0.455	0.2×0.2
S_v	0.411	0.391	0.432	0.435	0.408	0.3×0.3
S_{sk}	0.263	0.250	0.276	0.249	0.263	1.5×1.5
S_{ku}	1.959	1.861	2.057	1.841	1.979	0.4×0.4

4. CONCLUSIONS

Three surfaces finished by different machining procedures (hard turning, grinding and polishing) were analyzed. The findings of the applied minimization method are the following.

- For the S_a and S_q parameters the minimum evaluation areas vary depending on the applied machining procedure. When analyzing S_q the side length of this area is 0.2 mm but 1 mm when analyzing S_a for hard turned surfaces. The minimum side lengths are 0.5 and 0.7 mm for ground and polished surfaces, respectively.
- In the cases of the S_p and S_v parameter a side length of 0.3 mm is recommended for the minimum area in all three analyzed procedures.

- In the cases of the S_{sk} and S_{ku} parameters the minimum area sizes strongly vary in the three procedures. Due to the purely random feature of the ground surface, its minimum area is relatively low: 0.8 × 0.8 mm.

These statements are valid for the three procedures and within the applied cutting data and technology parameters.

References: 1. *Nagy, A., Kundrak, J.:* Changes in the values of roughness parameters on face-milled steel surface, Rezanie i Instrumenty v Tekhnologicheskih Sistemah 92, pp.85-95, 2020. **2.** *Zaghal, J., Mertinger, V., Filep, A., Varga, G., Benke, M.:* Characterization of residual stresses induced into bearing rings by means of turning in soft state using different turning parameters, Journal of Machine Engineering 21(4), pp.49-56, 2021. **3.** *Yong, Q., Chang, J., Liu, Q., Jiang, F., Wei, D., Li, H.:* Matt polyurethane coating: Correlation of surface roughness on measurement length and gloss, Polymers 12, paper 326, 2020. **4.** *Molnar, V.:* Minimization method for 3D surface roughness evaluation area, Machines 9, paper 192, 2021. **5.** *Grzesik, W., Rech, J., Zak, K.:* High-precision finishing hard steel surfaces using cutting, abrasive and burnishing operations, Procedia Manufacturing 1, pp.619–627, 2015. **6.** *Matras, A., Zębala, W., Machno, M.:* Research and method of roughness prediction of a curvilinear surface after titanium alloy turning, Materials 12, paper 502, 2019. **7.** *Grzesik, W., Zak, K., Kiszka, P.*: Comparison of surface textures generated in hard turning and grinding operations, Procedia CIRP 13, pp.84–89, 2014. **8.** *Legutko, S., Zak, K., Kudlacek, J.:* Characteristics of geometric structure of the surface after grinding, MATEC Web Conf. 94, paper 02007, 2017. **9.** *Wojciechowski, S., Twardowski, P., Chwalczuk, T.:* Surface roughness analysis after machining of direct laser deposited tungsten carbide, Journal of Physics: Conf. Ser. 483, paper 012018, 2014. **10.** *Schmahling, J., Hamprecht, F.A., Hoffmann, D.M.P.:* A three-dimensional measure of surface roughness based on mathematical morphology. Technical Report from Multidimensional Image Processing, IWR; University of Heidelberg, Germany, 2006. **11.** *Zhou, J., Han, X., Li, H., Liu, S., Shen, S., Zhou, X., Zhang, D.:* In-situ laser polishing additive manufactured AlSi10Mg: Effect of laser polishing strategy on surface morphology, roughness and microhardness, Materials 14, paper 393, 2021. **12.** *Zhou, H., Zhou, H., Zhao, Z., Li, K., Yin, J.:* Numerical simulation and verification of laser-polishing free surface of S136D die steel, Metals 11, paper 400, 2021. **13.** *Dzierwa, A., Markopoulos, A.P.:* Influence of ball-burnishing process on surface topography parameters and tribological properties of hardened steel, Machines 7, paper 11, 2019. **14.** *Nadolny, K., Kaplonek, W.:* Analysis of flatness deviations for austenitic stainless-steel workpieces after efficient surface machining, Measurement Science Reviev 14, paper 204, 2014. **15.** *Kundrak, J., Nagy, A., Markopoulos, A.P., Karkalos, N.E.:* Investigation of surface roughness on face milled parts with round insert in planes parallel to the feed at various cutting speeds, Rezanie i Instrumenty v Tekhnologicheskih Sistemah 91, pp.87–96, 2019. **16.** *Karolczak, P., Kowalski, M., Wisniewska, M.:* Analysis of the possibility of using wavelet transform to assess the condition of the surface layer of elements with flat-top structures, Machines 65, paper 8, 2020. **17.** *Deltombe, R., Kubiak, K.J., Bigerelle, M.:* How to select the most relevant 3D roughness parameters of a surface?, Scanning 36, pp.150–160, 2014. **18.** *Molnar, V.:* Designation of evaluation area in measuring 3d surface roughness, Rezanie i Instrumenty v Tekhnologicheskih Sistemah 93, pp.56-64,2020. **19.** *Molnar, V., Szabo, G.:* Designation of minimum measurement area for the evaluation of 3D surface texture, Journal of Manufacturing Processes 83, pp.40-48, 2022. **20.** *Kundrak, J., Felho, Cs., Nagy, A.*: Analysis and prediction of roughness of face milled surfaces using CAD model, Manufacturing Technology 22(5), pp.558-572, 2022. **21.** *Ferencsik, V., Varga, G.:* The influence of diamond burnishing process parameters on surface roughness of low-alloyed aluminium workpieces, Machines 10(7), paper 564, 2022. **22.** *Kundrak, J., Nagy, A., Markopoulos, A.P., Karkalos, N.E., Skondras-Giousios, D.:* Experimental study on surface roughness of face milled parts with round insert at various feed rates, Rezanie i Instrumenty v Tekhnologicheskih Sistemah 92, pp.96-106, 2020. **23.** *Ferencsik, V., Varga, G.:* The effect of burnishing process on skewness and kurtosis of the scale limited surface, Rezanie i Instrumenty v Tekhnologicheskih Sistemah 97, pp.83-90, 2022. **24.** *Molnar, V., Sztankovics, I.:*

Analysis of roughness parameters determining tribological properties in hard turned surfaces, Hungarian Journal of Industry and Chemistry 49(2), pp.77-84, 2021. **25.** *Zhu, X., Dong, Z., Zhang, Y., Cheng, Z.:* Fatigue Life Prediction of Machined Specimens with the Consideration of Surface Roughness, Materials 14, paper 5420, 2021. **26.** *Gapinski, B., Firlik, B., Mathia, T.G.:* Characteristics of tram wheel wear: Focus on mechanism identification and surface topography, Tribology International 150, paper 106365, 2020. **27.** *Molnar, V.:* Tribological properties and 3D topographic parameters of hard turned and ground surfaces, Materials 15(7), paper 2505, 2022. **28.** *Kundrak, J., Deszpoth, I., Molnar, V.:* Increasing productivity of combined procedure by reducing grinding allowance, Rezanie i Instrumenty v Tekhnologicheskih Sistemah 90, pp.26-35, 2019.

Джавад Загал, Мартон Бенке, Мішкольц, Угорщина

ВИЗНАЧЕННЯ НАДІЙНИХ РОЗМІРІВ ОБЛАСТІ ДЛЯ 3*D* ВИМІРЮВАННЯ ШОРСТКОСТІ

Анотація. *Характеристика шорсткості поверхні відіграє важливу роль у кваліфікації оброблених поверхонь. У результаті розробки методів 3D-сканування з високою роздільною здатністю дослідники та технологи мають більше можливостей для більш детального аналізу топографії поверхні. Метою даного дослідження є визначення мінімального розміру площі вимірювання поверхонь, оброблених одноточковим та абразивним інструментом. Було проаналізовано деякі важливі параметри висоти: S_a, S_q, S_p, S_v, S_{sk} та S_{ku}. Було виявлено, що мінімальні розміри площі різняться для різних параметрів шорсткості, однак у деяких випадках можлива мінімізація, залежно від мети аналізу поверхні. Вибір розміру зони вимірювання є нерозв'язною проблемою в 3D-аналізі топографії поверхні. Немає точного методу, який би гарантував, що відсканована область дасть надійні значення параметрів або аналітику. У той же час 3D-сканування поверхні є трудомістким і тому відносно дорогим процесом. Це означає, що визначення мінімальної поверхні, яка дає надійні результати, є важливим. Для вимірювання шорсткості використовувався тривимірний тестер шорсткості типу AltiSurf 520. Виміряна площа становила 1,75 × 1,75 мм, довжина сторони оцінюваної області становила 1,5 мм. Границя становила 0,25 мм. Роздільна здатність оптичного датчика (типу CL2) становила 1 мкм у напрямках x та y та 0,012 мкм у напрямку z. Швидкість сканування становила 1000 мкм/с. Для аналізу різних розмірів області була відсканована найвища область, а потім з неї вилучено менші області. Різниця в довжині сторін двох послідовних ділянок становила 0,1 мм. Проаналізовано 14 ділянок (довжина сторін від 0,2 до 1,5 мм). У цьому дослідженні площа оцінки була прийнята як мінімальна, якщо її значення шорсткості не перевищує ±5% від попередньо визначеного контрольного значення. Було проаналізовано три поверхні, оброблені різними процедурами механічної обробки (жорсте точіння, шліфування та полірування). Для параметрів S_a і S_q мінімальна площа оцінки змінюється в залежності від застосовуваної процедури обробки. При аналізі S_q довжина сторони цієї області становить 0,2 мм, та 1 мм при аналізі S_a для точених поверхонь. Мінімальна довжина сторін становить 0,5 і 0,7 мм для шліфованих і полірованих поверхонь відповідно. У випадку параметрів S_p і S_v рекомендована довжина сторони 0,3 мм для мінімальної площі в усіх трьох аналізованих процедурах. У випадку параметрів S_{sk} і S_{ku} мінімальні розміри області сильно відрізняються в трьох процедурах. Через чисто випадкову особливість поверхні ґрунту її мінімальна площа відносно мала: 0,8 × 0,8 мм. Ці твердження дійсні для трьох процедур і в межах застосовуваних даних різання та параметрів технології.*

Ключові слова: *жорстке точіння; шліфування; полірування; 3D рельєф поверхні.*

UDC 621.923: 661.65 **doi: 10.20998/2078-7405.2023.98.02**

V. Lavrinenko, Kyiv, Ukraine,
V. Fedorovich, Y. Ostroverkh, Kharkiv, Ukraine,
V. Solod, Kamianske, Ukraine

MODERN DEVELOPMENTS RELATED TO THE DIRECTED IMPACT ON THE CUTTING SURFACE OF A DIAMOND ABRASIVE TOOL AND ITS CONTACT ZONE IN THE PROCESSES OF MACHINING (REVIEW)

Abstract. *This article provides information on modern developments in the direction of directed impact on the cutting surface of a diamond-abrasive tool and its contact zone in machining processes. For the most part, such processing is faced with issues of influence on the cutting surface of diamond tools, including ruling mechanical and electrophysical, taking into account the defectiveness of the diamonds that undergo processing, the directed influence on the surface of such diamonds, thermal and modification of the surface of diamonds. Such developments make it possible to significantly intensify processing processes and increase the efficiency of the diamond abrasive tool. That is why, in this review, the main attention is paid to the presentation of modern developments, known from scientific publications, mainly for the last 5 years, related to the above-mentioned issues.*
Keywords: *diamond abrasive tool; cutting surface; contact zone; mechanical processing; defects of diamonds; electrophysical influence.*

1. Introduction

High-hard and high-strength materials, especially tool materials, are now widely used in industry. Their effective diamond processing is important for modern production. At the same time, the issue of effective processing, along with instrumental processing, of such fragile, difficult-to-process materials as mono- and polycrystalline diamonds, including CVD diamond films, sapphire, etc. For the most part, such processing is faced with issues of influence on the cutting surface of diamond tools, including ruling mechanical and electrophysical, taking into account the defectiveness of the diamonds that undergo processing, the directed influence on the surface of such diamonds, thermal and modification of the surface of diamonds. Also, great attention is paid to obtaining a high-quality defect-free surface processed layer of the above-mentioned difficult-to-process materials. That is why, in this review, the main attention is paid to the presentation of modern developments (mainly over the last 5 years) related to the above-mentioned issues.

2. Processing of brittle mono- and polycrystalline materials

At the beginning of this review, let's pay attention to the development of a grinding wheel with a diameter of 3.2 mm, which was made of nanopolycrystalline diamond (NPD), obtained by direct conversion sintering under high pressure

and temperature [1]. Using this NPD wheel as a grinding blade, a new useful method for investigating the micro-scale abrasive properties of single-crystal diamonds was developed. Since NPD has an extremely high hardness of about 130 GPa, the abrasive properties of various natural and synthetic single-crystal diamonds, whose hardness is usually around 70 to 125 GPa, can be appropriately evaluated. In addition, since the wheel diameter is very small, it is possible to measure the abrasion resistance in a minute region of several tens of μm in a diamond crystal. It was confirmed that the method can accurately evaluate the abrasive properties of minute regions of single-crystal diamonds using synthetic type IIa diamond. It was also demonstrated that it is possible to investigate how the abrasive properties of synthetic type Ib and natural type Ia diamonds change depending on the distribution of impurities or crystal defects in the crystals [1].

In work [2], a smooth nano-sized surface of polycrystalline diamond without damage was polished, on the contrary, with a rough diamond (D151) grinding wheel on a ceramic bond. Atomic force microscopy verified that surface roughness of S_a 4.20 nm, S_a 2.06 nm, and S_a 0.548 nm were achieved under grinding speeds of 750, 1050, and 1350 rpm, respectively. Electron energy loss spectroscopy spectra confirmed the existence of a graphitic layer (black layer) with a thickness of ~15 nm in the subsurface after grinding. The "black layer" showed an easy ability to be removed under scratch and high-temperature oxidation. Moreover, transmission electron microscopy demonstrated that no damaged layer was observed in the subsurfaces at 750 rpm and 1050 rpm grinding speed. For grinding speed of 1350 rpm, stacking faults and micro-crack appear in the subsurface, thus forming a damaged layer with several microns in thickness. This work [2] demonstrates a unique removal mechanism for abrasive processing of hard-and-brittle materials, as distinct from either mechanical grinding or chemical mechanical grinding.

In the article [3], the grinding of monocrystalline diamond substrates, which must have a super-smooth surface (atomic-order), was investigated. Known methods of polishing single crystal diamonds are based on pressure control processes and are capable of improving surface quality, but are inefficient. To obtain high-precision surface smoothness with greater process efficiency, the authors [3] have developed a method for diamond polishing that is based on a depth-control principle and employs an ordinary rotary grinder in which both the substrate and the grinding wheel are rotated simultaneously during the grinding. The resulting ground surface showed tiny crosshatch scratches. By progressively applying finer grinding wheels from #600 to #15000, the surface could be gradually improved, and finally a surface with a near-atomic-order surface roughness was obtained with the finest wheel (#15000); the average surface roughness was 0.13 nm for 5×5 μm^2 area. The removal rate with the #15000

wheel was 0.04 μm/min, which was markedly higher than that achievable by other methods capable of producing an atomic-order surface roughness on single-crystal diamond. The depth of subsurface damage induced by the grinding process was reduced by using finer grinding wheels. The processed surface was ultrasmooth with ~0.1 nm average surface roughness.

Polishing of polycrystalline diamond using the synergy of chemical and mechanical influences is considered in work [4]. Polycrystalline diamond (PCD), applied in the form of a thin film, is an attractive material due to the unique combination of its properties. But, since for many of its applications it is necessary that the PCD has a high quality of surface treatment, effective and economical polishing is important. In article [4], chemical-mechanical polishing of PCD is considered. Three main ways of material removal during diamond polishing are identified and summarized on the basis of experimental results: interphase mechano-chemical removal, chemically stimulated mechanical removal and mechano-chemical transformation of diamond.

The work [5] is focused on highly efficient and damage-free diamond polishing enhanced by atmospheric pressure inductively coupled plasma (ICP) modified silicon plate. A rapid decrease in the surface roughness from S_a 308 nm–0.86 nm over 300 μm^2 in 120 min proclaims ICP enhanced polishing a highly efficient technique (Fig 1). Simultaneously, an atomically smooth, high-quality diamond surface is obtained with a surface roughness of R_a 0.26 nm over 20 μm^2. The polishing mechanism based on the OH-modification of silicon plate and diamond surface, dehydration condensation reaction occurring at the interface of OH-terminated surfaces, and subsequent mechanical shearing of carbon, is proposed. TEM and Raman analysis of polished surfaces confirm that the use of ICP contributes to further damage-free removal of the mechanically caused damaged layer [5].

Ultrahard nanotwinned diamond (nt-D) is an ideal material for next-generation high-precision, high-efficiency cutting tools, due to its high hardness, enhanced fracture toughness, and increased oxidation resistance temperature, when compared with natural diamond. However, a critical problem that limits the application of such material is the grinding and polishing of nt-D material into suitable shapes. In article [6] confirmed the feasibility of classical mechanical polishing for nt-D through amorphization transition. The effect of mechanical loading and the catalysis of Fe nano-particles work together, promoting the transformation of nt-D into a hard sp^2–sp^3 amorphous carbon (Fig. 2). The surface of the amorphous carbon layer and the interface between amorphous carbon and nt-

D were both smooth after polishing. The results are valuable for the mechanical processing and further applications of ultrahard nanotwinned diamond.

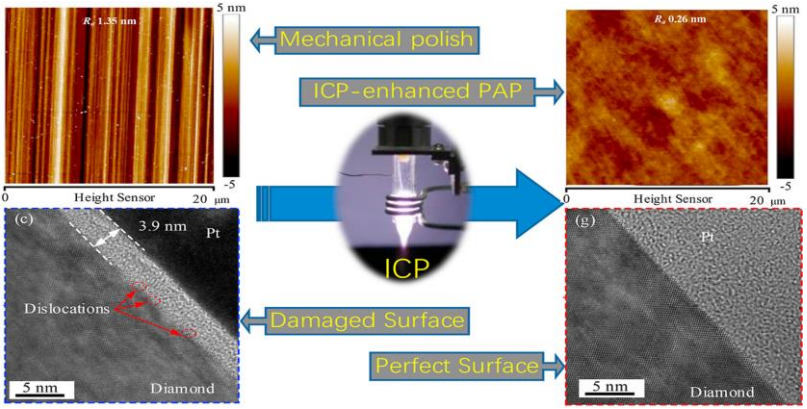

Figure 1 – Scientific principles underlying the mechanism of polishing single-crystal diamond enhanced by inductively coupled plasma [5]

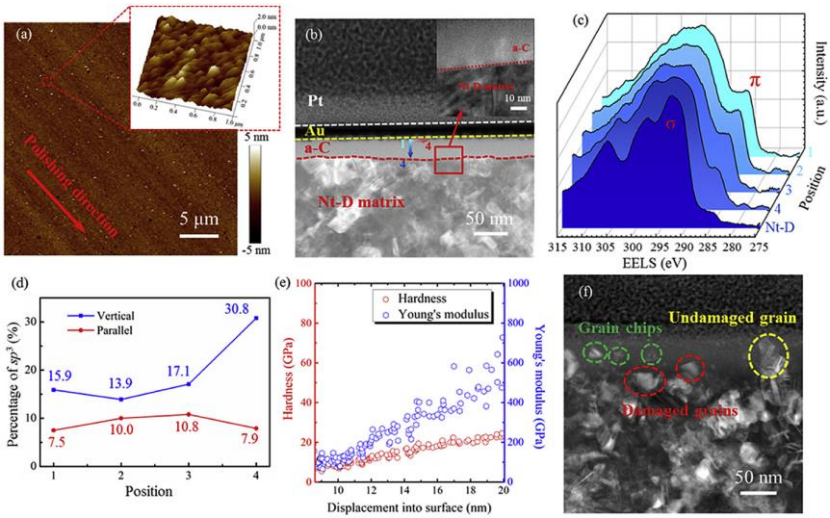

Figure 2 – Scientific principles underlying the mechanism of mechanical polishing for nt-D through amorphization transition [6]

Monocrystalline diamond possesses covalent bonding making diamond extremely hard and difficult to machine. In study [7] a microdiamond stylus typically used in measuring surface roughness is machined to exemplify the proposed 'microspark erosion-assisted machining with heat-avoidance path' technique. Based on the high thermal conductivity and weak electrical conductivity of boron-doped monocrystalline diamond, high-frequency pulsed discharge plasma is employed to efficiently perform microspark erosion machining on an extremely hard monocrystalline diamond blank. It was found that the pulse-on time and servo voltage respectively affect erosion plasma length and the erosion gap during diamond machining. Also, the safety distance and safety height of the erosion path dominate heat transfer to filler metal. These factors all affect the firmness of the brazed diamond blank on the substrate. Three mechanisms for removing carbon atoms from the diamond blank surface were observed. They are vaporization, melting, and graphitization of carbon atoms. This graphitized carbon atoms have weak electrical conductivity, which is conducive to inducing the wire-electrode to generate a greater electric field and secondary discharging, facilitating removal of additional carbon atoms. Experimental results indicate that a microdiamond stylus prototype with a tip of 10 μm can be safely formed using a 'microspark erosion-assisted machining with heat-avoidance path' technique, creating 93.7% repeatability of the minimum residual stylus diameter. The tangential micro-grinding facilitates the stylus tip to receive grinding from the grinding wheel's maximum tangential speed and create the precision microdiamond stylus with 1 μm in tip-radius (Fig. 3). The applied microspark erosion-assisted machining had a diamond material removal rate that was 54% more efficient than conventional grinding of a commercial microdiamond stylus. The formed microdiamond stylus was inspected by Raman spectroscopy and verified by the surface roughness standard gauge to be up to industry standards.

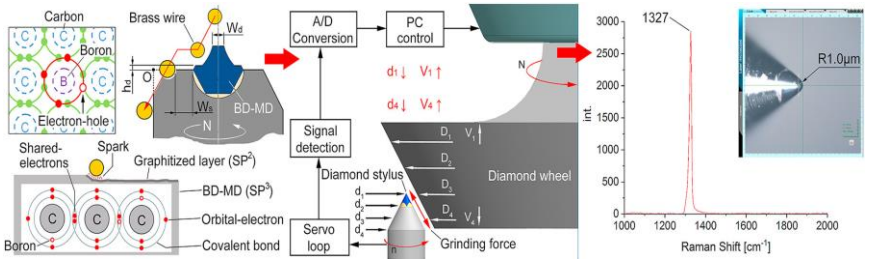

Figure 3 – Microdiamond stylus prototype with a tip of 10 μm can be safely formed using a 'microspark erosion-assisted machining with heat-avoidance path' technique and create the precision microdiamond stylus with 1 μm in tip-radius [7]

Above, we drew attention to the effect of boron impurities in diamond on its conductivity, so at the end of this part of the review, we will review the wear characteristics of cubic boron nitride grains during abrasive wear [8]. The wear phenomenon is an important issue that affects the grinding performance of polycrystalline cubic boron nitride (PCBN) grinding wheel. To explore the wear mechanism, single grain scratching tests were conducted on the nickel-based superalloy Inconel 718. Fractal theory was applied to evaluate the grain wear process, and the influences of undeformed chip thickness $a_{g\max}$ and grinding wheel speed v_s on grain wear were analysed. The variation in fractal dimension, grinding force and grinding force ratio were discussed. Results show that the micro-fracture is caused by the crack, and the adhered grinding chip leads to the attrition wear of PCBN grain. The average specific material removal volume of monocrystalline CBN grain is approximately 10.7% that of PCBN grain when macro-fracture occurs. The effect of a_{gmax} on grain macro-fracture is stronger than that of v_s. Furthermore, the grinding parameters should be set as follows: v_s of 80 m/s and a_{gmax} in the range of 0.1–0.67 μm. These settings help improve the grain micro-fracture phenomenon in high-speed grinding [8].

3. Features of precision adjustment of diamond abrasive wheels

Now let's move on from the above-mentioned modern studies of the wear characteristics of individual diamond grains to modern developments in precision straightening of diamond wheels, in which diamond grains are located.

The rapid wear of the dressing tools severely limits the further improvement of the truing accuracy and dressing sharpness of the arc-shaped diamond wheels used in ultra-precision grinding. In paper [9] thoroughly investigated the wear characteristics of electroplated diamond dressing wheels used for on-machine precision truing of arc-shaped diamond wheels. Firstly, wear topography and protrusion height of the diamond particles were researched. Secondly, the wear evolution mechanism of diamond particles with different grain sizes was systematically researched. Then, the wear mechanism of the metal bonded matrix was studied (Fig. 4). Subsequently, the Raman spectrum analysis of diamond particles before and after wear was carried out. Finally, the profile accuracy and surface topography of the trued arc-shaped diamond wheel were evaluated for distinguishing the wear resistance and sharpening performance of the electroplated diamond dressing wheels with different grain sizes.

The work [10] is devoted to the influence of the properties of grains and dressing on grinding mechanics and wheel performance: analytical assessment framework. This paper introduces an analytical assessment framework for evaluating grinding wheel performance derived from the model of cutting and sliding grinding force components. Four new parameters are proposed based on wheel topography. These parameters are normalized through the aggressiveness number, which circumvents the influences of grinding geometry and kinematics. The framework is validated through experiments with different wheel topographies obtained by changing dressing conditions and grit properties (toughness, thermal stability and shape). The framework and experiments quantify how wheel wear flat area influences the sliding component and how grit protrusion influences the intrinsic specific grinding energy. This framework provides a rational basis for evaluating grinding-wheel performance and abrasive-grit selection.

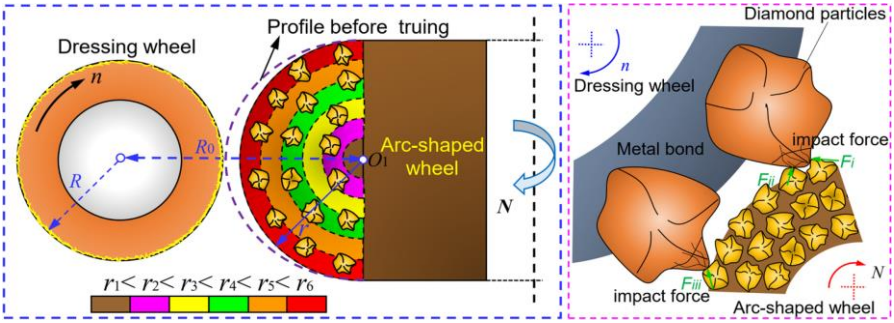

Figure 4 – Scheme of the truing of arc-shaped diamond wheels [9]

Precision grinding with ultrathin arc-shaped diamond (UAD) grinding wheels provides a satisfactory solution for the fabrication of high-quality microstructures on tungsten carbide (WC) molds. However, ultrathin grinding wheels are difficult to be trued, due to the limited small grinding wheel profile. In paper [11], an on-machine truing method for ultrathin arc-shaped diamond grinding wheels is proposed. First, a model of the three-axis linkage controlling truing for the diamond grinding wheel was introduced. Then, the effects of the setting and measurement errors of the grinding wheel on the profile radius were theoretically analyzed. Furthermore, an aspherical microstructure array of tungsten carbide was ground by the trued diamond grinding wheel. The experimental results demonstrated that the expected arc radius of the grinding wheel could be achieved and the binderless tungsten carbide mold could be ground efficiently and precisely. The profile error of the grinding wheel (diameter of 23 mm, thickness of 0.38 mm) reached 8.5 μm. An aspherical microstructure array surface of tungsten carbide

with a form accuracy of 15 μm was obtained by grinding with the trued diamond grinding wheel without additional compensation [11].

In paper [12,13] a modified U-Net neural network was used to evaluate the laser sharpening quality of diamond grinding wheels, and the laser sharpening parameters were optimized. The three-dimensional (3*D*) detection algorithm is researched, and a 3*D* detection algorithm for the diamond wheel surface matching the two-dimensional (2*D*) image and the 3*D* point cloud was proposed. The recognized 2*D* grain image is filtered to remove edge grains and connected grains, correct the 3*D* point cloud by eliminating the effect of curvature, and match grain pixels (Fig. 5). The laser sharpening experiment of the bronze-bonded diamond wheel was carried out by the orthogonal experiment method, and the quality evaluation of the laser sharpening pictures of the wheel obtained by the experiment was carried out. The embedding depth of the abrasive grains was obtained from the 2*D* area of the abrasive grains, and the evaluation index of abrasive grain height-depth distribution was proposed. The laser sharpening experiments was carried out to obtain grinding wheels with different sharpening qualities, and the grinding tests were carried out. The effectiveness of the sharpening evaluation index was verified by the amount of grinding force when grinding the workpiece and the surface roughness of the workpiece after grinding. The optimal dressing process parameters were obtained as the average power of 35 W, the repetition frequency of 100 kHz, the rotational speed of 300 r/min, and the scanning speed of 3.6 mm/min.

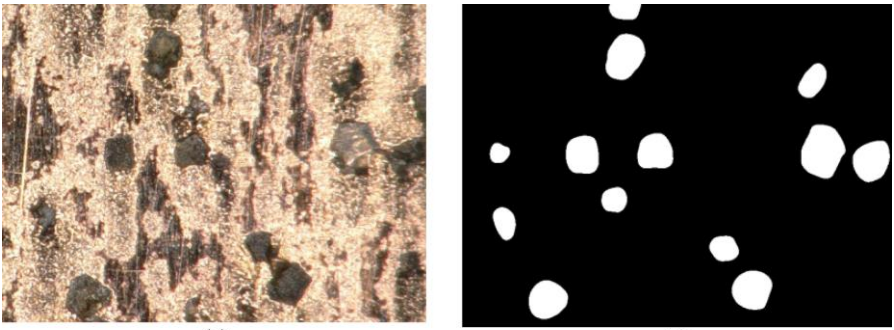

(a) (b)

Figure 5 – General view of the cutting surface of the wheel (a) and recognized 2D grain image (b) [12]

Affected by the characteristics of laser Gaussian beam, the spot size and laser energy irradiated on the grinding wheel surface change at any time with the dressing path, which makes it difficult to realize the dressing of high-precision arc-shaped diamond grinding wheel. In order to achieve high-efficiency and precise

dressing of arc-shaped diamond grinding wheels, a composite dressing method using laser rough dressing and electrical discharge precision dressing was first proposed (Fig. 6) [14]. Laser rough dressing method is used to quickly remove the excess abrasive layer to obtain an arc-shaped profile. Electrical discharge precision dressing not only improved the accuracy of arc-shaped contour, but also realized the grinding wheel sharpening. The optimization of kinematic parameters on the dressing profile accuracy in laser dressing and electrical discharge dressing was explored. An arc-shaped profile with a radius of 13 mm was tested on a diamond grinding wheel with a grain size of 120#. The radius of the final dressed arc-shaped profile is 13,007 μm, and the PV value of the profile error is 10.67 μm. It was found that the abrasive grains on the surface of the grinding wheel were slightly graphitized. The damage degree of the abrasive particles in laser dressing was more serious than that of in electrical discharge dressing. Most of the graphite layer on the surface of abrasive particles could be removed by grinding alumina ceramics. The fitting radius of the arc profile of the workpiece is 13.013 mm, and the profile error PV value is 11.91 μm.

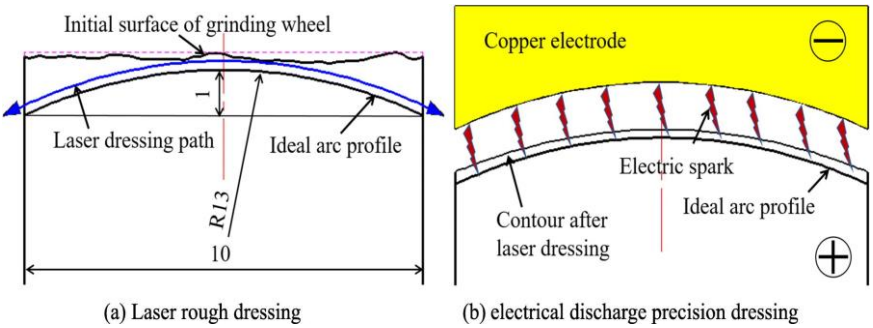

Figure 6 – Scheme of laser rough (a) and electrical discharge precision (b) dressing [14]

Although significant work has been done on the application of acoustic emission (AE) to grinding and to dressing of grinding wheels, several fundamental AE relationships between have not been established. These are: 1) the relationship between dressing energy and the measured AE signal; 2) how different diamond/grit contact modes (fracture, plastic deformation, rubbing, etc.) affect AE energy; and 3) how this can be used to quantify dressing efficiency, wheel sharpness and wear-induced changes in diamond shape. In paper [15] describes an investigation into these fundamental concepts, with quantification of the relationship between AE intensity and dressing energy and the influence of different diamond/grit contact modes. A new parameter is introduced, the *specific*

acoustic-emission dressing energy, which can be used to quantify dressing efficiency and wheel sharpness. Finally, the use of the AE intensity in evaluating diamond wear is explored, allowing the operator to know the size of the wear flat and when changes are necessary to avoid workpiece burn.

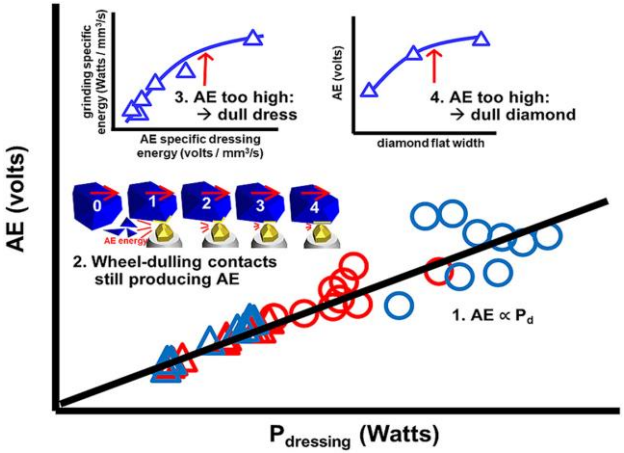

Figure 7 – Scientific principles underlying the mechanism of AE during correction [15]

4. Research on directional impact on the cutting surface of a diamond wheel and its contact zone

To improve the durability and self-sharpening ability of traditional coated abrasives for efficient automated manufacturing, structured patterns and super hard materials were utilized for the fabrication of coated tools. In study [16], the polymer matrix was synthesized by 50 wt% polyurethane and 50 wt% epoxy, the tensile strength and elongation at break is 53.6 MPa and 36.8%, respectively. Then the thermosetting PU/EP diamond composites were prepared by roller embossing successfully (Fig. 8).

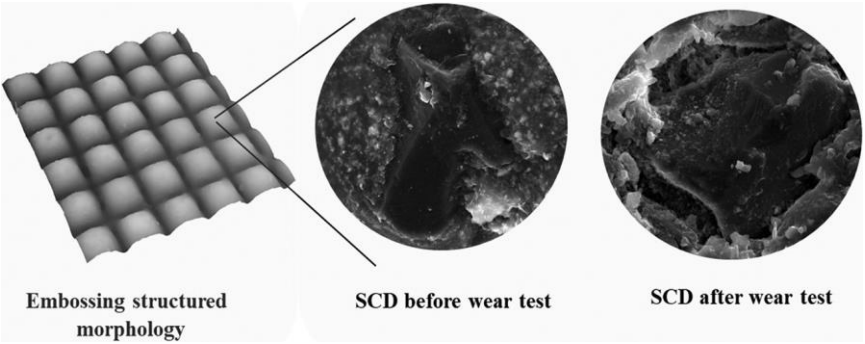

Figure 8 – Technological features of the surface of thermosetting diamond wheels made by roller embossing [16]

The wear performance tests of the composites were performed with the difficult-to-machine material 304 stainless steel. The maximum height of the summit of the 400# and 800# diamond composite grits declined by 13.6% and 8.2%, respectively after wear tests. Also, the composite grits could retain material removal ability and renew themselves due to the domed pyramid structure. The surface roughness of the workpiece decreased to 0.405 μm by 80% after the first wear test for 400# diamond and eventually approached 0.036 μm. The improvement on the surface of the workpiece could be accomplished in no more than 90 s [16].

Micro diamond tools are indispensable for machining microstructured arrays. The cutting edge durability and consistency of micro diamond tools are the determinants of the microstructure quality and accuracy, in addition to the motion accuracy of the machine tool. In article [17] a strength distribution model of the working area including the cutting edge and rake and flank faces was established considering diamond anisotropy and chip flow direction. Comprehensive wear resistances of micro diamond tools with different crystal orientation combinations were analyzed based on the model, and the wear prone areas of different tools were successfully predicted. The evolution processes of the sharpness and wear topography were monitored for every micro diamond tool in the micromachining experiments (Fig. 9).

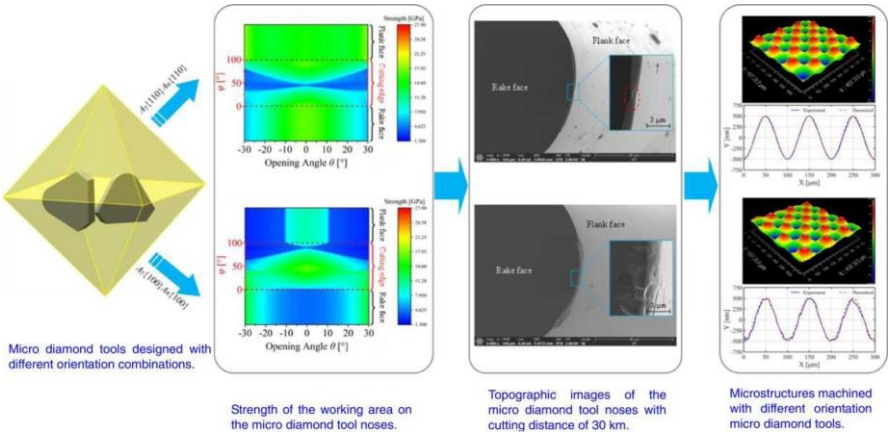

Figure 9 – Micro diamond tools designed with different orientation combinations [17]

The morphologies, profile errors and topological characteristic of the microstructures machined with different micro diamond tools with increasing cutting distance were analyzed. Finally, a conclusion was drawn that the wear resistances of the micro diamond tools in ascending order are $A_\gamma\{100\}A_\alpha\{100\}$, $A_\gamma\{100\}A_\alpha\{110\}$, $A_\gamma\{110\}A_\alpha\{100\}$, and $A_\gamma\{110\}A_\alpha\{110\}$. The three working areas of the $A_\gamma\{100\}A_\alpha\{100\}$ tool are prone to wear; in contrast, those of the $A_\gamma\{110\}A_\alpha\{110\}$tool are resistant to wear. The tool wear of $A_\gamma\{100\}A_\alpha\{110\}$is caused by flank face wear, and that of $A_\gamma\{110\}A_\alpha\{100\}$ is caused by rake face wear [17].

Coupling of multiple abrasive grains is crucial for the efficiency in the grinding process and grinder design. In [18] the coupling effect in a double-grain model in vibration-assisted scratch of single-crystal silicon carbide (SiC) have been investigated using the molecular dynamics simulations for both simultaneous and sequential scratch processes. The coupling between the double abrasive grains affect the scratch force, stress, amorphous layer and surface morphology. The reduction ratios of tangential and normal force and the influenced material volume show that the critical distance for the inhibition of the coupling of vibration-assisted scratch is significantly greater than that in conventional scratch (Fig. 10). The change of overlap ratio can reflect the change trend of the scratch force reduction ratio. In the vibration-assisted grinding, the increase of overlap ratio also intensifies the coupling of the abrasive grains, resulting in faster material removal, smaller scratch force and better surface finish. Insights obtained through the molecular dynamics analysis in this work into the coupling effects of abrasive

grains in the vibration-assisted grinding process is believed to be beneficial in the development of grinding wheels and the optimization of machining processes.

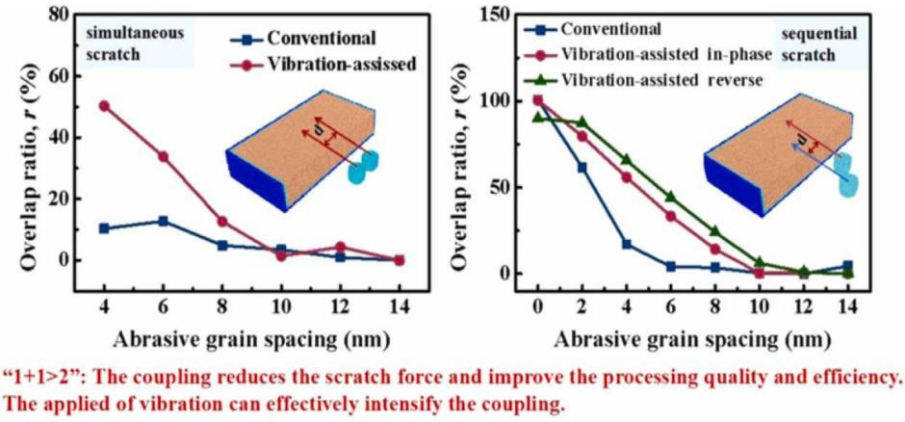

Figure 10 – The coupling between the double abrasive grains affect the scratch force, stress, amorphous layer and surface morphology [19]

In article [19] Single pass scratch tests were carried out in three different grades of WC/Co, containing 6, 11, 28% of cobalt and in different environmental conditions: dry, distilled water (pH 6), acid (pH 2) and basic (pH 10) solutions in order to analyze its influence on wear and friction coefficient. Tests were conducted with increasing normal load ranging from 2 to 102 N. A drop of liquid was placed between the indenter tip and the sample at the beginning of the test. At the end of the test, sample was cleaned and dried. The total exposure time to liquid is around 200 s in order to minimize corrosion effects. Worn surfaces were analyzed by Scanning Electron Microscopy (SEM) and optical profilometry. Co% has a significant effect on mechanisms transition loads and on friction coefficient. The later increased with Co% due to the larger extent of plastic deformation. Results indicated that at loads inferior to 62 N, liquid nature does not affect friction or critical loads. However, at higher loads, liquid media effect is statistically significant and distilled water presented the lower friction coefficient and fluid wettability. The liquid acted as a lubricant resulting in lower friction when compared to dry conditions. In Rockwell tests, wear is controlled by plastic deformation, whereas, in Vickers tests, brittle-mechanisms such as cracking took place [19].

Thermally sprayed tungsten carbide coating is extensively engaged in wear resistance applications due to its good tribological properties. For some

applications in aerospace, automotive, printing and forming industries, these coated components require a nanolevel surface finish. In the investigation [20], magnetorheological fluid based finishing (MRF) process is carried out on the pre-polished tungsten carbide coating using standard magnetorheological (MR) fluid which contains diamond powder as the abrasive particles. In this case, the lower gripping strength of non-magnetic abrasives into the chain structures of carbonyl iron particles (CIPs) is responsible for inadequate material removal rate (MRR) and irregular polishing. To overcome these problems, MRF is conducted with a chemical etchant and that leads to a higher finishing rate due to the integrated effect of etching and polishing. The mechanism of material removal in normal MRF operation is schematically shown in Fig. 11. In the traditional MR fluid, abrasive particles are loosely gripped in between CIPs chains under the effect of magnetic flux lines. However, the gripping force of CIP chains on abrasive particles is not sufficient to restrict the rolling motion of the abrasive particles during finishing of hard materials. Hence, a lower penetration depth is accomplished by the rolling motion of abrasives as shown in Fig. 11. Thus, material is removed by both rolling and sliding motions of the abrasive particles. Therefore, the material removal mechanism is similar to the three-body abrasive wear and that leads to an inefficient and nonuniform material removal. In addition to that, the abrasives may also be thrown away from the MR fluid ribbon at a high wheel speed due to the lack of gripping of abrasive particles into the CIP chain structures. So, it is difficult or time consuming to finish hard materials due to less abrasive particles and low forces.

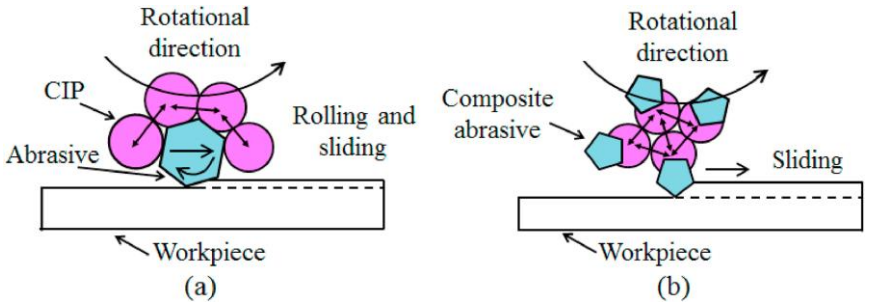

Figure 11 – Mechanism of material removal in MRF with (a) conventional MR fluid and (b) MR fluid with magnetic abrasives

As a result of presenting the available modern developments, it is possible to draw the following conclusions.

Attention is drawn to the processing of polycrystalline diamonds using the synergy of chemical and mechanical effects. Three main ways of material removal during diamond polishing are identified and summarized on the basis of experimental results: interphase mechanochemical removal, chemically stimulated mechanical removal and mechanochemical transformation of diamond. Attention is drawn to the fact that developments in the polishing of monocrystalline diamond without damage at the atomic level can be enhanced by inductively coupled plasma at atmospheric pressure.

It is shown that the accuracy of straightening diamond arc-shaped grinding wheels can be significantly increased by reducing the wear of diamond particles of the galvanic straightening tool. Graphitization appears in the ruling circle with a large grain size of diamond particles, and the wear rate of diamond particles will be accelerated. It was established that to achieve high-performance and accurate straightening of arc-shaped diamond grinding wheels, a combined method using laser rough straightening and electric discharge precision straightening is used. Moreover, the laser roughing method is used to quickly remove the excess abrasive layer to obtain an arc-shaped profile. Electroerosion precision correction not only increased the accuracy of the arc-shaped contour, but also improved the cutting ability of the grinding wheel. The use of acoustic emission intensity for the assessment of diamond wear was studied, which allows the operator to estimate the size of the worn surface and when changes are necessary to avoid burnishing of the working surface.

In order to increase the durability and self-sharpening ability of abrasive materials for efficient automated production, structured models and superhard materials have been developed and researched. In vibratory sanding, increasing the overlap ratio also increases the adhesion of the abrasive grains, resulting in faster material removal, less scratch force, and better surface finish. It is believed that the data obtained by molecular dynamics analysis on the effects of abrasive grain bonding in the vibration grinding process will be useful for the design of grinding wheels and the optimization of machining processes.

References: 1. *H. Sumiya, K. Harano*. Micro-scale abrasion investigations of single-crystal diamonds using nano-polycrystalline diamond wheels. Diamond and Related Materials. Volume 126, June 2022, 109108. **2.** Nanoscale smooth and damage-free polycrystalline diamond surface ground by coarse diamond grinding wheel / *Yunxiang Lu, Bo Wang, Qing Mu, Ke Yang, He Li, Andreas Rosenkranz, Nan Jiang, Ping Zhou*. Diamond and Related Materials. Volume 125, May 2022, 108971. **3.** Mirror-grinding of single-crystal diamond substrates with a rotary grinder / *Hideo Aida, Ryuji Oshima, Hiroki Minamigata, Shogo Kawaguchi, Junpei Tokutake, Juan Manuel Del Angel Sifuentes, Yutaka Kimura*. Diamond and Related Materials. Volume 121, January 2022, 108733. **4.** Polishing of polycrystalline diamond using synergies between chemical and mechanical inputs: A review of mechanisms and

processes / *Chen Xiao, Feng-Chun Hsia, Alexander Sutton-Cook, Bart Weber, Steve Franklin*. Carbon. Volume 196, 30 August 2022, pp. 29–48. **5.** Atomic-scale and damage-free polishing of single crystal diamond enhanced by atmospheric pressure inductively coupled plasma / *Hu Luo, Khan Muhammad Ajmal, Wang Liu, Kazuya Yamamura, Hui Deng*. Carbon. Volume 182, September 2021, pp. 175–184. **6.** Mechanical polishing of ultrahard nanotwinned diamond via transition into hard sp^2-sp^3 amorphous carbon / *Tianye Jin, Mengdong Ma, Baozhong Li, Yufei Gao, Qingliang Zhao, Zhisheng Zhao, Junyun Chen, Yongjun Tian*. Carbon. Volume 161, May 2020, pp. 1–6. **7.** *Shun-Tong Chen, Chien-Chih Chen, Sheng-Yu Shih.* Efficient microspark erosion-assisted machining of a monocrystalline microdiamond stylus using a heat-avoidance path. Precision Engineering. Volume 72, November 2021, pp. 426–436. **8.** *Yejun Zhu, Wenfeng Ding, Zhiwen Rao, Changyong Yang.* Micro-fracture mechanism of polycrystalline CBN grain during single grain scratching tests based on fractal dimension analysis. Precision Engineering. Volume 59, September 2019, pp. 26–36. **9.** *Sheng Wang, Qingliang Zhao, Bing Guo.* Wear characteristics of electroplated diamond dressing wheels used for on-machine precision truing of arc-shaped diamond wheels. Diamond and Related Materials. Volume 129, November 2022, 109372. **10.** *Nastja Macerol, Luiz F.P. Franca, Radovan Drazumeric, Peter Krajnik.* The effects of grit properties and dressing on grinding mechanics and wheel performance: Analytical assessment framework. International Journal of Machine Tools and Manufacture. Volume 180, September 2022, 103919. **11.** On-machine precision truing of ultrathin arc-shaped diamond wheels for grinding aspherical microstructure arrays / *Shimeng Yu, Peng Yao, Chuanzhen Huang, Dongkai Chu, Hongtao Zhu, Bin Zou, Hanlian Liu*. Precision Engineering. Volume 73, January 2022, pp. 40–50. **12.** Laser sharpening evaluation of diamond wheels based on 3*D* recognition / *Wei Zhou, Genyu Chen, Mengyang Gao, Mingquan Li*. Diamond and Related Materials. Volume 129, November 2022, 109354. **13**. *Molnar, V.*: Designation of Evaluation Area in Measuring 3*D* Surface Roughness, Rezanie i Instrumenty v Tekhnologicheskih Sistemah 93, pp. 56–64., 2020. doi: 10.20998/2078-7405.2020.93.07. **14.** Efficient and precision dressing of arc-shaped diamond grinding wheel by laser dressing and electrical discharge dressing / *Longzhou Dai, Genyu Chen, Mingquan Li, Shangyong Yuan*. Diamond and Related Materials. Volume 125, May 2022, 108978. **15.** *Jeffrey Badger, Stuart Murphy, Garret E. O'Donnell*. Acoustic emission in dressing of grinding wheels: AE intensity, dressing energy, and quantification of dressing sharpness and increase in diamond wear-flat size. International Journal of Machine Tools and Manufacture. Volume 125, February 2018, pp. 11–19. **16.** Preparation and characterization of coated abrasives with domed pyramid thermosetting polyurethane/epoxy/diamond composites by roller embossing: Wear performance / *Xudong Song, Yaliu Jian, Wenjun Zou, Jin Peng, Pengzhan Liu, Furen Xiao*. Diamond and Related Materials. Volume 120, December 2021, 108632. **17.** *Hanzhong Liu, Wenjun Zong, Zhipeng Cui*. Durability of micro diamond tools with different crystallographic planes. Journal of Materials Processing Technology. Volume 305, July 2022, 117600**. 18.** Coupling of double grains enforces the grinding process in vibration-assisted scratch: Insights from molecular dynamics / *Zhongwei Hu, Yue Chen, Zhiyuan Lai, Yiqing Yu, Xipeng Xu, Qing Peng, Long Zhang*. Journal of Materials Processing Technology. Volume 304, June 2022, 117551. **19.** Liquid media effect on the abrasion response of WC/Co hardmetal with different cobalt percent / *R.V. Magnol, T. Gatti, M.C. Romero, A. Sinatora, C. Scandian*. Wear. Volume 477, 18 July 2021, 203815. **20.** *Gourhari Ghosh, Ajay Sidpara, P.P. Bandyopadhyay.* Performance improvement of magnetorheological finishing using chemical etchant and diamond-graphene based magnetic abrasives. Precision Engineering. Volume 79, January 2023, pp. 221–235.

Валерій Лавріненко, Київ, Україна,
Володимир Федорович, Євгеній Островерх, Харків, Україна,
Володимир Солод, Кам'янське, Україна

СУЧАСНІ РОЗРОБКИ ЩОДО СПРЯМОВАНОГО ВПЛИВУ НА РІЗАЛЬНУ ПОВЕРХНЮ АЛМАЗНО-АБРАЗИВНОГО ІНСТРУМЕНТУ ТА ЙОГО КОНТАКТНУ ЗОНУ В ПРОЦЕСАХ МЕХАНІЧНОЇ ОБРОБКИ (ОГЛЯД)

Анотація. *В даній статті наведені відомості з сучасних розробок у напрямку спрямованого впливу на різальну поверхню алмазно-абразивного інструменту та його контактну зону в процесах механічної обробки. Здебільшого така обробка стикається із питаннями впливу на ріжучу поверхню алмазних інструментів, в т.ч. правлячого механічного та електрофізичного, врахуванню дефектності алмазів, якими піддається обробка, спрямованого впливу на поверхню таких алмазів, теплового та модифікуванням поверхні алмазів. Встановлено, що для досягнення високої продуктивності та точності правки алмазних шліфувальних кругів з дугоподібним профілем використовується комбінований метод лазерної чорнової правки та електророзрядної прецизійної правки. Крім того, метод лазерної чорнової обробки використовується для швидкого видалення надлишків абразивного шару для отримання дугоподібного профілю. Електроерозійна прецизійна корекція не тільки підвищила точність дугоподібного контуру, але й покращила різальну здатність шліфувального круга. Вивчено використання інтенсивності акустичної емісії для оцінки зносу алмазу, що дозволяє оператору оцінити розмір зношеної поверхні та коли необхідні зміни, щоб уникнути вигорання робочої поверхні.*

Щоб підвищити довговічність і здатність до самозаточування абразивних матеріалів для ефективного автоматизованого виробництва, були розроблені та досліджені структуровані моделі та надтверді матеріали. Під час вібраційного шліфування збільшення коефіцієнта перекриття також збільшує адгезію абразивних зерен, що призводить до швидшого видалення матеріалу, меншої сили подряпин і кращої обробки поверхні. Вважається, що дані, отримані за допомогою аналізу молекулярної динаміки про вплив зв'язки абразивних кругів у процесі вібраційного шліфування, будуть корисні для проектування шліфувальних кругів та оптимізації процесів обробки. Такі розробки дозволяють значно інтенсифікувати процеси оброблення та збільшити ефективність алмазно-абразивного інструменту. Саме тому, в даному огляді основна увага і приділена викладенню сучасних напрацювань, відомих із наукових публікацій, переважно за останні 5 років, пов'язаних із вказаними вище питаннями.

Ключові слова: *алмазно-абразивний інструмент; різальна поверхня; контактна зона; механічна обробка; дефектність алмазів; електрофізичний вплив.*

UDC 658.511 **doi: 10.20998/2078-7405.2023.98.03**

V. Meczkó, T. Bányai, Miskolc, Hungary

OPTIMISATION OF OPERATOR-MACHINE ASSIGNMENT PROBLEM USING EXCEL SOLVER

Abstract. *Although the fourth industrial revolution has greatly accelerated the automation of production processes, the importance of human resources has not diminished, as evidenced by the fact that multinational companies are increasingly investing more and more effort in determining the optimal allocation of machines and operators. In this paper, the authors present an approach to the operator-machine assignment task through a suitable model. The mathematical model presented is suitable to support the design of an appropriate human resource management strategy and the implementation of operative human resource management tasks in production systems of different sizes.*
Keywords: *assignment; operator; optimization; cost-efficiency; reject rate.*

1. INTRODUCTION

The design of material flow systems is becoming increasingly important in both on- and off-site value chains. The main reason for this is that, in addition to technological processes, the logistics processes that serve them are becoming increasingly important. The aim of this research is to identify possible solutions in the area of assignment task design, an important area of material flow system design, and to propose a solution that goes beyond these. In order to achieve this goal, a systematic literature review has been carried out as a first step, resulting in an examination of the main relevant design methods discussed in the literature. Subsequently, we briefly review the structuring of design tasks in material flow systems in order to identify the areas where it is possible to formulate specific design tasks as assignment tasks.

In the main part of the paper, we demonstrate the potentials of Excel Solver for different operator-machine allocation problems by solving optimization problems of different complexity. The article discusses the mathematical models of two typical assignment tasks that allow to describe different types of operator-machine assignment problems. Then, the implementation of the discussed assignment problems is described.

By examining the models and methods compared in the research work, we investigate the significance of transforming certain constraints into an objective function component and the impact of added constraint sets on the objective function value.

The models and methods presented in this work are suitable for optimising the allocation of process equipment, manufacturing and assembly cells and the operators serving them, even in large enterprises, resulting in increased production

process efficiency, improved product quality through reduced reject rates and increased economic efficiency.

2. LITERATURE REVIEW

All research activities should be preceded by a literature review, which aims to identify areas of research relevant to the research objectives by looking at the existing research in the literature. In this chapter, we present the results of a systematic literature review to identify research results in the field of transportation and assignment problems and to identify areas where new research directions could be identified. To this end, we have divided the literature review into three major parts. In the first part, we describe a descriptive analysis of the literature sources in the relevant publication databases. In the second part, we provide an overview of the content of the literature sources identified and selected on the basis of various criteria, while in the third part we formulate our findings that contribute to the precise limitation of the research objective.

As a first step in the systematic literature review, we had to define search criteria to identify literature sources that fit well with our research objectives related to the study of transportation and assignment tasks. For our review, we first used the Scopus database and searched using the keyword (TITLE ("assignment problem") OR TITLE-ABS-KEY ("transportation problem")).

The search based on the keyword (TITLE ("assignment problem") OR TITLE-ABS-KEY ("transportation problem")) resulted 8771 publications. The research of assignment problems has a history of more than 60 years, while interestingly the earliest publication in the Scopus database in the field of transportation problems dates back to 1899 [1]. The first publication on solving assignment problems appeared in 1957 and focused on methods for solving assignment problems in directed graphs [2].

The number of publications shows a continuous increase (with the exception of a few years), but the trend in the number of publications shows that the research area is still relevant today, which we see as a result of the need to solve complex logistics problems in complex supply systems that require the development of increasingly complex solution methods.

An examination of the sources revealed that the majority of the articles were published in journals covering the fields of operations research, discrete applied mathematics and computer science. Based on the title and discipline of the sources that published a large number of articles, it can be concluded that heuristic optimization methods and artificial intelligence methods are playing an important role in solving assignment and transportation problems in complex supply chain planning. We found an interesting result when we examined the distribution of the number of published scientific results among researchers. Surprisingly, we were

able to identify several researchers who had published more than 30 scientific results in Scopus database papers. This number indicates to us that several scientific workshops have developed over the decades that have made significant achievements in the field of research on transportation and assignment tasks.

We found similar results when analysing the affiliation of authors. Research groups with a large number of publications can be found in many countries around the world, in Europe, in America and in Asia. The same result is supported by the distribution of scientific papers by country, with the countries with the largest number of articles being China, India, France, Canada, Germany, Italy, Japan, Italy, Turkey, United Kingdom and the United States of America.

Focusing on the research topics, it can be observed that transportation and assignment tasks cover a wide range of different disciplines, with the following being of particular importance: computer science (4140 articles), engineering (3431 articles), mathematics (3315 articles), decision theory (1682 articles), social sciences (772 articles), business and management (765 articles), environmental science (278 articles).

This classification shows that our chosen research area fits well with engineering and applies knowledge from both computer science and mathematics. The explanation for this is that, since the transportation and assignment problems mainly seek solutions to problems that arise in the design of logistics processes in a large enterprise environment, the transport and assignment tasks are also mainly (but not exclusively) in the field of logistics. The importance of the information sciences lies in the fact that the design and management of complex supply chains requires the application of information and telecommunication technologies. The importance of the field of engineering implies that the problems involved in solving transportation and assignment tasks can generally be conceptualized as complex engineering systems. The large number of mathematical and decision making articles supports the fact that transportation and assignment problems require increasingly advanced solution methods, so that the use of newer and newer analytical and heuristic methods is inevitable. And the importance of business sciences draws attention to the important fact that cost-effectiveness is of great importance in the design of logistics systems, while environmental considerations are also inevitable. The categorization of the articles by keywords confirms the same facts from the point of view of the keywords used.

Following the statistical analysis, we examined a narrowed set of literature on assignment problems, analyzing the content of journal articles that are no older than 5 years and have the most independent citations. For the purpose of this analysis, we have chosen to analyze the content of articles focusing only on assignment problems. Articles focusing on assignment problems cover the following typical application areas: production logistics, supply chain planning,

transportation management, warehousing logistics, warfare, education. The importance of these areas is demonstrated by the results of the following main research areas: modelling of real time ride sharing by linear assignment [3], traffic assignment problem [4], storage location assignment problems [5], assignment problems in socio-economic systems [6], assignment problems in optical networks [7], rapid drone assignment problems [8], weapon-target assignment [9], assignment of maintenance workers to maintenance tasks [10], assignment in education [11], restricted assignment problems [12], e-scooter assignment problems [13], period stochastic assignment problem for social engagement and opportunistic IoT [14], traffic assignment problems [15], assignment of nurse and patient [16], tail assignment problem [17], knapsack assignment problem [18].

Although an analytical solution of the assignment problem is possible, the constraints increase the complexity of the optimization problem to such an extent that the following heuristic and metaheuristic algorithms can be used: Whale algorithm and Tabu search [19], deep neural networks [20], Pareto-Ant Colony optimization [21], Birnbaum-heuristics [22], Discrete Bat heuristics [23].

In summary, research on assignment tasks has a history going back several decades. There are a number of applications that are not only of logistical relevance, but also concern many areas of production and civil services. A wide range of mathematical methods is available for solving transportation and assignment problems. These can be analytical methods for basic models of assignment problems, while for a large number of constraints the search space of the optimization problem requires the use of heuristic and metaheuristic algorithms. Based on the above conclusions drawn from the reviewed literature, we intend to investigate in our research to what extent the solution of transportation and assignment problems can be supported by Solver.

3. ASSIGNMENT PROBLEMS IN MATERIAL HANDLING DESIGN

The design problems of material flow systems can be traced back to a number of operational research problems. This chapter briefly describes examples of potential design problems that can be traced back to assignment problems [24, 25]. Layout planning, facility location: assignment of empty sites and objects to be installed, packaging, planning of unit loading: selection of optimal unit loading and packaging device, route planning: assignment of vehicles to routes, supply tasks to routes and assign collection and distribution tasks to routes and vehicles, design of queuing systems: assigning service tasks to resources, reliability of material flow

systems: assigning tasks to resources and assigning resources to subsystems in order to design an optimal system structure to increase reliability.

4. OPERATOR MACHINE ASSIGNMENT WITH TRAINING OPTIONS

In the model, we consider as given the cost of assigning human resources (operators) to each technological resource (machine), the predicted reject rate of each operator on a given machine, the value of the planned quantities to be produced per shift on each machine, the cost of training of operators and the performance improvement as a result of training, which is reflected in the improvement of the reject rate:

- k_{ij}: assignment cost of operator *i* to machine *j*,
- s_{ij}: reject rate of operator *i* assigned to machine *j*,
- e_j: value of products to be produced on machine *j* within a shift,
- w: training cost of an operator, which can lead to a reject rate decrease of β.

The decision variable of the optimization problem is the matrices describing the assignment of human resources and technological resources and the training of human resources:

- x_{ij}: assignment of operator *i* to machine *j*:

$$\forall i,j\colon x_{ij} \in (0,1) \tag{1}$$

- x_i^*: training of operator *i*:

$$\forall i\colon x_i^* \in (0,1) \tag{2}$$

The objective function of the optimization task is to minimize the total cost:

$$C_6 = \sum_{i=1}^{m}\sum_{j=1}^{n} x_{ij} \cdot k_{ij} + \sum_{i=1}^{m}\sum_{j=1}^{n} x_{ij} \cdot \frac{s_{ij}}{1+x_i^* \cdot \beta} \cdot e_j + \sum_{i=1}^{m} w \cdot x_i^* \rightarrow min. \tag{3}$$

We can define two different constraints:

- each operator can be assigned to one machine:

$$\forall i\colon \sum_{j=1}^{n} x_{ij} = 1 \tag{4}$$

- each machine can be assigned to one operator:

$$\forall j\colon \sum_{i=1}^{m} x_{ij} = 1 \tag{5}$$

The input parameters of the scenario are the cost shown in Figure 1, the reject rate shown in Figure 2, the total value of products to be produced per shift per machine shown in Figure 3 and the training cost, which in this case study is 10 EURO/person.

Technological resources

Human resources / Cost	1	2	3	4	5	6	7	8	9	10	11	12
1	86	76	37	47	42	18	32	82	20	85	20	62
2	35	66	47	52	52	24	40	69	54	42	81	65
3	56	52	67	38	60	74	79	76	85	48	55	66
4	24	69	85	75	25	31	66	61	64	82	14	16
5	29	29	23	31	64	86	27	76	24	56	22	49
6	27	39	41	56	54	58	47	79	54	49	41	19
7	28	65	62	52	29	35	82	67	85	68	35	66
8	77	58	50	82	21	46	81	62	17	10	59	42
9	72	22	39	29	29	86	77	63	51	80	26	21
10	51	56	21	83	67	25	37	43	18	44	42	65
11	45	76	18	47	49	57	74	35	21	47	81	66
12	24	87	44	62	39	80	88	40	64	79	33	42

Figure 1 – The assignment cost of operators and machines

Technological resources

Human resources / Reject rate	1	2	3	4	5	6	7	8	9	10	11	12
1	2	5	1.1	1.2	0.8	4.3	1.3	0.3	3.6	1.3	4.4	2.7
2	0.4	2.7	1.6	4.3	3.9	0.3	3.7	0.6	1	3	0.2	4.8
3	1.9	3.9	2.7	0.8	3.3	0.5	3.1	3.4	0.9	4.4	3.3	0.1
4	1.9	4.9	3.2	1.3	1.1	4.9	4.8	0.1	3.7	2.5	0.3	3.5
5	1.4	3.5	3.7	1.6	2.9	4.6	2.3	1.1	2.3	1.3	0.8	4.1
6	0.8	1	0.1	0.9	3.2	3.5	2	1	2.6	1.9	1.2	3.2
7	3.5	3.8	1.8	3.6	4.4	1.6	0.6	0.6	0.8	4.1	2.6	2
8	4.1	3.8	1.2	5	1.3	4.6	4	4.9	0.2	0.6	2.8	2.6
9	3	3.5	1.9	3.5	2.7	2.4	0.1	3.9	4.5	1.8	3.1	1.2
10	0.3	3.1	5	2.4	0.3	5	1.9	3	1.2	0.5	1.2	1.7
11	5	2.9	1.7	0.2	1.3	4.8	0.2	0.1	1.3	0.3	4.3	1
12	2.1	2.1	2.5	0.6	3.6	3.2	1.8	3.1	4.1	3.9	4.5	1.8

Figure 2 – The reject rate of operators assigned to different machines

Technological resources

	1	2	3	4	5	6	7	8	9	10	11	12
Value to be produced	3500	5600	1500	2650	4570	9510	1500	980	12000	5400	3200	6540

Figure 3 – Value to be produced per shift per machine

The solution is illustrated in Figure 4 and Figure 5. The integrated assignment matrix shown in Figure 4 contains both the assignment of human resources and technological resources and the assignment of human resources to training.

Human resources \ Technological resources	1	2	3	4	5	6	7	8	9	10	11	12	Training
1	0	0	0	0	1	0	0	0	0	0	0	0	1
2	0	0	0	0	0	1	0	0	0	0	0	0	0
3	0	0	0	1	0	0	0	0	0	0	0	0	1
4	0	0	0	0	0	0	0	0	0	0	1	0	0
5	0	0	0	0	0	0	1	0	0	0	0	0	1
6	0	1	0	0	0	0	0	0	0	0	0	0	1
7	0	0	0	0	0	0	0	1	0	0	0	0	0
8	0	0	0	0	0	0	0	0	1	0	0	0	1
9	0	0	0	0	0	0	0	0	0	0	0	1	1
10	0	0	0	0	0	0	0	0	0	1	0	0	1
11	0	0	1	0	0	0	0	0	0	0	0	0	1
12	1	0	0	0	0	0	0	0	0	0	0	0	1

Figure 4 – The integrated assignment matrix

The integrated assignment matrix in Figure 4 can be used to calculate the modified value of the reject rates shown in Figure 2, which is summarized in Figure 5. The cells in blue show the reduced reject rates.

Human resources \ Technological resources	1	2	3	4	5	6	7	8	9	10	11	12
1	1	2.5	0.55	0.6	0.4	2.15	0.65	0.15	1.8	0.65	2.2	1.35
2	0.4	2.7	1.6	4.3	3.9	0.3	3.7	0.6	1	3	0.2	4.8
3	0.95	1.95	1.35	0.4	1.65	0.25	1.55	1.7	0.45	2.2	1.65	0.05
4	1.9	4.9	3.2	1.3	1.1	4.9	4.8	0.1	3.7	2.5	0.3	3.5
5	0.7	1.75	1.85	0.8	1.45	2.3	1.15	0.55	1.15	0.65	0.4	2.05
6	0.4	0.5	0.05	0.45	1.6	1.75	1	0.5	1.3	0.95	0.6	1.6
7	3.5	3.8	1.8	3.6	4.4	1.6	0.6	0.6	0.8	4.1	2.6	2
8	2.05	1.9	0.6	2.5	0.65	2.3	2	2.45	0.1	0.3	1.4	1.3
9	1.5	1.75	0.95	1.75	1.35	1.2	0.05	1.95	2.25	0.9	1.55	0.6
10	0.15	1.55	2.5	1.2	0.15	2.5	0.95	1.5	0.6	0.25	0.6	0.85
11	2.5	1.45	0.85	0.1	0.65	2.4	0.1	0.05	0.65	0.15	2.15	0.5
12	1.05	1.05	1.25	0.3	1.8	1.6	0.9	1.55	2.05	1.95	2.25	0.9

Figure 5 – The modified reject rates

The optimization resulted the following costs: cost of assignment of human resources to technological resources 375 EURO, training cost 90 EURO, reject value 232.4 EURO and total cost 697.4 EURO. The Excel Solver implementation of the solution and its relation to the mathematical model is illustrated in Figure 6.

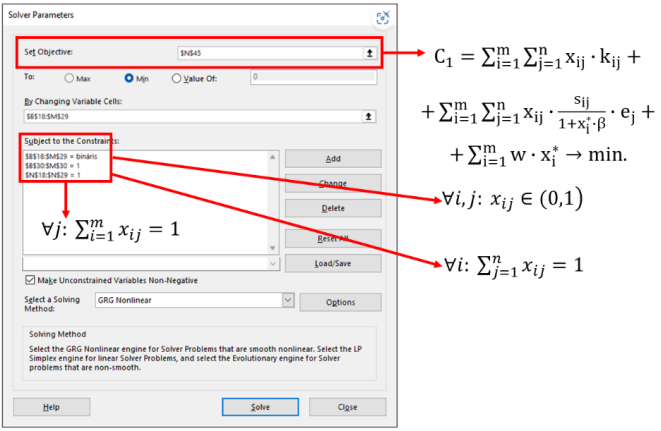

Figure 6 – The Excel Solver implementation of the solution and its relation to the mathematical model

The impact of training cost on the cost structure of the optimal solution is shown in Figure 7.

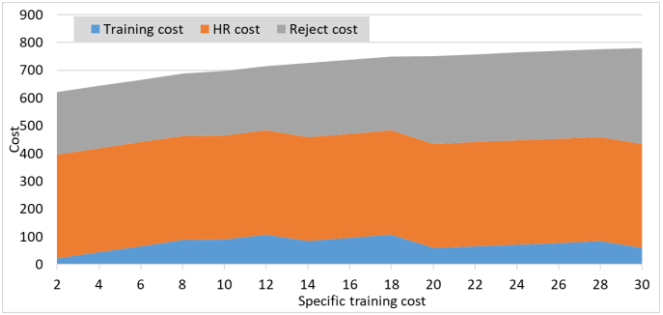

Figure 7 – Impact of specific training cost on the cost structure of optimal solution

5. DISCUSSION AND CONCLUSIONS

An important part of the design and operation of material flow systems in manufacturing processes is the solution of transportation and assignment tasks. The goal of this research work was to develop a mathematical model for the optimal assignment of operators (human resources) and machines (technological resources)

in complex manufacturing environment. To achieve this goal, the main tasks in the design of material flow systems (especially in in-plant supply) have been investigated and the typical assignment tasks they represent have been presented. Several methods are available for solving these assignment problems (Northwest corner method, minimum cost method, Vogel method), but when the objective functions and constraints subject to optimization are complex, new solutions are needed to solve the problem under consideration. In this research work, we investigated whether Excel Solver is suitable for solving complex assignment tasks. Having established that Excel Solver is suitable for solving complex assignment tasks, we have developed a mathematical model that is suitable for assigning operators to machines, while also analyzing the potential performance improvements that can be achieved through worker training. The most important consequences of our analysis can be summarized as follows:

- The more constraints are taken into consideration, the more the optimal solution decreased. This is a trivial fact follows from the nature of optimization problems. It is important to note that this statement is only trivial and true if we add constraints to an existing constraint set. Replacing a smaller set of constraints with a larger set of constraints does not necessarily imply a decreasing objective function value in the case of maximization.
- If a constraint is integrated into the objective function, the solution can be significantly improved. For example, as long as only a constraint on the reject rate that can be produced on technological resources is formulated, a worse solution is obtained than when this reject value is integrated into the cost function as objective function.
- Training of operators can improve their performance, which can lead to a decreased reject rate, but since training has also significant cost, training of human resources may not be appropriate. This conclusion should be treated with caution, as the time horizon over which the return of training is interpreted is very important. In the case of short-term employment, the cost of training is less profitable than in the case of long-term employment.

The practical impact of the research work presented above can be summarized as follows:

- the presented model and solution method can be used to assign human resources (operators) to production resources (production tasks) in a real production environment,
- as a result of the optimization discussed, the utilization of human resources can be increased, the quality of products can be improved by reducing the reject rate, and a more cost-efficient production system can be operated.

Future research plans include further extension of the models and the investigation of methods for solving large-scale complex problems. An important further development could be the inclusion of uncertainty factors.

References: 1. *Higgins, E.E.:* Some of the larger transportation problems in cities, Journal of the Franklin Institute vol.147(4) (1899) pp. 315-327. https://doi.org/10.1016/s0016-0032(99)90253-3 **2.** *Suits, D.B.:* Solution of assignment problems by directed graphs, American Journal of Agricultural Economics vol.39(4) (1957) pp. 975–983. https://doi.org/10.2307/1234208 **3.** *Simonetto, A., Monteil, J., Gambella, C.:* Real-time city-scale ridesharing via linear assignment problems, Transportation Research Part C: Emerging Technologies vol.101 (2019) pp. 208–232. https://doi.org/10.1016/j.trc.2019.01.019 **4.** *Xu, S., Jiang, W., Deng, X., Shou, Y.:* A modified Physarum-inspired model for the user equilibrium traffic assignment problem, Applied Mathematical Modelling vol.55 (2018) pp. 340–353. https://doi.org/10.1016/j.apm.2017.07.032 **5.** *Reyes, J.J.R., Solano-Charris, E.L., Montoya-Torres, J.R.:* The storage location assignment problem: A literature review, International Journal of Industrial Engineering Computations vol.10(2) (2019) pp. 199–224. https://doi.org/10.5267/j.ijiec.2018.8.001 **6.** *Zaitseva, I., Malafeyev, O., Poddubnaya, N., Vanina, A., Novikova, E.:* Solving a dynamic assignment problem in the socio-economic system, Journal of Physics: Conference Series vol.1172(1) (2019) 012092. https://doi.org/10.1088/1742-6596/1172/1/012092 **7.** *Hai, D.T., Morvan, M., Gravey, P.:* Combining heuristic and exact approaches for solving the routing and spectrum assignment problem, IET Optoelectronics vol.12(2) (2018) pp. 65-72. https://doi.org/10.1049/iet-opt.2017.0013 **8.** *Zhu, M., Du, X., Zhang, X., Luo, H., Wang, G.:* Multi-UAV Rapid-Assessment Task-Assignment Problem in a Post-Earthquake Scenario, IEEE Access vol.7 (2019) pp. 74542–74557. https://doi.org/10.1109/ACCESS.2019.2920736 **9.** *Li, X., Zhou, D., Pan, Q., Tang, Y., Huang, J.:* Weapon-target assignment problem by multiobjective evolutionary algorithm based on decomposition, Complexity, vol.2018, 8623051. https://doi.org/10.1155/2018/8623051 **10.** *Chaabane, K., Khatab, A., Diallo, C., Aghezzaf, E.-H., Venkatadri, U.:* Integrated imperfect multimission selective maintenance and repairpersons assignment problem, Reliability Engineering and System Safety vol.199 (2020) 106895. https://doi.org/10.1016/j.ress.2020.106895 **11.** *Faudzi, S., Abdul-Rahman, S., Abd Rahman, R.:* An Assignment Problem and Its Application in Education Domain: A Review and Potential Path, Advances in Operations Research 2018, 8958393. https://doi.org/10.1155/2018/8958393 **12.** *Jansen, K., Rohwedder, L.:* On the configuration-LP of the restricted assignment problem, Proceedings of the Annual ACM-SIAM Symposium on Discrete Algorithms (2017) pp. 2670–2678. https://doi.org/10.1137/1.9781611974782.176 **13.** *Masoud, M., Elhenawy, M., Almannaa, M.H., Liu, S.Q., Glaser, S., Rakotonirainy, A.:* Heuristic Approaches to Solve E-Scooter Assignment Problem, IEEE Access vol.7 (2019) pp. 175093–175105. https://doi.org/10.1109/ACCESS.2019.2957303 **14.** *Fadda, E., Perboli, G., Tadei, R.:* Customized multi-period stochastic assignment problem for social engagement and opportunistic IoT, Computers and Operations Research vol.93 (2018) pp. 41–50. https://doi.org/10.1016/j.cor.2018.01.010 **15.** *Jafari, E., Pandey, V., Boyles, S.D.:* A decomposition approach to the static traffic assignment problem, Transportation Research Part B: Methodological vol.105 (2017) pp. 270–296. https://doi.org/10.1016/j.trb.2017.09.011 **16.** *Carello, G., Lanzarone, E., Mattia, S.:* Trade-off between stakeholders' goals in the home care nurse-to-patient assignment problem, Operations Research for Health Care vol.16 (2018) pp. 29–40. https://doi.org/10.1016/j.orhc.2017.12.002 **17.** *Vikstål, P., Grönkvist, M., Svensson, M., Andersson, M., Johansson, G., Ferrini, G.:* Applying the quantum approximate optimization algorithm to the tail-assignment problem, Physical Review Applied vol.14(3) (2020) 034009. https://doi.org/10.1103/PhysRevApplied.14.034009 **18.** *Martello, S., Monaci, M.:* Algorithmic approaches to the multiple knapsack assignment problem, Omega vol.90 (2020) 102004. https://doi.org/10.1016/j.omega.2018.11.013 **19.** *Abdel-Basset, M., Manogaran, G., El-Shahat, D., Mirjalili, S.:* Integrating the whale algorithm with Tabu search for quadratic assignment problem: A new approach for locating hospital departments, Applied Soft Computing Journal vol.73 (2018) pp. 530–546. https://doi.org/10.1016/j.asoc.2018.08.047 **20.** *Lee, M., Xiong, Y., Yu, G., Li, G.Y.:* Deep neural networks for linear sum assignment problems, IEEE Wireless Communications Letters vol.7(6) (2018) pp. 962–965. https://doi.org/10.1109/LWC.2018.2843359 **21.** *Li, Y., Kou, Y., Li, Z., Xu, A., Chang, Y.:* A Modified Pareto Ant Colony Optimization Approach to Solve Biobjective Weapon-Target Assignment Problem, International Journal of Aerospace Engineering (2017) 1746124. https://doi.org/10.1155/2017/1746124 **22.** *Zhu, X., Fu, Y., Yuan, T., Wu, X.:* Birnbaum importance based heuristics for multi-type component assignment problems, Reliability Engineering and System Safety vol.165 (2020) pp. 209–221.

https://doi.org/10.1016/j.ress.2017.04.018 **23.** *Riffi, M.E., Saji, Y., Barkatou, M.:* Incorporating a modified uniform crossover and 2-exchange neighborhood mechanism in a discrete bat algorithm to solve the quadratic assignment problem Incorporating a modified uniform crossover and 2-exchange neighborhood mechanism, Egyptian Informatics Journal vol.18(3) (2017) pp. 221–232. https://doi.org/10.1016/j.eij.2017.02.003 **24.** *Cselényi, B., Illés B.:* Design and control of material handling systems (in Hungarian), University of Miskolc, 2006. **25.** Telek, P. Kostal, P. Material handling equipment selection algorithm for production workplaces, Advanced Logistic Systems – Theory and Practice vol.16(2) (2022) pp. 37–46. https://doi.org/10.32971/als.2022.011.

Вікторія Мечко, Тамаш Баняї, Мішкольц, Угорщина

ОПТИМІЗАЦІЯ ЗАДАЧІ ПРИЗНАЧЕННЯ ОПЕРАТОР-МАШИНА ЗА ДОПОМОГОЮ EXCEL SOLVER

Анотація. *Незважаючи на те, що четверта промислова революція значно прискорила автоматизацію виробничих процесів, важливість людських ресурсів не зменшилася, про що свідчить той факт, що багатонаціональні компанії все частіше вкладають все більше зусиль у визначення оптимального розподілу машин і операторів. Розробка систем матеріальних потоків стає все більш важливою в ланцюжках створення вартості як на місці, так і за його межами. Основна причина цього полягає в тому, що, крім технологічних процесів, все більшого значення набувають логістичні процеси, які їх обслуговують. Важливою частиною проектування та експлуатації систем матеріальних потоків у виробничих процесах є вирішення завдань транспортування та призначення. Метою цієї дослідницької роботи була розробка математичної моделі для оптимального розподілу операторів (людських ресурсів) і машин (технологічних ресурсів) у складному виробничому середовищі. Для досягнення цієї мети були досліджені основні завдання при проектуванні систем матеріальних потоків (особливо при внутрішньозаводському постачанні) та представлені типові завдання призначення, які вони представляють. Існує кілька методів для вирішення цих проблем призначення (метод північно-західного кута, метод мінімальних витрат, метод Фогеля), але коли цільові функції та обмеження, що підлягають оптимізації, є складними, для вирішення проблеми, що розглядається, необхідні нові рішення. У цій дослідницькій роботі автори з'ясували, чи підходить Excel Solver для розв'язування складних завдань. Встановивши, що Excel Solver підходить для вирішення складних завдань призначення, автори розробили математичну модель, яка підходить для призначення операторів машинам, а також аналізуючи потенційні покращення продуктивності, яких можна досягти шляхом навчання працівників. Найважливіші наслідки аналізу авторів можна підсумувати таким чином: чим більше обмежень береться до уваги, тим більше зменшується оптимальне рішення. Якщо сформульовано лише обмеження на відсоток браку, який може бути створений за допомогою технологічних ресурсів, буде отримано гірше рішення, ніж коли це значення браку інтегровано у функцію витрат як цільову функцію. Навчання операторів може підвищити їх продуктивність, що може призвести до зниження відсотка відмов, але оскільки навчання також вимагає значних витрат, навчання людських ресурсів може бути недоречним. Представлена модель і метод рішення можуть бути використані для призначення людських ресурсів (операторів) виробничим ресурсам (виробничим завданням) у реальному виробничому середовищі. В результаті обговорюваної оптимізації можна підвищити використання людських ресурсів, покращити якість продукції за рахунок зменшення відсотка браку та запровадити більш економічно ефективну систему виробництва.*
Ключові слова: *призначення; оператор; оптимізація; економічність; брак.*

UDC 621.9.048 **doi: 10.20998/2078-7405.2023.98.04**

A. Mitsyk, V. Fedorovich, Kharkiv, Ukraine

REGULARITIES OF VIBRATION FINISHING AND GRINDING PROCESSING AND DIRECTIONS OF IMPROVEMENT OF ITS INTENSITY AND QUALITY

Abstract. *The data on the labor intensity of manufacturing engineering products and the share of finishing and grinding operations in the total labor costs of their manufacture are presented. The list and the degree of mastering the technological operations of finishing and grinding processing, performed in the conditions of machine-building industries during the last years are given. The grounds are given for highlighting the method of vibration processing as the most promising for ensuring complete mechanization of the process of finishing and cleaning, as well as achieving high technological characteristics of the surface roughness of parts. An assessment was made of the influence of modes, the trajectory of the movement of the reservoir and the grain size of the granules of the abrasive medium on metal removal. It is indicated that the intensity and quality of vibration treatment is estimated quantitatively by the weight removal of metal and qualitatively by the roughness of the processed surface. It is indicated that the determining factor in this case is the speed of the oscillating movement of granules and parts, the difference of which represents the speed of vibration processing, depending on the speed of the oscillating movement of the medium. It is noted that in order to increase the productivity of the process, it is necessary to increase the speed of the medium by increasing the frequency and amplitude of the reservoir oscillations. The layer-by-layer transmission of a force impulse from the bottom of the reservoir to the bulk medium is considered. The physical meaning of increasing productivity by increasing the amplitude of the reservoir oscillations is indicated. The conditions for obtaining metal removal are indicated, which provide increased efforts for the interaction of granules with parts at high micro-cutting speeds. Experimental studies are described to determine the influence of the amplitude and frequency of oscillations on the results of vibration finishing and grinding. Graphic dependences of metal removal were obtained for various ratios of the sample weight to the weight of the medium granule. The dependence of metal removal on the ellipticity coefficient and the amplitude of the reservoir oscillations was obtained in a similar way. It is noted that the vertical component of the amplitude during in-plane oscillations of the reservoir is the determining factor of the complex influence of the parameters of the ellipse coefficient of the trajectory of the reservoir and its amplitude of oscillations. It has been established that when using a coarse-grained abrasive, the penetration of grains into the metal of the part occurs to a greater depth and larger metal chips are removed with a large metal removal. With a small grain size of the abrasive, small chips are removed with a small metal removal and a decrease in the height of micro-roughness.*

Keywords: *vibration treatment; technological capabilities; intensity and quality; amplitude and frequency of oscillations; trajectory of the reservoir; metal removal; ellipse coefficient; granularity of the medium material.*

With the growth of production volumes and the requirements for the quality of products of mechanical engineering and instrumentation, there is a constant increase in the volume of finishing and grinding processing.

It is known from domestic and foreign experience that at the present stage, the share of finishing and grinding processing reaches 10 ... 20 % of the total labor

intensity of manufacturing parts. In some cases, for example, in the manufacture of parts from materials that are difficult to machine by cutting and pressure processes, the labor intensity of finishing and grinding operations can reach 40 – 70 % of the labor costs for manufacturing the part [1].

The technological operations of finishing and grinding processing include: deburring; removal of flash and grata; edge rounding; surface cleaning from scale, corrosion; molding sand residues; grinding and polishing to give shade and shine, etc. [2].

Studies of various types of finishing and grinding processing have made it possible to establish the degree of their development in the metalworking industry in the recent period. These data are as follows: vibration treatment – 23 %; jet-abrasive – 18 %; belt grinding – 11 %; tumbling – 6 %; polishing wheels and metal brushes – 5 %; treatment with a stream of compacted abrasive – 2 ... 3 %.

An analysis of technological capabilities and experience in practical application made it possible to single out the vibratory processing method from the variety of industrial methods of finishing and cleaning, as the most effective from the position of mechanization of manual labor while achieving high technological characteristics of surface roughness and ensuring complete mechanization of the process of vibration finishing and grinding.

Further, in order to improve the intensity and quality of vibration finishing and cleaning processing, we will evaluate the influence of the modes and trajectory of the reservoir movement, as well as of the material grain size of the abrasive medium granules on the resulting metal removal.

It is accepted that the intensity and quality of vibration treatment is estimated quantitatively by the weight metal removal from a unit surface area per unit time and qualitatively by the roughness of the processed surface [3,4].

The determining factor in this case is the speed of the oscillating movement of abrasive granules and parts, the difference of which represents the speed of vibration processing. The latter depends on the damping coefficient of the bulk medium, which in its urn is determined by its elastic properties, the thickness of the medium layer, the size and shape of the granules, the relative content of the chemically active solution in the reservoir, the internal friction in the medium, its air permeability and a number of other factors, the influence of which should be taken into account almost impossible analytically.

Obviously, to increase the productivity of the process, it is necessary to increase the speed of the oscillating movement of the medium by increasing the frequency and amplitude of the reservoir oscillations. Usually, the oscillation frequency is in the range of 1500 ... 3000 vpm and its increase is limited by the design capabilities of the vibrating machine units. Running at lower frequencies causes significant performance degradation. The amplitude of oscillations during vibration processing is selected within the range of 0.5 ... 6.0 mm. Increasing it

more than 6.0 mm causes a sharp decrease in the service life of bearing assemblies of inertial vibration exciters.

The transfer of a force impulse from the bottom of the reservoir to the bulk medium is carried out in layers – from one layer to another. During vibration processing, a phase lag is observed in the movement of various layers. There may be a mode of operation in which the inner or upper layers are in suspension state, and the lower layer, falling on the surface of the reservoir bottom, again receives and transmits an impulse to the upper layer, when it has not yet completed its upward movement. Such a transfer of motion reduces productivity, since layers of abrasive granules, which are far from the walls of the reservoir, practically stop removing metal from parts [5, 6].

In this case, the most effective measure to improve productivity is to increase the amplitude of the reservoir oscillations. The physical meaning of this lies in the fact that when the reservoir moves upwards, first there is a compaction and elastic compression of the medium layers with a thickness of δ located near the wall. When the reservoir wall is moved by an amount equal to the amplitude of A, the layer is compacted and decreases by an amount Δ.

Thus, it is shifted by an amount of $A-\Delta$. The next layer will not receive an impulse if the compaction and compression of the first layer by Δ is greater than A. The same will happen with the n-th layer, when $\Delta_n \geq A$.

The force F_n of the mutual pressure of the parts and the abrasive granule is determined by the expression:

$$F_n = \varepsilon MA\omega^2; \quad (1)$$

where $\varepsilon = k^2/k_1$, k and k_1 – coefficients are not constant in value; k – takes into account the damping properties of the medium and the inertia of the part; k_1 – takes into account the decrease in amplitude due to the damping of the medium. Each point of the cross section of the reservoir has its own values k and k_1, which vary depending on the distance of parts from the reservoir walls and some other reasons.

By increasing the oscillation amplitude, it is possible to transfer the force impulse to a layer of much greater thickness. According to dependence (1) at $A = 2.5$ mm we have $F_n = \varepsilon\, 2.5 \cdot 43600 = 109000$ grams.

Increasing the amplitude from $A = 1.5$ mm to $A = 2.5$ mm makes it possible to obtain a greater force than it is achieved by increasing the frequency by 1000 rpm. With an increase in amplitude to $A = 4.0$ mm,

$F_n = \varepsilon 4 \cdot 43600 \square 175000$ grams, that is, the force increases by 1.7 times compared to the first case.

Thus, for the vibration grinding process, when it is necessary to remove a defective metal layer from the surface to be treated, as well as for cleaning operations, large amplitudes should be used, providing increased interaction forces between granules and parts, as well as high micro-cutting speeds along with high values of the parameters of the elastic-plastic deforming.

For finishing operations, on the contrary, large vibration amplitudes are unacceptable, since in this case it is not required to remove a significant layer of metal from the surface to be treated, but to increase its purity with a decrease in the height of micro-roughness., Therefore, the designs of vibrating machines that allow changing the amplitude and frequency of processing in a wide range receive all greater distribution [7].

It is extremely difficult to analytically determine the influence of the amplitude and frequency of vibrations on the results of grinding and polishing due to the large number of factors that affect the results of processing. This can be done more simply and accurately experimentally. The corresponding experiments were carried out on cylindrical samples of steel 45 DSTU 7809:2015 (steel 45C DIN EN 10083-2) weighing 25, 50, 100 and 300 grams. Mineral-ceramic plates weighing 10 grams were used as an abrasive medium for all experiments.

Obtained as a result of the experiment, the dependence of metal removal from 1 cm^2 of the surface of the samples on the oscillation frequency at a different ratio of the weight of Q sample to the weight of q granules of the medium is presented graphically (Fig. 1).

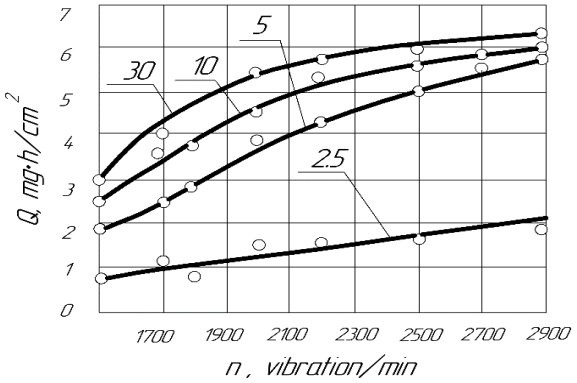

Figure 1 – Dependence of metal removal on the oscillation frequency and relationships $Q/q = 2.5; 5; 10; 30$

The difference in the removal of metal from the samples when the ratio Q/q changes from 2.5 to 30 is explained by a large decrease in the speed of movement of heavy parts when they are removed from the reservoir walls compared to light ones. This leads to an increase in the relative speed between the part and the granules and, therefore, to an increase in the efficiency of the operation.

As the frequency increases, metal removal increases rapidly at first, then slows down. This can be explained as follows. With an increase in the oscillation frequency, the impulse from the walls and bottom of the reservoir is transmitted only to the layers located near these surfaces, with a frequency corresponding to the oscillation frequency of the reservoir. The layers, however, remote from the walls and the bottom, receive an impulse of the opposite sign even before the end of the movement in the original direction. So their movement is damped [8].

The dependence of metal removal on the ellipse coefficient K_A and the amplitude A of the reservoir oscillations has been obtained in a similar way (Fig. 2). It can be considered linear within $A = 0.5...6.0$ mm.

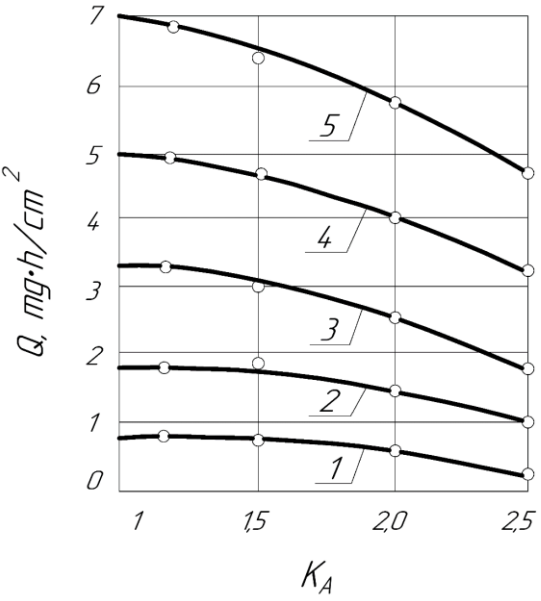

Figure 2 – Dependence of metal removal on the ellipse coefficient and the amplitude of the reservoir oscillations: 1 – $A_y = 1$ mm; 2 – $A_y = 2$ mm; 3 – $A_y = 3$ mm; 4 – $A_y = 4$ mm; 5 – $A_y = 5$ mm

The results of experiments to determine the removal of metal, depending on the grain size of the material of the granules of the abrasive medium, are presented graphically (Fig. 3).

The greatest removal of metal at all investigated amplitudes is observed at $K_A = 1.0...1.5$, and within these limits of fluctuations K_A the removal of metal changes insignificantly. This allows you to adjust the trajectory of the reservoir motion with less accuracy, which speeds up and simplifies the adjustment of vibrating machines.

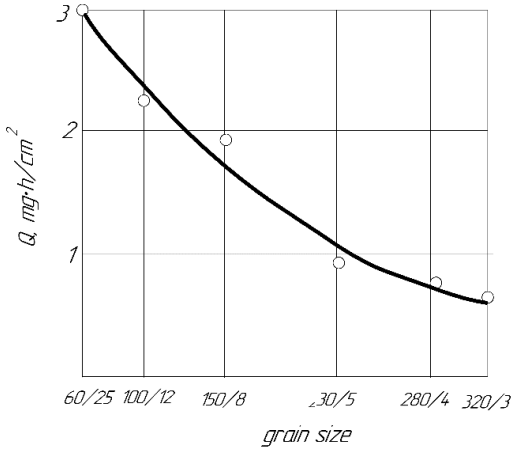

Figure 3 – Dependence of metal removal on the grain size of the material of the granules of the abrasive medium

At a value of $K_A = 2.0...2.5$, an increased number of micro-nicks are observed on the processed surfaces of parts, the depth of which reaches 0.1 mm. For grinding, the most productive modes will be those that have K_A close to unity.

The removal of metal is decreased with a decrease in the material grain size of the abrasive medium granules. This is especially noticeable in the grain size range of 2.5 ... 5.0 μm. An increase in the grain size of grinding powders in the range from 5.0 to 7.0 μm also leads to a decrease in metal removal. However, the use of fine-grained abrasive media allows to obtain a higher surface quality.

Conclusions

1. An analysis of the theoretical and experimental studies carried out showed that an increase in the frequency of oscillations, depending on the accepted ranges of its change, has a different effect on the intensity and quality of the process. However, in all cases, there is a clear tendency to increase the productivity of vibration processing with an increase in the frequency of vibrations of the vibrating machine reservoir.

2. The amplitude of the reservoir oscillations, as well as its frequency, has a significant impact on the intensity of the vibration treatment process, where the fundamental effect on the medium is the vertical component of the amplitude during in-plane oscillations of the reservoir. The conducted studies have a general tendency to increase the intensity of vibration treatment with an increase in the amplitude of vibrations of the vibrating machine reservoir.

3. Experimental studies have established that when using a coarse-grained abrasive, the number of grains in contact with the processed surface decreases. In this case, the penetration of grains into the metal occurs to a greater depth and larger metal chips are removed with a significant metal removal. With a small grain size of the abrasive, the number of contacts with the processed surface increases. This contributes to the removal of small chips and a decrease in the height of the micro-roughness of the processed surface with a small metal removal.

References: **1.** Primenenie vibracionnyh tehnologij na operacijah otdelochno-zachistnoj obrabotki detalej (ochistka, mojka, udalenie obloja i zacsencev, obrabotka kromok): monografija / Babichev A.P., Motrenko P.D., Gillespi L.K. i dr.; pod red. A.P. Babicheva. Rostov-na-Donu: Izd-vo DGTU, 2010. 289 p. **2.** *Kulakov Ju.M., Hrulkov Ju.M.* Otdelochno-zachistnaja obrabotka detalej. Moskva: Mashinostroenie, 1979. 216 p. **3.** *Kartashov I.N., Shainskij M.E., Vlasov V.A.* Obrabotka detalej svobodnymi abrazivami v vibrirujushhih rezervuarah. Kyiv: Vishha shk., 1975. 188 p. **4.** *Molnar, V.*: Tribology and Topography of Hard Machined Surfaces, Rezanie i Instrumenty v Tekhnologicheskih Sistemah 94, pp. 49–59., 2021. https://doi.org/10.20998/2078-7405.2021.94.06 **5.** *Mitsyk, A., Fedorovich, V., Grabchenko, A. (2023).* Wave Nature of the Abrasive Granules Action on the Surface of Parts During Vibration Processing. In: Tonkonogyi, V., Ivanov, V., Trojanowska, J., Oborskyi, G., Pavlenko, I. (eds) Advanced Manufacturing Processes IV. InterPartner 2022. Lecture Notes in Mechanical Engineering. Springer, Cham. https://doi.org/10.1007/978-3-031-16651-8_17 **6.** *Mitsyk A.V., Fedorovich V.A.* The nature of the formation of surface micro-roughness in vibration finishing and grinding processing. *Cutting & Tools in Technological System.* Kharkiv, NTU «KhPI». 2022. № 97. pp. 103 – 112. https://doi.org/10.20998/2078-7405.2022.97.09 **7.** *Mitsyk A.V., Fedorovich V.A., Grabchenko A.I.* The effect of a shock wave in an oscillating working medium during vibration fishing-grinding processing. *Cutting & Tools in Technological System.* Kharkiv, NTU «KhPI». 2020. № 93. pp. 43 – 55. https://doi.org/10.20998/2078-7405.2020.93.06 **8.** *Mitsyk A.V.* Rozvytok procesiv obrobky vil'nym abrazyvnym seredovyshhem v kolyvnyh rezervuarah i formuvannja i'h fizyko-tehnologichnyh mozhlyvostej. Visnyk SNU im. V. Dahl. Sjevjerodonec'k, SNU im. V. Dahl, 2020. № 4 (260). pp. 55 – 65.

Андрій Міцик, Володимир Федорович, Харків, Україна

ЗАКОНОМІРНОСТІ ПРОЦЕСУ ВІБРАЦІЙНОЇ ОЗДОБЛЮВАЛЬНО-ЗАЧИЩУВАЛЬНОЇ ОБРОБКИ І НАПРЯМКИ ВДОСКОНАЛЕННЯ ЇЇ ІНТЕНСИВНОСТІ ТА ЯКОСТІ

Анотація. *Наведено дані трудомісткості виготовлення виробів машинобудування та частки оздоблювально-зачищувальних операцій у загальних трудовитратах їх виготовлення. Дано перелік та ступінь освоєння технологічних операцій оздоблювально-зачищувальної обробки, що виконуються в умовах машинобудівних виробництв за останній період. Наведено підстави для виділення методу вібраційної обробки як найбільш перспективного для забезпечення повної механізації процесу оздоблювально-зачищувальної обробки, а також досягнення високих технологічних характеристик шорсткості поверхні деталей. Здійснено оцінку впливу режимів, траєкторії руху резервуара та зернистості гранул абразивного середовища на зйом металу. Вказано, що інтенсивність та якість вібраційної обробки оцінюється кількісно за ваговим зйомом металу і якісно за шорсткістю оброблюваної поверхні. Вказано, що визначальним фактором при цьому є швидкість осциляційного руху гранул і деталей, різниця яких представляє швидкість вібраційної обробки, яка залежить від швидкості осциляційного руху середовища. Відзначено, що підвищення продуктивності процесу слід шляхом збільшення частоти та амплітуди коливань резервуара збільшити швидкість руху середовища. Розглянуто пошарову передачу силового імпульсу від днища резервуара до насипного середовища. Вказано фізичне значення підвищення продуктивності шляхом збільшення амплітуди коливань резервуара. Вказано умови отримання зйому металу, що забезпечують підвищені зусилля взаємодії гранул з деталями на високих швидкостях мікрорізання. Описано проведення експериментальних досліджень щодо визначення впливу амплітуди та частоти коливань на результати вібраційної оздоблювально-зачищувальної обробки. Отримано графічні залежності зйому металу при різному співвідношенні ваги зразка до ваги гранули середовища. Аналогічним чином отримана залежність зйому металу від коефіцієнта еліпсності та амплітуди коливань резервуара. Зазначено, що вертикальна складова амплітуди при площинних коливаннях резервуара є визначальним фактором комплексного впливу параметрів коефіцієнта еліпсності траєкторії руху резервуара та його амплітуди коливань. Встановлено, що при використанні крупнозернистого абразиву проникнення зерен у метал деталі відбувається на велику глибину та видаляється більша металева стружка з великим зйомом металу. При малій зернистості абразиву відбувається видалення дрібної стружки з малим зйомом металу та зменшенням висоти мікронерівностей.*

Ключові слова: *вібраційна обробка; технологічні можливості; інтенсивність та якість; амплітуда та частота коливань; траєкторія руху резервуара; зйом металу; коефіцієнт еліпсності; зернистість матеріалу середовища.*

UDC 620.179.112 **doi: 10.20998/2078-7405.2023.98.05**

V. Molnar, Miskolc, Hungary

ANALYZING SURFACE INTEGRITY ELEMENTS OF HARD TURNED 16MNCR5 STEEL

Abstract. *Surface integrity plays a determinant role in the functional requirement of precision machined parts. In the automotive industry billions of components are manufactured by using case hardened steels. In this study some surface integrity elements, such as surface roughness or residual stress are analyzed based on systematic machining experimental plan to optimize the applied cutting parameters. Recommendations are made for these parameters based on the measurement data and some widely used functional requirements.*
Keywords: *hard turning; surface integrity; design of experiment.*

1. INTRODUCTION

Case hardened materials are widely used in precision machined industrial components where surface layers must fulfill certain functional requirements in their operating time, such as wear-resistance or high fatigue strength [1]. These components are mainly shafts of disc-shaped elements, e.g., bearings or gears. 16MnCr5 is a widely used low-carbon content steel which is applicable for case hardening. To ensure the required accuracy and surface quality, the hardened surfaces (55-65 HRC) can be machined by hard cutting or grinding [2, 3]. The applied machining procedure determines the surface topography among other surface integrity elements [4]. If a random surface is not needed, hard turning is a suitable option for machining cylindrical components [5].

Maximum height (S_z) of the surface topography is a height parameter that provides a simple piece of information about how rough a surface is. In calculating the theoretical value of the maximum height, cutting data are used [6]. The arithmetical mean height (S_a) provides the same information, but its use is more widespread in part drawings. The importance of these parameters is that they are directly or indirectly connected with several mechanical and material-related characteristics of the surface, e.g., fatigue life [7]. Another two parameters are the maximum peak height (S_p) and maximum pit height (S_v). The former is related to lubricant-retention ability and, through micro-crack propagation, with fatigue strength [8, 9]. The latter provides information about the load-bearing capacity and wear resistance of a surface. The higher-order moments of the height are skewness (S_{sk}) and kurtosis (S_{ku}). A surface that is more filled in the peak zone has negative skewness, which results in a higher load-bearing capacity and a lower extent of wear [10, 11]. A kurtosis higher than 3 indicates that fewer peaks and valleys are located on the surface [12].

The fewer peaks leads to less debris formation during operation and better wear resistance [13].

Residual stress is another determining factor of surface integrity. Due to the case hardening process, an initial residual stress can be observed in the surface layer; however, the machining procedure results generally in a higher extent of it than the initial value [14]. By hard turning, basically compressive residual stress is evolved, which is useful in cases when e.g., the risk of fatigue or corrosion is recommended to be minimized [15]. The reason for the relatively high compressive residual stress is that in hard turning the cutting tool has a negative rake angle [16] and therefore high radial-direction (passive) force arises during the material removal process.

In this paper the functionality of hardened surfaces is in focus. Based on a design of experiment, hard machining experiments and measurements have been carried out to determine the cutting parameter values that fulfill the following functionality requirements: reduction in S_a, S_z, and S_v increases the fatigue life; reduction in S_p and S_{sk} and increase in S_{ku} improves the wear resistance. At the same time, increase in the cutting and passive force components, and therefore, increase in the compressive residual stress state (-σ), results in increased fatigue strength.

The novelty and contribution of the study is that it provides information for cutting parameter selection when functionality-related surface integrity aspects (residual stress, roughness) must be considered in designing the hard turning procedure for 16MnCr5 case hardened steel in the case of external cylindrical surfaces.

2. METHODS OF THE EXPERIMENT AND MEASURMENTS

Hard turning (dry machining) experiments were carried out to analyze surface roughness, cutting force and residual stress values of the machined surfaces. The machine tool was a hard machining center: EMAG VSC 400 DDS. The applied insert was 4NC-CNGA 120408 coated CBN and the tool holder was PCLNR 2020-K12. The material was 16MnCr5 (HRC 60–63), the diameter and the length of the machined workpieces were 60 mm and 13 mm, respectively. The analyzed cutting parameter values were selected based on the recommendation of the tool manufacturer. The minimum and the maximum values of the three cutting data were varied in the experiment, which resulted in eight setups.

- Depth-of-cut (a_p): 0.05 and 0.35 mm
- Cutting speed (v_c): 120 and 240 m/min
- Feed rate (f): 0.04 and 0.2 mm/rev

The effects of the medium values of these parameters were also analyzed: a_p = 0.2 mm; v_c = 180 m/min and f = 0.12 mm/rev.

For the force measurement a Kistler dynamometer type 9257A was used (5000 sample/sec). For the 3*D* roughness measurement an Altisurf 520 machine with an optical sensor type CL2 was used. The evaluation area of the surface was 2 × 2 mm, the cut-off length was 0.08 or 0.8 mm based on the periodicity of the topography, the resolution in x and y directions was 1 μm and in z direction 0.012 μm, the measurement range in z direction was 0–300 μm. For the residual stress measurement a Stresstech type G3R *X*-ray diffractometer was used, the source was Cr *X*-ray.

3. RESULTS

In the following figures the analyzed parameter values are designated by dots. These values show quite well-separable levels for the two considered feed rates. The parameter values that belong to the minimum (0.04 mm/rev) and the maximum (0.2 mm/rev) feed rates are designated by black and gray dots, respectively.

The maximum height and arithmetical mean height of the surface should be decreased when lower fatigue strength is required from the precision machined surface. The S_z values of the surfaces machined at the 0.04 mm/rev feed rate are between 0.49 and 0.70 μm, and those machined at 0.2 mm/rev are between 4.57 and 5.51 μm. The relative deviations of these two groups are 15% and 10%, respectively (Fig. 1a). The S_a values of the surfaces machined by 0.04 mm/rev feed rate are between 0.08 and 0.10 μm, and those machined by 0.2 mm/rev are between 1.07 and 0.33 μm. The relative deviation of each group is 11% (Fig. 1b).

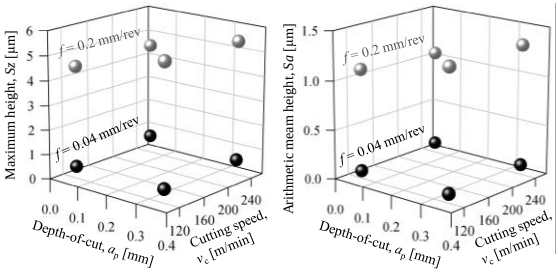

a) b)

Figure 1 – The S_z (a) and S_a (b) parameter values of the machined surfaces

The maximum peak height (S_p) and the maximum pit height (S_v) provide information about several tribological characteristics of a surface. If the peak zone is relatively high, and includes thin peaks, they wear relatively fast, which results in debris that influences the surface. If the peak zone is low, it indicates that the

surface is quite filled, i.e. the load-bearing capacity and the wear resistance of the surface is high. On the other hand, the valleys of the surface are useful from a lubricating point of view, i.e. the valleys are able to retain lubricating fluid, but they can also be the initiation places of micro-cracks. In this study the wear resistance and fatigue strength are in focus, therefore the minimization of these two parameters is the aim. The S_p values of the surfaces machined at the 0.04 mm/rev feed rate are between 0.22 and 0.33 µm, and those machined at 0.2 mm/rev are between 2.82 and 3.29 µm. The relative deviations of these two groups are 17% and 8%, respectively (Fig. 2a). The *Sv* values of the surfaces machined at 0.04 mm/rev feed rate are between 0.27 and 0.37 µm, and those machined at 0.2 mm/rev are between 1.67 and 2.23 µm. The relative deviation of each group is 15% (Fig. 2b).

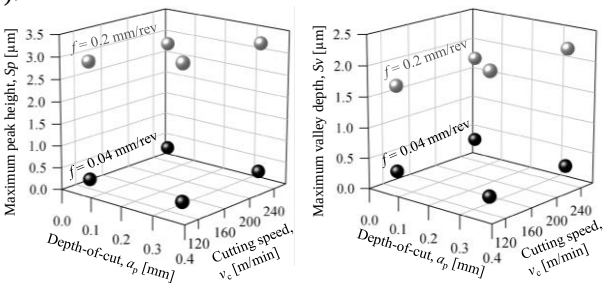

a) b)

Figure 2 – The S_p (a) and S_v (b) parameter values of the machined surfaces

A surface with negative S_{sk} and relatively high S_{ku} (>3) is asymmetric, filled, and among other characteristics, wear-resistant. In the present study these requirements are fulfilled in some cutting parameter combinations.

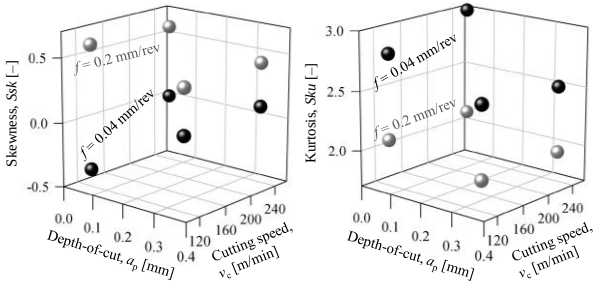

a) b)

Figure 3 – The S_{sk} (a) and S_{ku} (b) parameter values of the machined surfaces

The S_{sk} values of the surfaces machined at the 0.04 mm/rev feed rate are between -0.37 and 0.10, and those machined at 0.2 mm/rev are between 0.43 and 0.60 (Fig. 3a). The S_{ku} values of the surfaces machined at the 0.04 mm/rev feed rate are between 2.51 and 3.01, and those machined at 0.2 mm/rev are between 1.95 and 2.12 (Fig. 3b). These results show that the lower feed rate results in favorable skewness and kurtosis values.

The cutting force components determine the stress state of a machined surface. Here the F_c cutting force and the F_p passive force are analyzed. The hard turned surfaces typically show high compressive residual stress, which is useful in the fatigue life of the components. The F_c values of the surfaces machined at the 0.04 mm/rev feed rate are between 34 and 79 N, and those machined at 0.2 mm/rev are between 87 and 248 N. The relative deviations of these two groups are relatively high: 43% and 52%, respectively (Fig. 4a). The F_p values of the surfaces machined at the 0.04 mm/rev feed rate are between 35 and 106 N, and those machined at 0.2 mm/rev are between 72 and 230 N. The relative deviations of these two groups are 53% and 56%, respectively (Fig. 4b). It has to be noted that the higher force results in favorable residual stress, and the reason for a higher force value is the more intense cutting parameters (e.g. higher cutting speed of depth-of-cut), which results in higher material removal efficiency. However, the material removal process characterized by the increased force requires higher energy consumption by the machine tool.

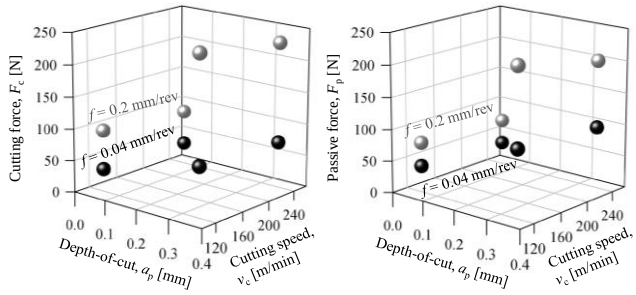

a) b)

Figure 4 – The F_c (a) and F_p (b) parameter values of the machined surfaces

The two components of residual stress are the axial and tangential. They have significance in hard turning operations. To decide which component plays a determinant role in the component, the main direction of load that affects the component has to be known. In the present experiment, the axial residual stress values were favorable at the 0.04 mm/rev feed rate, and the tangential residual

stress values at 0.2 mm/rev. The σ_A values of the surfaces machined at the 0.04 mm/rev feed rate are between -459 and -566 MPa, and those machined at 0.2 mm/rev are between -130 and -365 MPa. The relative deviations of these two groups are 9% and 43%, respectively (Fig. 5a). The σ_T values of the surfaces machined at the 0.04 mm/rev feed rate are between -235 and -535 MPa, and those machined at 0.2 mm/rev are between -706 and -816 MPa. The relative deviations of these two groups are 34% and 7%, respectively (Fig. 5b).

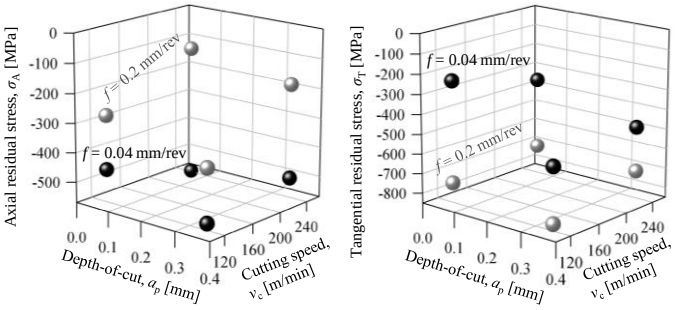

a) b)

Figure 5 – The σ_A (a) and σ_T (b) parameter values of the machined surfaces

4. DISCUSSION

Not only the possible minimal (a_p = 0.05 mm; v_c = 120 m/min; f = 0.04 mm/rev) and maximal (a_p = 0.35 mm; v_c = 240 m/min; f = 0.2 mm/rev) values of the cutting parameters were set in the experiments but also the medium values (a_p = 0.2 mm; v_c = 180 m/min; f = 0.12 mm/rev). The extra data can provide information for the technologist in the data selection, because not only surface integrity-related factors but economic, efficiency or energy consumption factors should also be considered in technology planning.

The most favorable (best) S_z, S_a, S_p and S_v values were obtained by setting all three cutting parameters at their minimum values (min). The least favorable (worst) values of these parameters were obtained at minimum cutting speed and maximum (max) depth-of-cut and feed rate values (Figs. 6 and 7). The medium value is 43% and the most favorable is 9% of the least favorable value of S_z. These values in the case of S_a are 43% and 6%, respectively. The medium value is 44% and the most favorable is the 7% of the least favorable value of S_p. These values in the case of S_v are 43% and 12%, respectively. When minimization of these roughness parameters is aimed for, it is recommended to choose the minimum values of the cutting data.

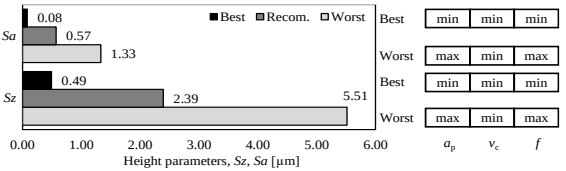

Figure 6 – The best and the worst S_z and S_a values
and their cutting parameter combinations

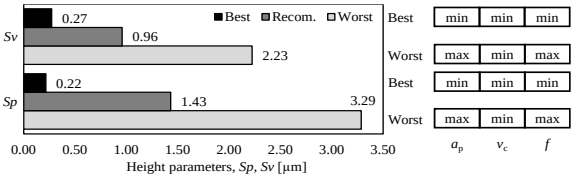

Figure 7 – The best and the worst S_p and S_v values
and their cutting parameter combinations

The most favorable value of the S_{sk} parameter was obtained at the minimum levels of all the three cutting parameters (Fig 8).

Figure 8 – The best and the worst S_{sk} and S_{ku} values
and their cutting parameter combinations

The relatively low cutting speed and feed rate supports the cutting edge (with negative rake angle) in burnishing the surface. The medium and the less favorable values are relatively close to each other, but the peak zones of the connecting surfaces are less filled, which results in poorer tribological characteristics. The most favorable value of the S_{ku} parameter was obtained at the minimum levels of the depth-of-cut and feed rate and the maximum level of the cutting speed (Fig 8). The other two S_{ku} values are close to each other and result in relatively poor tribological characteristics.

In Fig. 9 the F_c and F_p force components are demonstrated. The most favorable values were obtained at minimum depth-of-cut and feed rate and maximum cutting speed, if minimization (e.g. energy efficiency) is specified. The

medium value of the F_c is 38%, the most favorable value is 14% of the least favorable one. The medium value of the F_p is 51%, the most favorable value is 15% of the least favorable one. However, if the high values are considered favorable (residual stress, and therefore fatigue strength improvement), the recommended cutting data values are the opposite: depth-of-cut and feed rate at maximum and cutting speed at minimum level.

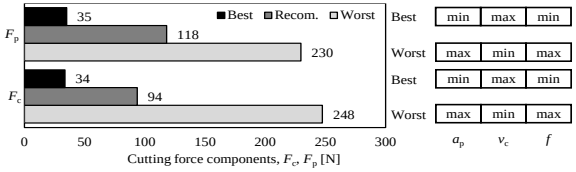

Figure 9 – The best and the worst F_c and F_p values and their cutting parameter combinations

Concerning the residual stress values (Fig. 10), their high negative values are favorable when fatigue strength and wear must be minimized. For the σ_T tangential residual stress, the most favorable value was obtained when the depth-of-cut and the feed rate were set to their maximum values, while the cutting speed was minimal. The highest values of the cutting force components F_c and F_p were obtained at this cutting parameter combination. The most favorable value for the σ_A axial residual stress was obtained when the F_c and F_p values were the lowest. The corresponding cutting parameter combination is the minimal depth-of-cut and feed rate and maximum cutting speed. It was observed that the lower feed rate whose direction is axial supports the higher compressive residual stress. The reason for that is that the tool moves more slowly and spends more time in one place, meanwhile loading the surface. In the case of the tangential residual stress, the same is observed in the perpendicular direction: the tangential direction cutting speed is relatively low, which increases the tangential residual stress value. The medium value of the axial residual stress is 2.3 times and the most favorable is 4.4 times better than the least favorable. The medium value of the axial residual stress is 2.5 times and the most favorable is 3.5 times better than the least favorable.

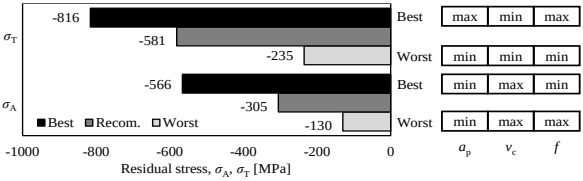

Figure 10 –The best and the worst σ_A and σ_T values
and their cutting parameter combinations

5. SUMMARY AND CONCLUSIONS

In this paper well-known surface roughness parameters (S_z, S_a, S_p, S_v, S_{sk} and S_{ku}), two cutting force components (F_c and F_p) and two residual stress components (σ_A and σ_T) were analyzed. They are determinant indicators for some surface integrity characteristics, such as wear resistance, fatigue strength or load-bearing capacity. Depending on the function of the surfaces of machine components or other (e.g., economic) purposes, these parameters can be minimized or maximized. This study focused on how this optimization can be carried out by varying the cutting parameter values. The following findings were made.

- To minimize the parameter values of maximum height (S_z), arithmetical mean height (S_a), maximum peak height (S_p), maximum pit height (S_v) and skewness (S_{sk}), it is recommended to set the depth-of-cut (a_p), cutting speed (v_c) and feed rate (f) to their minimum values.
- To maximize the kurtosis (S_{ku}) parameter value, maximum v_c and minimum a_p and f are recommended.
- The F_c (cutting speed direction) and F_p (depth-of-cut direction) cutting force components reach their maximum values at maximum a_p and f levels.
- The highest compressive axial residual stress can be reached at minimum a_p and f and maximum v_c. The highest compressive tangential residual stress can be reached at maximum a_p and f and minimum v_c.

These findings are valid for hard turning by the applied CBN insert (4NC-CNGA 120408) in the investiaged cutting parameter ranges (a_p = 0.05–0.35 mm; v_c = 120–240 m/min; f = 0.04–0.2 mm/rev), and for the applied material (16MnCr5). The limitation of the study is that only the maximum and minimum cutting parameter values were considered. The experiments are recommended to be extended to other insert geometries and material grades.

References: 1. *Grzesik, W., Zak, K., Kiszka, P.:* Comparison of Surface Textures Generated in Hard Turning and Grinding Operations, Procedia CIRP 13, pp. 84–89, 2014. **2.** *Chumak, A., Klimenko, S., Klimenko, S., Manokhin, A., Naydenko, A., Kopeikina, M., Burikin, V., Bondarenko, M., Burlakov, V.:* Finish Machining of the Cutting Inserts from Cubic Borine Nitride Bl Group Composite, Cutting & Tools in Technological System 94, pp. 102-114, 2021. **3.** *Mamalis, A.G., Kundrak, J., Horvath, M.:* On a Novel Tool Life Relation for Precision Cutting Tools, Journal of Manufacturing Science and Engineering 127(2), pp. 328–332, 2005. **4.** *Sztankovics, I., Kundrak, J.:* Theoretical Value and Experimental Study of Arithmetic Mean Deviation in Rotational Turning, Cutting & Tools in Technological System 96, pp. 73-81, 2022. **5.** *Kundrak, J.:* Alternative Machining Procedures of Hardened Steels, Manufacturing Technology 11, pp. 32–39, 2011. **6.** *Lavrinenko, V., Solod, V.:* The Ralationship between the Parameters of Roughness and Features of Surface Formation with a Special Microprofile, Cutting & Tools in Technological System 96, pp. 99–109, 2022. **7.** *Balanou, M., Papazoglou, L.-E., Markopoulos, A.P., Karmiris-Obratanski, P.:* Experimental Investigation of Surface

Topography of Al7075-T6 Alloy Machined by EDM, Cutting & Tools in Technological System 94, pp. 3–10, 2021. **8.** *Zhao, B., Song, J., Xie, L., Hu, Z., Chen, J.:* Surface Roughness Effect on Fatigue Strength of Aluminum Alloy Using Revised Stress Field Intensity Approach, Scientific Reports 11, paper 19279, 2021. **9.** *Xiao, W.L., Chen, H.B., Yin, Y.:* Effects of Surface Roughness on the Fatigue Life of Alloy Steel, Key Engineering Materials 525–526, pp. 417–420, 2013. **10.** *Flack, K.A.; Schultz, M.P.; Barros, J.M.:* Skin Friction Measurements of Systematically-Varied roughness: Probing the Role of Roughness Amplitude and Skewness, Flow, Turbulence and Combustion 104, pp. 317–329, 2020. **11.** *Sedlacek, M., Gregorcic, P., Podgornik, B.:* Use of the Roughness Parameters Ssk and Sku to Control Friction—A Method for Designing Surface Texturing, Tribology Transactions 60, pp. 260–266, 2016. **12.** *Nagy, A.:* Investigation of the Effect of Areal Roughness Measurement Length on Face Milled Surface Topographies, Cutting & Tools in Technological System 94, pp. 60–69, 2021. **13.** *Maruda, R.W., Krolczyk, G.M., Wojciechowski, S., Powalka, B., Klos, S., Szczotkarz, N., Matuszak, M., Khanna, N.:* Evaluation of Turning with Different Cooling-Lubricating Techniques in terms of Surface Integrity and Tribologic Properties, Tribology International 148, paper 106334, 2020. **14.** *Jouini, N., Revel, P., Thoquenne, G.:* Influence of Surface Integrity on Fatigue Life of Bearing Rings Finished by Precision Hard Turning and Grinding, Journal of Manufacturing Processes 57, pp. 444–451, 2020. **15.** *Zaghal, J., Mertinger, V., Filep, A., Benke, M.:* Characterization of Residual Stress State after Turning of Bearing Rings, Doktorandusz Almanach 1, pp. 313–318, 2022. **16**. *Manovytskyi, O., Klymenko, S., Burykin, V.:* Calculation of Shear Angle when Cutting with a Tool of a Negative Rake Angle, Cutting & Tools in Technological System 97, pp. 59–69, 2022.

Віктор Мольнар, Мішкольц, Угорщина

АНАЛІЗ ЦІЛІСНОСТІ ПОВЕРХНІ ЕЛЕМЕНТІВ ЗІ СТАЛІ 16MNCR5 ПІСЛЯ ТОЧІННЯ

Анотація. *Цілісність поверхні відіграє вирішальну роль у функціональних вимогах до деталей, оброблених на верстаті. В автомобільній промисловості мільярди компонентів виготовляються з використанням загартованої сталі. У цьому дослідженні деякі елементи цілісності поверхні, такі як шорсткість поверхні або залишкові напруження, аналізуються на основі експериментального плану систематичної обробки для оптимізації застосовуваних параметрів різання. Для цих параметрів розроблені рекомендації на основі даних вимірювань і деяких широко використовуваних функціональних вимог. У цій статті були проаналізовані добре відомі параметри шорсткості поверхні (S_z, S_a, S_p, S_v, S_{sk} і S_{ku}), два компоненти сили різання (F_c і F_p) і два компоненти залишкових напружень (σ_A і σ_T). Вони є визначальними показниками для деяких характеристик цілісності поверхні, таких як зносостійкість, втомна міцність або несуча здатність. Залежно від функції поверхонь деталей машини або інших (наприклад, економічних) цілей ці параметри можна мінімізувати або максимізувати. Це дослідження були зосереджені на тому, як цю оптимізацію можна здійснити шляхом зміни значень параметрів різання. Були зроблені такі висновки. Для мінімізації значень параметрів максимальної висоти (S_z), середньої арифметичної висоти (S_a), максимальної висоти піку (S_p), максимальної висоти ями (S_v) і перекосу (S_{sk}), рекомендується встановити глибину різання (a_p), швидкість різання (v_c) і швидкість подачі (f) до їх мінімальних значень. Для максимізації значення параметра ексцесу (S_{ku}) рекомендується максимальна v_c і мінімальні a_p і f. Компоненти сили різання F_c (напрямок швидкості різання) і F_p (напрямок глибини різання) досягають своїх максимальних значень на максимальних рівнях a_p і f. Найвищі осьові залишкові напруження стиску можуть бути досягнуті при мінімумах a_p і f і максимумі v_c. Найвище тангенціальне залишкове напруження стиску може бути досягнуто при максимальних a_p і f і мінімальних v_c.*

Ключові слова: *жорстке точіння; цілісність поверхні; план експерименту.*

UDC 621.9.01 **doi: 10.20998/2078-7405.2023.98.06**

F. Novikov, Kharkiv, Ukraine

OPTIMISATION OF INTERRUPTED GRINDING PARAMETERS ACCORDING TO THE TEMPERATURE CRITERION

Abstract. *In the paper analytical optimization of discontinuous grinding parameters according to temperature criterion is carried out and on its basis conditions for significant reduction of cutting temperature, which consist mainly in increasing the number of contacts of working ledges of discontinuous wheel with fixed cross-section of machined workpiece, are determined. It is established by calculations that providing 20 contacts the cutting temperature may be reduced up to 3 times in comparison with the conventional grinding by a continuous wheel. This is achieved in the conditions of deep interrupted grinding with relatively low workpiece speed, as in the conditions of traditionally used multipass interrupted grinding not more than 6 contacts of working ledges of an interrupted wheel with the fixed cross-section of the workpiece are realized and the cutting temperature is reduced only in the range of 50 %. It is established by calculations that the minimum of cutting temperature at discontinuous grinding is achieved under conditions of equality of lengths of the working shoulder and the notch on the discontinuous grinding wheel and their reduction. It is also established that excess of the length of the working ledge over the length of the notch of the discontinuous wheel leads to insignificant increase of the cutting temperature. This reduces the wear of the discontinuous wheel and increases the machining capacity without actually increasing the cutting temperature. The paper shows that the obtained theoretical solutions are a necessary condition for ensuring a significant reduction of cutting temperature in discontinuous grinding. A sufficient condition should be considered as complete or partial cooling of grinding zone between contacts of machined workpiece with working jaws of discontinuous grinding wheel by intensive supply of effective technological media into the grinding zone.*
Keywords: *cutting force; machining quality; working ledge of wheel; adiabatic bar; process medium; cutting ability of wheel.*

Introduction. Interrupted grinding is one of the most efficient methods of finishing abrasives which ensures high quality machined surfaces and prevents the formation of burn marks and other temperature defects. The main effect of interrupted grinding is a reduction in cutting temperature without sacrificing productivity. This is due to shock-cyclic interaction of the working ledges of discontinuous wheel with the workpiece, which allows, firstly, to maintain high cutting ability of discontinuous wheel in the process of grinding and, secondly, provides partial cooling of the machined surface in the period of passing over the cutting zone of discontinuous wheel notch. As Professor Yakimov A. V. in work [1], such double machining effect is inherent only in the method of discontinuous grinding, as it is impossible to achieve in conditions of conventional grinding with a continuous wheel.

The method of interrupted grinding is widely used for machining products made of various hard metal and non-metal materials, especially when machining critical parts of aircraft technology [2] in finish grinding operations that require

high quality machining. Thanks to its application, it is possible to reduce the cutting temperature by up to 50 % compared to conventional grinding with a continuous wheel. However, more significant reductions in cutting temperatures are required for more productive grinding operations. A positive example should be considered the work [3] which experimentally substantiated the conditions of grinding temperature reduction below the critical value during productive machining of titanium alloy Ti-6Al-4V with a special segmented wheel. In works [4, 5] technological possibilities of reduction of force and temperature of cutting, increase of productivity of processing of products from ceramic SiC at intermittent grinding by a segment wheel of special design T-Tool are also proved. Thus, it is established that the use of special designs of discontinuous wheels can reduce the cutting temperature. However, it is difficult to solve the problem of theoretically determining the conditions for significant reduction of cutting temperature during discontinuous grinding.

The most rigorous mathematical models for determining the cutting temperature in intermittent grinding have been developed by Yakimov A. V. [2] and Sizyy Yu. A. [6] on the basis of solving the differential equation of heat conduction of materials for various initial and boundary conditions taking into account the main regularities of the grinding process. It is theoretically established that due to periodical interruption of grinding process, contact time of working shoulder of discontinuous wheel with workpiece is much less than contact time of continuous wheel with workpiece. This, in fact, makes it possible to reduce the cutting temperature in discontinuous grinding. But the condition of additional removal by working ledge of discontinuous circle of layer of machined material, not removed for the period of grinding area passage by cutout of discontinuous circle, as a result of which actual material removal and cutting force at the moment of contact of working ledge of discontinuous circle with workpiece are increased and result in increase of cutting temperature. Similar theoretical solutions are given in [7, 8]. It follows from this that the process of discontinuous grinding is subject to more complex physical laws, which limit the possibility of more significant reduction of cutting temperature and increase productivity and quality of machining.

Further development of mathematical models of thermal processes in discontinuous grinding are the works [9, 10]. They give theoretical solutions for justification of cutting temperature reduction conditions for various grinding conditions, including the use of effective technological media and highly porous wheels, impregnation technology of discontinuous wheels. Calculation of lengths of working protrusions and troughs of discontinuous grinding wheels has been made [11]. However, it is rather difficult to use these solutions for optimisation calculations of discontinuous grinding parameters according to the temperature criterion because they are derived from the solution of differential equation of

thermal conductivity of materials and are represented by complex mathematical dependences requiring numerical calculations. At the same time, in [12] it has been theoretically and experimentally quite unambiguously established that a significant reduction of cutting temperature in flat interrupted grinding can be achieved by increasing the number of thermal pulses in the grinding zone. This opens up new technological possibilities for determining the conditions for significant reduction of cutting temperature in discontinuous grinding. Therefore, in works [13, 14], the scientific prerequisites of this provision are substantiated.

For their further development it is necessary to carry out optimization of interrupted grinding parameters according to the temperature criterion on the basis of application of new mathematical approaches to calculation of cutting temperature. The aim of the work is theoretical determination of optimum conditions of interrupted grinding taking into account possibility of significant reduction of cutting temperature and development of practical recommendations on creation of highly efficient interrupted grinding processes

Research methodology. The theoretical approach proposed in [1, 15] was used to achieve this objective. Its essence is to determine the cutting temperature when grinding based on the conditions of interrupted circle cutting adiabatic rods, which conventionally represent the removed allowance of the workpiece (Fig. 1)

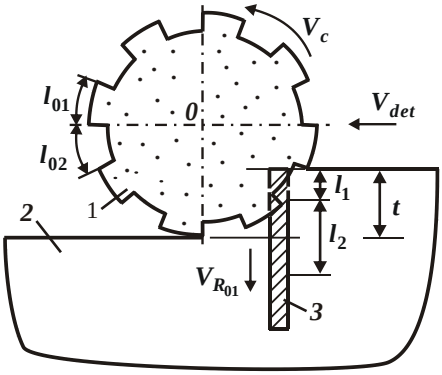

Figur 1 – Cutting temperature design for surface grinding, taking into account the cutting around adiabatic rods, the set of which represents a removable allowance: 1 - grinding wheel; 2 - processed material; 3 - adiabatic rod (l_1 is the length of the cut part of the adiabatic rod; l_2 is the depth of heat penetration into the surface layer of the workpiece; l_{01} is the length of the working protrusion of the intermittent circle; l_{02} is the length of the notch on the interrupted circle; V_c is the speed of the circle; V_{det} is the speed of the part; t – grinding depth)

Based on Fig. 1, the condition of continuity of the cut of an adiabatic rod of length h of time $(\tau_{01} + \tau_{02})$ determined by the dependency:

$$h = V_R \cdot (\tau_{01} + \tau_{02}) = V_{R_{01}} \cdot \tau_{01}, \quad (1)$$

where $V_R = V_{det} \cdot \sqrt{0{,}5 \cdot t / R_c}$ is the cutting speed of the adiabatic rod in a continuous circle, m/s; t – grinding depth, m; R_c – circle radius, m; $V_{R_{01}}$ is the speed of cutting the adiabatic rod by the working ledge of the discontinuous circle, m/s; $\tau_{01} = l_{01} / V_c$ is the time for the working protrusion (length l_{01}) to pass through the intermittent circle of the grinding zone, s; $\tau_{02} = l_{02} / V_c$ is the time of passing through the cutout (length l_{02}) of the discontinuous circle of the grinding zone, s.

From dependence (1) obtained:

$$V_{R_{01}} = V_R \cdot \left(1 + \frac{\tau_{02}}{\tau_{01}}\right). \quad (2)$$

As you can see, the speed $V_{R_{01}}$ is always greater than the speed V_R. Under the condition τ_{02} = 0, i.e. when grinding with a solid circle, these speeds are equal. As the time τ_{02} increases, the $V_{R_{01}}$ speed increases and can significantly exceed the V_R speed. Therefore, increasing the length of the notch on a discontinuous circle can lead to a significant increase in speed $V_{R_{01}}$. This is due to a decrease in the number of cutting grains on the working surface of the intermittent circle. Accordingly, the productivity of processing Q_k at the moment of contact of the working ledge of the intermittent wheel with the processed adiabatic rod will also increase due to the increase in the ratio τ_{02} / τ_{01} and will exceed the productivity of $Q = \Delta S \cdot V_R$ when grinding with a solid wheel:

$$Q_k = \Delta S \cdot V_{R_{01}} = Q \cdot \left(1 + \frac{\tau_{02}}{\tau_{01}}\right), \quad (3)$$

where ΔS is the cross-sectional area of the adiabatic rod, m^2.

In this case, the average processing performance during intermittent grinding will remain the same as when grinding with a solid circle, i.e. equal to $Q = \Delta S \cdot V_R$.

Let us establish the patterns of change in the cutting force and temperature during grinding, with continuous and intermittent circles. The tangential P_z and

radial P_y components of the cutting force when grinding with a solid circle, as shown in the work [15], are described by analytical dependencies:

$$P_z = \sigma \cdot \frac{Q}{V_c}; \tag{4}$$

$$P_y = \frac{\sigma}{K} \cdot \frac{Q}{V_c}, \tag{5}$$

where σ is the conditional cutting stress, N/m^2; V_c – wheel speed, m/s; $K = P_z / P_y$ – grinding coefficient.

In intermittent grinding, dependences (4) and (5), taking into account dependence (3), take the form:

$$P_z = \sigma \cdot \frac{Q_k}{V_c} = \sigma \cdot \frac{\Delta S \cdot V_R}{V_c} \cdot \left(1 + \frac{\tau_{02}}{\tau_{01}}\right); \tag{6}$$

$$P_y = \frac{\sigma}{K} \cdot \frac{Q_k}{V_c} = \frac{\sigma}{K} \cdot \frac{\Delta S \cdot V_R}{V_c} \cdot \left(1 + \frac{\tau_{02}}{\tau_{01}}\right). \tag{7}$$

As can be seen, the tangential P_z and radial P_y components of the cutting force during intermittent grinding for the given values σ, K, ΔS, V_R and V_c are greater than when grinding with a solid wheel. This is because the $(1 + \tau_{02} / \tau_{01}) > 1$ multiplier, i.e. the longer the time τ_{02}, the greater the cutting force components P_z and P_y.

However, as established experimentally in the works of A. V. Yakimov [1, 2], the conditional cutting stress σ is less, and the grinding coefficient $K = P_z / P_y$ is greater for interrupted grinding. This is due to the fact that the intermittent circle, as a result of shock-cyclic interaction with the workpiece during the grinding process, actually operates in the continuous intensive dressing mode and constantly maintains high cutting ability, while the solid circle loses the cutting ability over time. Thus, it has been experimentally established that under conditions of intermittent grinding, abrasive wheels of increased hardness are operable, which, during normal grinding, quickly become dull and lose their cutting ability. In this case, the intensity of friction of the discontinuous circle with the material being processed is significantly reduced, i.e. in the process of intermittent grinding, the energy expended on the cutting process and the removal of the material being processed predominate.

The cutting temperature during grinding with a solid wheel in the first approximation is determined by the analytical dependence [15]:

$$\theta = \frac{q \cdot l_2}{\lambda}, \tag{8}$$

where $q = N / \Delta S$ is the heat flux density, W/m^2; $N = P_z \cdot V_c$ – grinding power, W; $l_2 = \sqrt{2a \cdot \tau}$ is the depth of heat penetration into the surface layer of the workpiece, m; a is the coefficient of thermal diffusivity of the processed material, m^2/s; τ is the contact time of the solid grinding wheel with the material being processed, s; λ is the thermal conductivity coefficient of the processed material, W/(m·deg.).

Taking into account dependence (4), dependence (8) takes the form:

$$\theta = \frac{\sigma \cdot Q \cdot \sqrt{2a \cdot \tau}}{\lambda \cdot \Delta S} = \frac{\sigma \cdot V_R \cdot \sqrt{2a \cdot \tau}}{\lambda}. \tag{9}$$

As follows from dependence (9), the main condition for reducing the cutting temperature θ is to reduce the conditional cutting stress σ by providing a high cutting ability of the grinding wheel. An important factor should also be considered to reduce the contact time τ of the grinding wheel with the material being processed. This is achieved, as a rule, by using a multi-pass grinding scheme, characterized by a small grinding depth and an increased speed of the part.

In intermittent grinding during one contact of the working ledge of the intermittent wheel with the material being machined, the cutting temperature is described by the dependence:

$$\theta = \frac{\sigma \cdot V_R}{\lambda} \cdot \left(1 + \frac{\tau_{02}}{\tau_{01}}\right) \cdot \sqrt{2 \cdot a \cdot \tau_{01}}. \tag{10}$$

For a generalized analysis of dependence (10), we represent it in the form:

$$\theta = \frac{\sigma \cdot V_R}{\lambda} \cdot \left(1 + \frac{\tau_{02}}{\tau_{01}}\right) \cdot \sqrt{2 \cdot a \cdot \frac{\tau_{01}}{\tau_{02}} \cdot \tau_{02}}. \tag{11}$$

The ratio τ_{01} / τ_{02} has an ambiguous effect on the cutting temperature θ. In table. 1 and in fig. 2 shows the nature of the change in the dimensionless variable $\alpha = \left(1 + \tau_{02} / \tau_{01}\right) \cdot \sqrt{\tau_{01} / \tau_{02}}$, included in dependence (11), with a change in the ratio τ_{01} / τ_{02}.

Table 1 – Calculated values of the dimensionless value α and the length of the working protrusion l_{01} of a broken circle for l_{02} = 10 mm

τ_{01}/τ_{02}	0	0,25	0,5	1,0	2	3	4	5	6
α	∞	2,5	2,12	2,0	2,12	2,31	2,5	2,68	2,86
l_{01}, mm	0	2,5	5	10	20	30	40	50	60

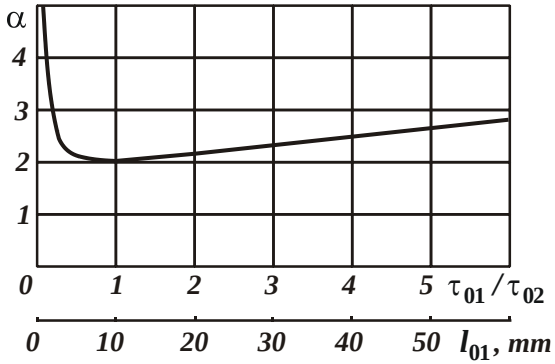

Figure 2 – Dependence of the dimensionless value α of the ratio τ_{01}/τ_{02} and the length of the working protrusion l_{01} of a broken circle: l_{02} = 10 mm

As you can see, the dimensionless value α passes the minimum point at the value of $\tau_{01}/\tau_{02}=1$. Therefore, there is a minimum of the cutting temperature θ under the condition $\tau_{01}/\tau_{02}=1$, i.e. provided $l_{01}=l_{02}$. In this case, an increase in the ratio τ_{01}/τ_{02} in the range $\tau_{01}/\tau_{02}>1$ leads to an insignificant increase in the dimensionless value α and, accordingly, the cutting temperature θ. So, with an increase in the ratio τ_{01}/τ_{02} of 2 times, the value α increased by only 6%, and with an increase in the ratio τ_{01}/τ_{02} by 6 times, by 43% (Table 1). This indicates the possibility of using intermittent circles that have $l_{01}>l_{02}$, which is the case in practice. As shown in [2], at such values of the ratio $l_{01}/l_{02}>1$, the wear intensity of the discontinuous wheel decreases and the grinding efficiency increases without increasing the cutting temperature.

In table. 1 and in fig. 2 shows the calculated values of the length of the working protrusion l_{01} of the intermittent circle, obtained based on the dependence $\tau_{01} / \tau_{02} = l_{01} / l_{02}$ for the given values of the ratio τ_{01} / τ_{02} and the length of the cutout on the intermittent circle l_{02} = 10 mm. Calculations have established that with an increase in the ratio τ_{01} / τ_{02}, the length of the working protrusion l_{01} of the intermittent circle increases.

To analytically determine the extreme value of the ratio τ_{01} / τ_{02}, the cutting temperature θ determined by dependence (10) should be subordinated to the necessary extremum condition: $\theta'_{\tau_{01}} = 0$. The result is:

$$\frac{\tau_{01}}{\tau_{02}} = 1. \tag{12}$$

Calculations have established that the second derivative $\theta''_{\tau_{01}}$ at the extremum point $\tau_{01} = \tau_{02}$ takes a positive value. Therefore, there is a minimum of the cutting temperature θ depending on the ratio τ_{01} / τ_{02}, which corresponds to the graph shown in Fig. 2. Then the minimum cutting temperature θ_{min}, taking into account dependences (10) and (12), will be determined by the dependence:

$$\theta_{min} = \frac{2 \cdot \sigma \cdot V_R \cdot \sqrt{2a \cdot \tau_{01}}}{\lambda}. \tag{13}$$

Let us compare the values of the cutting temperature during grinding, with continuous and intermittent wheels, determined by dependences (9) and (13) for the time $\tau = \tau_{01} + \tau_{02}$, i.e. for one contact of the working ledge of a discontinuous circle with an adiabatic rod (Fig. 1). To do this, we represent dependence (9), taking into account the condition $\tau_{01} = \tau_{02}$, in the form:

$$\theta = \frac{\sigma \cdot V_R \cdot \sqrt{2a \cdot 2\tau_{01}}}{\lambda}. \tag{14}$$

From the comparison of dependencies (13) and (14) it can be seen that the cutting temperature θ when grinding with a solid wheel is 1.41 times lower than the cutting temperature when grinding with an intermittent wheel. This is because dependence (13) is valid under the condition that the material being processed is removed from its one contact with the working ledge of the discontinuous circle.

With subsequent contacts, of course, the cutting temperature θ will increase due to the accumulation of the generated heat in the adiabatic rod. However, when providing intensive cooling of the adiabatic rod, as shown in [1, 2], it is possible to completely cool it down to subsequent contact with the working ledge of the discontinuous circle. In this case, the cutting temperature θ will periodically take on a maximum value equal to θ_{min} under the condition $\tau_{01} = \tau_{02}$. Therefore, the time τ_{01} can be significantly less than the time τ of contact between the solid grinding wheel and the adiabatic rod being machined. Therefore, the minimum cutting temperature θ_{min} will be less than the cutting temperature when grinding with a solid wheel, determined by dependence (9), which creates the main effect of interrupted grinding.

To compare the cutting temperatures during grinding, with intermittent and solid wheels, determined by dependencies (9) and (13), we consider their ratio, taking into account the conditions $\tau / (\tau_{01} + \tau_{02}) = n$ and $\tau_{01} = \tau_{02}$ for the given values σ, V_R, λ, a:

$$\frac{\theta_{min}}{\theta} = 2 \cdot \sqrt{\frac{\tau_{01}}{\tau}} = \sqrt{\frac{2}{n}}, \qquad (15)$$

where n is the number of contacts of the working ledges of a discontinuous circle with an adiabatic rod (Fig. 1) until it is completely cut, i.e. for the time τ.

From dependence (15) it follows that the ratio θ_{min} / θ is quite unambiguously determined by the value n: the larger it is, the smaller the ratio θ_{min} / θ and the more efficient the use of intermittent grinding compared to conventional grinding with a solid wheel.

Research results. In table. 2 and in Fig. 3 shows the calculated values of the ratio θ_{min} / θ and the length of the working protrusion l_{01} of the intermittent circle for V_c =30 m/s and τ =10^{-2} s.

Table 2 – Calculated values of the ratio θ_{min} / θ and the length of the working ledge l_{01} of a broken circle for V_c = 30 m/s and τ = 10^{-2} s

n	2	4	6	8	10	20	40	80	160
θ_{min} / θ	1	0,7	0,58	0,5	0,447	0,316	0,22	0,158	0,11
l_{01}, mm	75	38	25	19	15	8	4	2	1

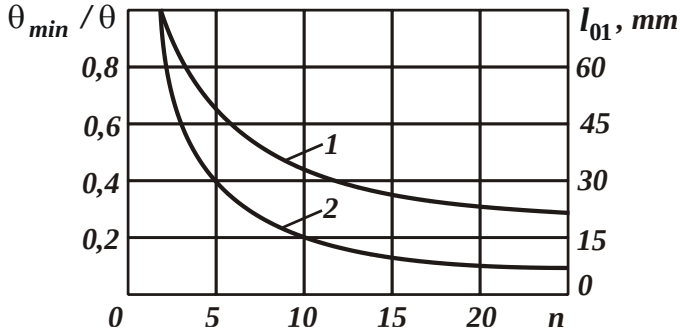

Figure 3 – Dependences of the ratio θ_{min} / θ (1) and the length of the working protrusion l_{01} (2) of the intermittent circle on the value of n: V_c =30 m/s; τ =10^{-2} s

Calculation of l_{01} values is made using dependencies: $l_{01} = \tau_{01} \cdot V_c$; $\tau / (\tau_{01} + \tau_{02}) = n$ and $\tau_{01} = \tau_{02}$. As a result, it was found $l_{01} = \tau \cdot V_c / 2n$.

The calculated value τ =10^{-2} s (Table 2) was obtained on the basis of the dependence [15]: $\tau = l / V_{det} = \sqrt{2t \cdot R_c} / V_{det}$ for initial data: t =0.02 mm; R_c =100 mm; V_{det} = 0.2 m/s; V_c =30 m/s, where $l = \sqrt{2 \cdot t \cdot R_c}$ is the length of the arc of contact of the solid circle with the workpiece, m.

As follows from Table 2, with an increase in n, the ratio θ_{min} / θ decreases over a wide range, reaching a value of 0.11 at n =160 and l_{01} =1 mm. Therefore, by reducing the length of the working ledge l_{01} of the intermittent wheel, it is possible to reduce the cutting temperature by up to 10 times when grinding with an intermittent wheel compared to grinding with a solid wheel.

In the works of Professor Yakimov A. V. [1, 2] it is shown that due to the use of intermittent grinding, it is possible to reduce the cutting temperature by up to 50%. Based on the table 2, this is due to the increase in n within n = 6 and the use of intermittent circles with an increased length of the working protrusion $l_{01} >$ 20 mm. Therefore, by increasing the value n within large limits (n >10) and, accordingly, reducing the length of the working protrusion l_{01} (to values l_{01} = 1 mm), it is possible to more significantly reduce the cutting temperature during interrupted grinding. The main limitation of reducing the length of the working

ledge l_{01} is a decrease in its strength and increased wear of the discontinuous circle. This confirms the effectiveness of the use of intermittent circles in the operations of cutting materials, carried out with a cutting depth of up to 100 mm or more [16]. As a result, the thermal and power intensity of the machining process and, accordingly, the cutting temperature are sharply reduced, which makes it possible to ensure high quality and productivity of machining.

As follows from dependence (15), under the condition $\tau_{01}/\tau < 4$, the cutting temperature during grinding with an intermittent wheel will be less than the cutting temperature during grinding with a solid wheel. Therefore, let us consider more fully the main regularities of the decrease in cutting temperature during flat grinding with a discontinuous circle.

Taking into account the contact time of the working ledge of the discontinuous circle with the workpiece $\tau_{01} = l_{01}/V_c$, dependence (15) will take the form:

$$\frac{\theta_{min}}{\theta} = 2 \cdot \sqrt{\frac{l_{01}}{l} \cdot \frac{V_{det}}{V_c}} = 2 \cdot \sqrt{\frac{l_{01} \cdot Q_0}{\sqrt{2t \cdot R_c} \cdot t \cdot V_c}}, \qquad (16)$$

where $Q_0 = t \cdot V_{det}$ is the specific processing capacity, m^2/s.

Based on dependence (16), it is possible to reduce the ratio of cutting temperatures during grinding with intermittent and solid wheels θ_{min}/θ for a given specific processing productivity Q_0 by reducing the length of the working ledge of the intermittent wheel l_{01}, increasing the grinding depth t and the wheel speed V_c. Obviously, the greatest effect from the use of discontinuous circles is achieved under conditions of deep-feed grinding with a relatively low speed of the part V_{det}, since the grinding depth t is included in dependence (16) with the highest exponent.

For example, the value n, taking into account the dependencies $\tau/(\tau_{01}+\tau_{02}) = n$ and $\tau_{01} = \tau_{02}$ for the given values t =0.1 mm; R_c =100 mm; V_{det} =0.05 m/s; V_c =30 m/s; l_{01}=10 mm is equal to n =134. Accordingly, the ratio θ_{min}/θ = 0.122, i.e., under conditions of deep interrupted grinding, it is possible to significantly (up to 10 times) reduce the cutting temperature compared to conventional grinding with a solid wheel. In this case, the specific productivity

of processing Q_0 is equal to 300 mm^2/min, which is a rather high value, which is achieved in practice under conditions of high-performance grinding.

Under the conditions of multi-pass intermittent grinding (t =0.01 mm; R_c =100 mm; V_{det} =0.5 m/s; V_c =30 m/s; l_{01}=10 mm; Q_0 =300 mm^2/min), the value n =5, and the ratio θ_{min} / θ =0.632, which allows only slightly (within 50%) to reduce the cutting temperature compared to conventional grinding with a solid wheel. Therefore, it is most effective to use intermittent wheels in creep grinding conditions. This is consistent with the practice of using diamond intermittent wheels when removing significant allowances in the operations of grinding products from highly hard non-metallic materials, including the operations of cutting materials, grinding deep grooves [16, 17], etc.

Dependence (15) was obtained for the condition of the extremum (minimum) of the cutting temperature during interrupted grinding, i.e. conditions $\tau_{01} = \tau_{02}$.

In the general case, the ratio of cutting temperatures during grinding with intermittent and solid circles $\theta_{int} / \theta_{sol}$, determined by dependencies (10) and (9), is described by:

$$\frac{\theta_{int}}{\theta_{sol}} = \left(1 + \frac{\tau_{02}}{\tau_{01}}\right) \cdot \sqrt{\frac{\tau_{01}}{\tau}} . \qquad (17)$$

As can be seen, under the condition $\tau_{01} = \tau_{02}$, dependences (17) and (15) are identical.

For a given time τ of contact of a solid grinding wheel with the material being processed, the nature of the change in the ratio $\theta_{int} / \theta_{sol}$ with a change in the length of the working ledge of the discontinuous wheel l_{01} is identical to the nature of the change in the dimensionless quantity $\alpha = (1 + \tau_{02} / \tau_{01}) \cdot \sqrt{\tau_{01} / \tau_{02}}$ included in dependence (11). Under the condition $\tau_{01} > \tau_{02}$, the ratio $\theta_{int} / \theta_{sol}$ will increase with an increase in the ratio τ_{01} / τ_{02} and the length of the working protrusion of the discontinuous circle l_{01} (Table 1), but not so significantly. This makes it possible to effectively use interrupted wheels that have a shoulder length longer than the length of the cutout on the circle, reducing the wear of the broken circle and increasing productivity without actually increasing the cutting temperature and reducing the quality of processing.

References: 1. Teplofizyka mekhanichnoyi obrobky : pidruchnyk / *O. V. Yakymov, A. V. Usov, P. T. Slobodyanyk, D. V. Iorhachov*. – Odesa: Astroprynt, 2000. – 256 p. **2.** *Yakimov A. V.* Preryvistoye shlifovaniye / A. V. Yakimov. – Kyiv – Odesa: Vid. ob"yed. Vishcha shkola, 1986. – 175 p. **3.** *Handa, D., Kumar, Sh., Babu S., Surendran Th., Sooraj, V.S.:* Simulation of Intermittent Grinding for Ti-6Al-4V with Segmented Wheel. Materials Today: Proceedings, 44(1), pp. 2537–2542 (2021). **4.** *Tawakoli, T., Azarhoushang, B.:* Intermittent Grinding of Advanced Ceramic with the T-Tool Grinding Wheel. Advanced Materials Research, 126-128, pp. 615–620 (2010). **5.** *Tawakoli, T., Azarhoushang, B.:* Theoretical and experimental investigation of intermittent grinding of SiC with a segmented grinding wheel. Int J Abras Technol. 4 (1), pp. 90–99 (2011). https://doi. org/10.1504/IJAT.2011. 039005. **6.** *Sizyy Yu. A.* Dinamika i teplofizika shlifovaniya / Yu. A. Sizyy, D. V. Stalinskiy. – Kharkiv: GP "UkrNTTS "Energostal"', 2016. – 448 p. **7.** Modelirovaniye sistem : monografiya / *G. A. Oborskiy, A. F. Dashchenko, A. V. Usov, D. V. Mitrishin*. – Odesa: Astroprint, 2013. – 664 p. **8.** *Lischenko, N. V., Larshin V. P., Yakimov, A. V.:* Opredelenie temperaturyi preryivistogo shlifovaniya. PratsI Odeskogo politehnIchnogo universitetu. Vip.2 (39), pp. 80–85 (2012). **9.** *Larshin,V. P., Lishchenko, N. V., Pitel, J. (2020).* Intermittent grinding temperature modeling for grinding system state monitoring. Applied Aspects of Information Technology. Simulation of Physical Objects and Processes. 2020; Vol.3 No.2: pp. 58–73. **10.** *Oleksiy Yakimov, Liubov Bovnegra, Vladimir Tonkonogyi, Vladyslav Vaysman, Viktor Strelbitsyi and Inna Sinko:* Influence of the geometric characteristics of the discontinuous profile working surfaces of abrasive wheels for precision and temperature when grinding // Rizannya ta instrumenty v tekhnolohichnykh systemakh. - KhPI, 2021, № 94. – pp. 115–125. (2021) https://doi.org/10.20998/2078-7405.2021.94.13 **11.** *Tonkonogiy, V., Yakimov, A., Bovnegra, L., Beznos, S., Dobrovolskiy, V.:* Reduction of the Heat Factor in Flat Abrasive Grinding. Technical Science and Technology, 4, pp. 16–26 (2017). **12.** *Fang C., Xu, X.* Analysis of temperature distributions in surface grinding with intermittent wheels. The International Journal of Advanced Manufacturing Technology. 71, pp. 23–31 (2014). https://doi.org/10.1007/S 00170013-5472-1 **13.** *Novikov F.V.* Zakonomernosti izmeneniya temperatury rezaniya pri obychnom i preryvistom shlifovanii / F. B. Novikov, I. A. Ryabenkov // Visnyk NTU “KHPI”. Zbirnyk naukovykh prats′. Seriya: Tekhnolohiyi v mashynobuduvanni. – KH.: NTU “KHPI”. − 2016. − № 5 (1177). − pp. 90–96. **14.** *Yakimov A.V.* Fizicheskaya sushchnost' i tekhnologicheskiye vozmozhnosti preryvistogo shlifovaniya / A.V. Yakimov, F.V. Novikov, G.V. Novikov // Suchasni systemy tekhnolohiy u mashynobuduvanni. Zbirnyk naukovykh prats′, prysvyachenyy 90-richchyu z dnya narodzhennya profesora Odes′koho natsional′noho politekhnichnoho universytetu (ONPU) Yakymova O.V. – Dnipro: LIRA. – 2015. – pp. 38-43. **15.** *Novikov F. V.* Rozroblennya teoretychnoho pidkhodu do vyznachennya temperatury rizannya pry shlifuvanni ta umov yiyi zmenshennya / F. V. Novikov, V. I. Polyans′kyy // Visnyk Natsional′noho tekhnichnoho universytetu «KHPI». Seriya: Tekhnolohiyi v mashynobuduvanni : zb. nauk.pr. / Nats. tekhn. un-t «Kharkiv. politekhn. in-t». – Kharkiv : NTU «KHPI», 2022. – № 2 (6) 2022. – pp. 96–103. – ISSN 2079-004X, https://doi.org/10.20998/2079-004X.2022.2(6).13. **16.** *Lavrinenko V. I.* Nadtverdi materialy v mekhanoobrobtsi / V. I. Lavrinenko, M. V. Novikov; za red. M. V. Novikova. – Kyiv: INM im. V. M. Bakulya NAN Ukrayiny, 2013. – 456 p. **17.** *Kundrak, J., Deszpoth, I., Molnar, V.*: Increasing Productivity of Combined Procedure by Reducing Grinding Allowance, Rezanie i Instrumenty v Tekhnologicheskih Sistemah 90, pp. 26–35., 2019.

Федір Новіков, Харків, Україна

ОПТИМІЗАЦІЯ ПАРАМЕТРІВ ПЕРЕРИВЧАСТОГО ШЛІФУВАННЯ ЗА ТЕМПЕРАТУРНИМ КРИТЕРІЄМ

Анотація. *У роботі проведено аналітичну оптимізацію параметрів переривчастого шліфування за температурним критерієм та на її основі визначено умови суттєвого зменшення температури різання, які полягають, головним чином, у збільшенні кількості контактів робочих виступів переривчастого круга із фіксованим поперечним перерізом оброблюваної деталі. Розрахунками встановлено, що за умови забезпечення 20 контактів температура різання може бути зменшена до 3-х разів порівняно із звичайним шліфуванням суцільним кругом. Це досягається в умовах глибинного переривчастого шліфування із відносно невеликою швидкістю оброблюваної деталі, оскільки в умовах багатопрохідного переривчастого шліфування із більш значною швидкістю оброблюваної деталі, яке традиційно застосовується, реалізується не більше 6 контактів робочих виступів переривчастого круга із фіксованим поперечним перерізом оброблюваної деталі і температура різання зменшується лише у межах 50 %. Розрахунками встановлено, що за умови рівності довжин робочого виступу та вирізу на переривчастому крузі досягається мінімум температури різання, зменшити який можна зменшенням довжин робочого виступу та вирізу на переривчастому крузі. Встановлено також, що перевищення довжиною робочого виступу довжини вирізу переривчастого круга призводить до несуттєвого збільшення температури різання. Це дозволяє зменшити зношування переривчастого круга і підвищити продуктивність обробки фактично без збільшення температури різання і, відповідно, зниження якості обробки завдяки виключенню припікань та інших температурних дефектів, які виникають на оброблюваних поверхнях. У роботі показано, що отримані теоретичні рішення є необхідною, але недостатньою умовою забезпечення суттєвого зменшення температури різання під час переривчастого шліфуванні. Достатньою умовою слід розглядати необхідність повного або часткового охолодження зони шліфування між контактами оброблюваної деталі із робочими виступами переривчастого круга шляхом інтенсивного підведення у зону шліфування ефективних технологічних середовищ.*

Ключові слова: *сила різання; якість обробки; робочий виступ круга; адіабатичний стержень; технологічне середовище; ріжуча здатність круга.*

UDC 620.179.112 **doi: 10.20998/2078-7405.2023.98.07**

N. Nagy, Miskolc, Hungary

EXPERIMENTAL INVESTIGATION OF TRIBOLOGY-RELATED SURFACE TOPOGRAPHY PARAMETERS AND HARDNESS OF 16MNCR5 CASE HARDENED STEEL

Abstract. *Tribological properties are determinant in the functionality of contacting surfaces of machine elements. The wear resistance or load bearing capacity influence the lifetime of these parts. In this study tribology-related surface topography parameters (S_{sk}, S_{bi}) and the hardness of hard turned surfaces are analyzed after hardness and topography measurements. Correlation coefficients were calculated for their relationships. It was found that the cutting parameters affect the wear resistance and the hardness in the opposite direction.*

Keywords: *HV hardness; surface roughness; S_{sk}; S_{bi}; hard machining.*

1. INTRODUCTION

Case hardened steels play an important role in machined components whose surfaces are required to be wear resistant and/or have high hardness or load bearing capacity [1]. These and other characteristics are determinant in the functionality and the lifetime of the components [2]. A high number of industrial parts, e.g. gears that require hardened surfaces, are machined in the automotive industry [3, 4]. Hardened surfaces are machined conventionally by grinding; however hard turning is also a suitable technology to reach the desired roughness (mainly R_a and R_z) or equal the accuracy of a ground surface [5, 6]. At the same time, hard turning is a more productive technology because of its high material removal rate [7] and the fact that grinding burn [8] can be eliminated by its application. One of the main reasons of applying grinding, despite the advantages of hard turning, is that in certain cases ground topography [9] is needed.

A determining field of functionality of hardened surfaces is their tribological characteristics [10, 11]. Among others, wear resistance and load bearing capacity have high importance when the lifetime of a component is in the focus. The skewness (S_{sk}) provides information about the asymmetry of the surface [12, 13]. If its value is negative and decreases, the surface becomes more filled in its peak zone. This results in higher load-bearing capacity due to the increased bearing area. At the same time, such a surface is characterized by fewer peaks, which results in a relatively short wear-in phase, i.e. the surface is more wear resistant [14, 15]. Some tribological characteristics are related to the S_{sk} parameter [16], and several studies have analyzed this in detail [e.g., 17, 18]. It has to be noted that this parameter is sensitive to sharp peaks of the surface [19]. The Surface bearing index (S_{bi}) also characterizes the peak zone of a surface; however, this parameter provides the

same information by a different calculation method [20, 21]. Selecting the suitable roughness or topography parameters requires complex consideration [22, 23]; for analyzing one phenomenon, it is recommended to compare a few available parameters [24, 25]. 3*D* scanning technology is recommended for measuring surface topography, because it provides more detailed information about the surface than its conventional 2*D* counterpart [26, 27], there are a number of parameters and analytic tools available to analyze the topography in more detailed way [28, 29], and the reliability of the results can also be considered higher [30].

In this study tribological-related (mainly wear resistance) 3*D* surface topography parameters (S_{sk} ; S_{bi}) and the Vickers hardness of hard turned surfaces were analyzed. The experiments were carried out at varying levels of feed rate and cutting speed, and by two CBN inserts with different geometry. Correlation relationships were calculated for the numerical results.

2. EXPERIMENTAL METHODS

The workpiece material was 16MnCr5 steel (diameter: 60 mm). Before cutting, the workpieces were case hardened: after 14 h of carburization, quenching in oil was carried out from 860 °C. In the third step, the pieces were tempered at 190 °C. In Fig. 1 the time-temperature diagram of the process is presented.

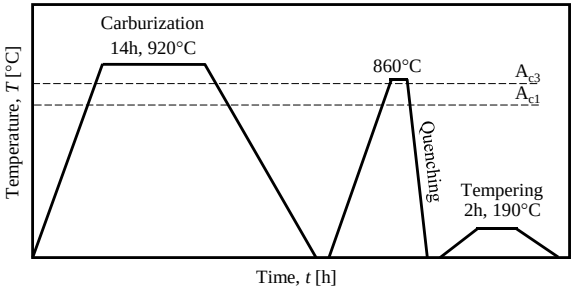

Figure 1 – Heat treatment process

In the hard turning experiment two cutting parameters were varied, the feed rate (f = 0.04; 0.12; and 0.2 mm/rev) and the cutting speed (v_c = 120; 180; and 240 m/min). The depth-of-cut was fixed (a_p = 0.2 mm). The used CNC lathe was Optiturn S600, the used tool holder was CLNR 2524 M12. Two inserts with different edge geometries were compared in the experiments: NP-CNGA 120408 TA4 and 4NC-CNGA 120408 (hereinafter inserts A and B, respectively). They differed from each other in the α angle and the w negative land width: α_A: 35°; α_B: 25°; w_A: 0.13 mm; w_B: 0.12 mm (Fig. 2). Nine surfaces (a total of 18 for the two inserts) were machined at all of the f and v_c data combinations.

The hard turning experiments were followed by hardness testing and roughness measurement and analysis. The roughness measurement was carried out on a 3*D* machine (Altisurf 520), equipped by an optical sensor. The resolution of the sensor in z directions was 0.012 μm. The measured area was 2 × 2 mm, with 2000 scanned points in both x and y directions. The cut-off length was 0.8 mm, and Gauss filter was applied for the preprocessing of the scanned data. The skewness (S_{sk}) is the third moment of the heights distribution of the surface; the surface bearing index (S_{bi}) is the ratio of the root-mean square deviation over the surface height at 5% bearing area. Two other parameters, the maximum height (S_z) and the arithmetical mean height (S_a), were also analyzed. They are widely applied parameters for qualification of surfaces. For the analysis of the parameters the standard ISO 25178 was applied.

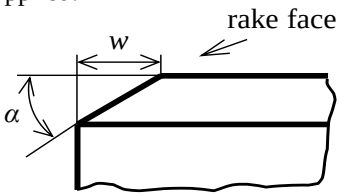

Figure 2 – Varying geometrical parameters of the applied tools

The hardness tests were carried out on a universal hardness tester (Reicherter UH250). The load was 10 kp and the dwell time was 10 s. For the measurement the standard DIN EN ISO 18265 was applied.

3. RESULTS AND DISCUSSION

As a result of the heat treatment, the thickness of the hardened layer was around 1 mm. The microstructure of this layer is basically martensitic (Fig. 3).

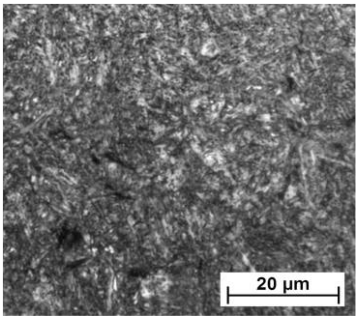

Figure 3 – Microstructure of the hardened layer (500×)

In Figs. 4 and 5 the *HV* hardness data are summarized as a function of the cutting parameters for the A and B inserts, respectively. The hardness values are between 752 and 854 in the case of insert A and between 695 and 825 in the case of insert B. The hardness values increased by the feed rate by applying bot inserts. The values increased with the cutting speed in the case of insert B. This was not observed in the case of insert A. The change in hardness results from the layer hardened during machining, which caused by the relatively high cutting forces, mainly the passive (radial) force.

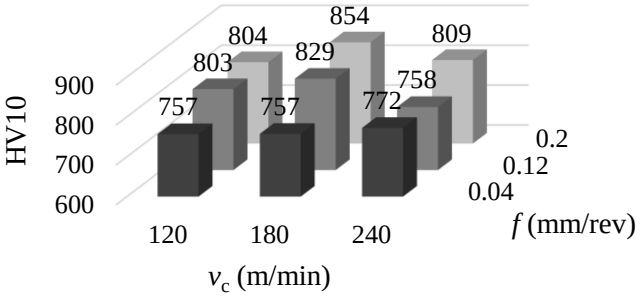

Figure 4 – Hardness data – insert A

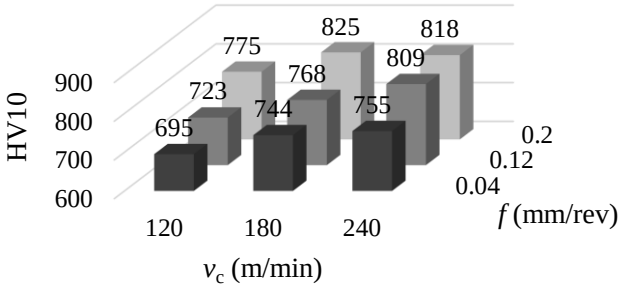

Figure 5 – Hardness data – insert B

In Fig. 6 the maximum height (S_z) values are presented as a function of the cutting speed and the feed rate. At 0.04 and 0.12 mm/rev feed rates the values are similar in the case of the two inserts. At the highest feed rate (0.2 mm), a higher deviation is observed in S_z in the case of insert B. The roughness values are not sensitive to the cutting speed; however, they increase with the feed rate. The S_z values at different feed rates are 0.10–0.21 μm lower for insert B than for insert A.

Similar results were found in the case of the arithmetical mean height (S_a); however, no deviation can be observed in the values at the highest feed rate (Fig.7). Here, at the two lower feed rates a slight decrease can be observed when the cutting speed is increased. The S_a values at different feed rates are 0.03–0.28 μm lower for insert B than for insert A.

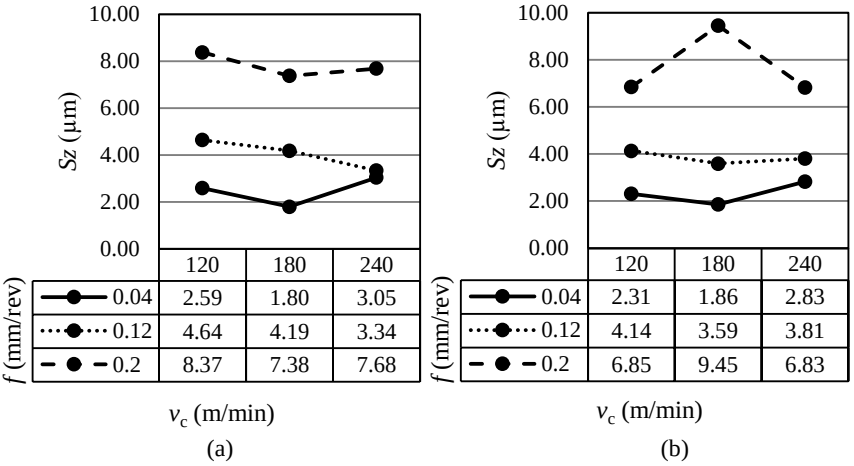

Figure 6 – Maximum height values – insert A (a); insert B (b)

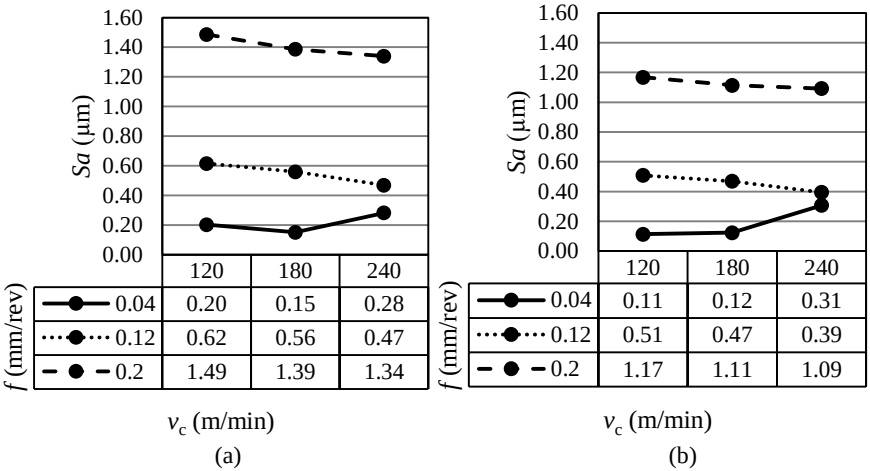

Figure 7 – Arithmetical height values – insert A (a); insert B (b)

The skewness values of the surfaces machined at the lowest feed rate show a relatively high deviation (Fig. 8). In the case of insert A S_{sk} is between -0.17 and 0.10, and in the case of insert B between -0.24 and 0.46. The negative S_{sk} values are favorable from a wear resistance point of view because the peak zone of such a surface is more filled. At the two higher feed rates the S_{sk} values are relatively close to each other, i.e., the feed rate has no significant influence on the skewness. In the case of insert B the skewness at the lowest feed rate increases with the cutting speed.

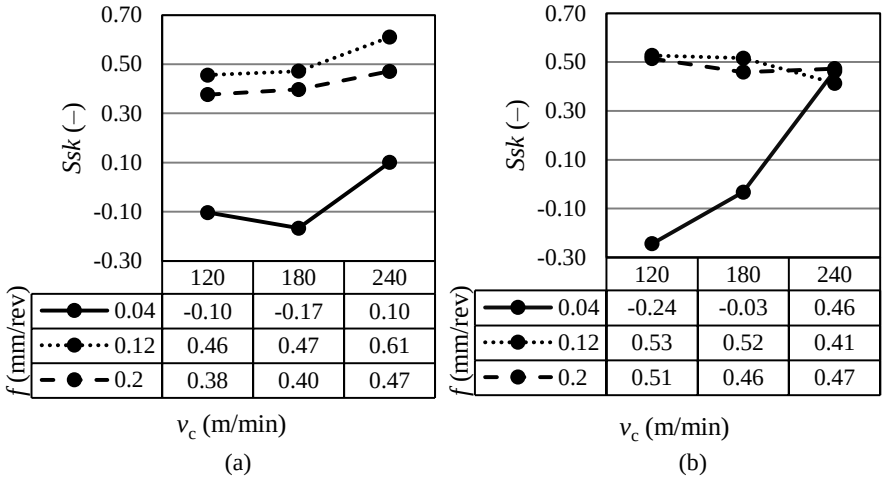

Figure 8 – Skewness values – insert A (a); insert B (b)

Concerning the S_{bi} parameter (Fig. 9), the lower value is more favorable for wear resistance. In the case of insert B the values are lower than in the case of insert A by 0.06–0.30. The skewness value does not provide sufficient information on the wear resistance at the analyzed cutting parameter values. However, the surface bearing index indicates clearer differences in the values. This demonstrates that more than one parameter is needed for obtaining more reliable information about the functionality of the surfaces.

It was found that the higher cutting forces result in a more hardened surface layer. In Fig. 10 the correlation between the S_{sk} and the hardness values is demonstrated. It was seen that both the S_{sk} and the S_{bi} values and the hardness also increase with the feed rate. In Figures 10 and 11 it can be observed that the hardness values increase with the roughness values. At the same time, the lower S_{sk} and lower S_{bi} values are favorable from a wear resistance point of view (more filled surface, larger bearing area).

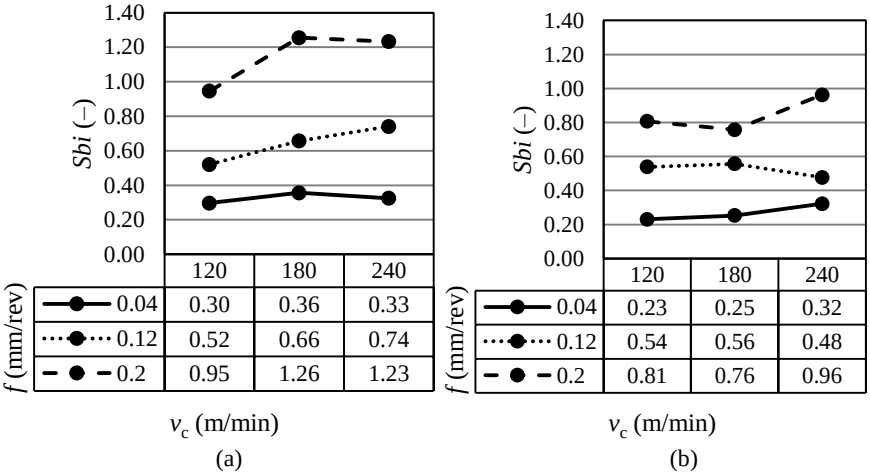

Figure 9 – Surface bearing index values – insert A (a); insert B (b)

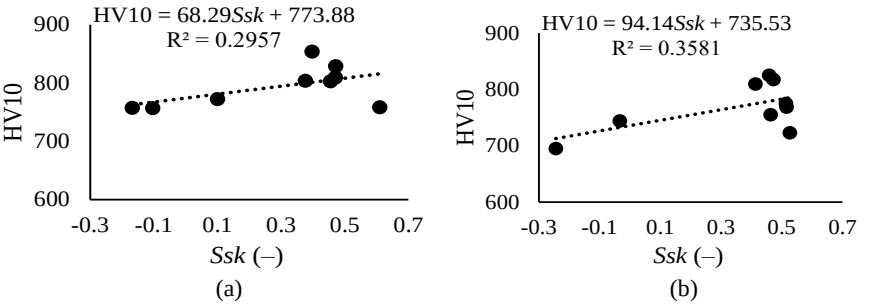

Figure 10 – Relationship between the skewness
and the hardness values – insert A (a); insert B (b)

This indicates that if the topographical parameters are favorable, the hardness value tends to be less favorable. It has to be noted, however, that the relationship between the hardness and topography values is not strong. Based on the correlation coefficients (*R*), the relationships are medium strong or weak. The correlation coefficient on the second power is the coefficient of determination. These values can be seen in the figures. The values between 0.2 and 0.4 indicate a weak relationship and between 0.4 and 0.7 a medium-strength relationship. The former is valid for the S_{sk} values (Fig. 10) and the latter for the S_{bi} values (Fig. 11).

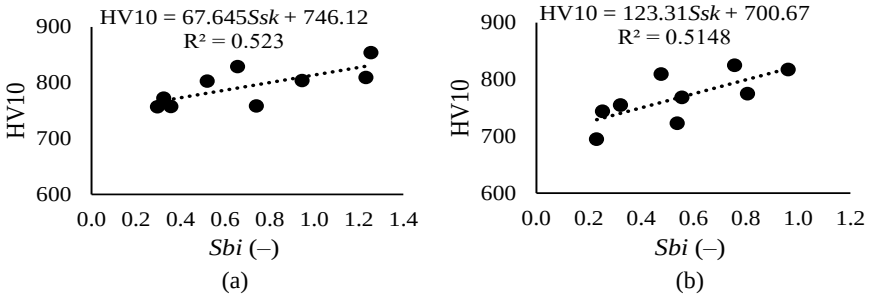

Figure 11 – Relationship between the surface bearing index and the hardness values – insert A (a); insert B (b)

5. SUMMARY

Hard turned surfaces were analyzed from a wear resistance and load bearing capacity point of view. The S_z, S_a, S_{sk} and S_{bi} topography parameters and the HV10 hardness values were analyzed and compared to each other. The following was found.

- The S_z, S_a, S_{bi} and HV10 parameters increase by the feed rate. This is valid for the S_{sk} parameter in the case of insert A (NP-CNGA 120408 TA4; $\alpha = 35°$).
- The S_z, S_a, S_{bi} and HV10 values are lower in the case of insert B (4NC-CNGA 120408; $\alpha = 25°$).
- The relationship between the hardness values and the S_{sk} values is weak, while the S_{bi} values have a medium-strong relationship with the hardness values. When the topography parameters improve, less favorable values are obtained for the hardness values.

The above findings are valid in the analyzed ranges of the hard turning parameters (a_p = 0.2 mm; v_c = 120–240 m/min; f = 0.04–0.2 mm/rev).

The analysis can be extended to the analysis of more depth-of-cut levels, more tools and more surface integrity or tribology related properties.

References: 1. *Fedorovich,V., Pyzhov, I., Ostroverkh, Y., Pupan, L., Garachenko, Y.:* Methodology for developing an expert system for the grinding of superhard materials, Rezanie i Instrumenty v Tekhnologicheskih Sistemah 96, pp. 82–88, 2022. **2.** *Lavrinenko, V., Solod, V.:* The ralationship betwheen the parameters of roughness and features of surface formation with a special microprofile, Rezanie i Instrumenty v Tekhnologicheskih Sistemah 96, pp. 99–109, 2022. **3.** *Kovalchuk, O., Nezhebovsky, V., Permyakov, O., Klochko, O., Ryabchenko, S.:* Processing of hardened cylindrical gear wheels of the cutting gearbox of the combine UKD 200-500, Rezanie i Instrumenty v Tekhnologicheskih Sistemah 95, pp. 57–70, 2021. **4.** *Yakimov, O., Uminsky, S., Klimenko, N., Kirkopulo, K., Pavlyshko, A., Vaysman, V.:* Improving grinding of gear wheels applied in gearboxes of power engineering, Rezanie i Instrumenty v Tekhnologicheskih Sistemah 95, pp. 45–56, 2021. **5.** *Kundrak, J., Sztankovics, I., Molnar, V.:* Accuracy and topography analysis of hard machined surfaces, Manufacturing Technology 21(4), pp. 512–519, 2021. **6.** *Zawada-Tomkiewicz, A.:* Analysis of surface

roughness parameters achieved by hard turning with the use of PCBN tools, Estonian Journal of Engineering 17, paper 88, 2011. **7.** *Kundrak, J., Deszpoth I., Molnar V.:* Decision support method for the applicability of hard turning, Rezanie i Instrumenty v Tekhnologicheskih Sistemah 96, pp. 110–120. 2022. **8.** *Heinzel, J., Jedamski, R., Rößler, M., Karpuschewski, B., Epp, J., Dix, M.:* Hybrid approach to evaluate surface integrity based on grinding power and Barkhausen noise, Procedia CIRP 108, pp. 489–494, 2022. **9.** *Kundrak J., Deszpoth, I., Molnar, V.:* Comparative study of material removal in hard machining of bore holes, Tehnicki Vjesnik-Technical Gazette 21(1), pp 183–189, 2014. **10.** *Gapinski, B., Firlik, B., Mathia, T.G.:* Characteristics of tram wheel wear: Focus on mechanism identification and surface topography, Tribology International 150, paper 106365, 2020. **11.** *Alok, A., Das, M.*: White layer analysis of hard turned AISI 52100 steel with the fresh tip of newly developed HSN2 coated insert, Journal of Manufacturing Processes 46, pp. 16–25, 2019. **12.** *Molnar V.:* Asymmetric height distribution of surfaces machined by hard turning and grinding, Symmetry 14(8), paper 1591, 2022. **13.** *Sedlacek, M., Podgornik, B., Vizintin, J.:* Correlation between standard roughness parameters skewness and kurtosis and tribological behaviour of contact surfaces, Tribology International 48, pp. 102–112, 2012. **14.** *Sedlacek, M., Gregorcic, P., Podgornik, B.:* Use of the roughness parameters S_{sk} and S_{ku} to control friction – a method for designing surface texturing, Tribology Transactions 60, pp. 260–266, 2017. **15.** *Molnar, V., Sztankovics, I.:* Analysis of roughness parameters determining tribological properties in hard turned surfaces, Hungarian Journal of Industry and Chemistry 49(2), pp. 77–84, 2021. **16.** *Yu, N., Polycarpou, A.A.:* Combining and contacting of two rough surfaces with asymmetric distribution of asperity heights, Journal of Tribology 126, pp. 225–232, 2004. **17.** *Pawlus, P., Reizer, R., Zelasko, W.:* Prediction of parameters of equivalent sum rough surfaces, Materials 13, paper 4898, 2020. **18.** *Orrillo, P.A., Santalla, S.N., Cuerno, R., Vazquez, L., Ribotta, S.B., Gassa, L.M., Mompean, F.J., Salvarezza, R.C., Vela, M.E.:* Morphological stabilization and KPZ scaling by electrochemically induced co-deposition of nanostructured NiW alloy films, Scientific Reports 7, paper 17997, 2017. **19.** *Gadelmawla, E.S., Koura, M.M., Maksoud, T.M.A., Elewa, I.M., Soliman, H.H.:* Roughness parameters, Journal of Material Processing Technology 123, pp. 133–145, 2002. **20.** *Grzesik, W.:* Prediction of the functional performance of machined components based on surface topography: state of the art, Journal of Materials Engineering and Performance 25(10), pp. 4460–4468, 2016. **21.** *Molnar V.:* Analysis of the S_{bi} and S_{vi} functional indices in hard machining, Rezanie i Instrumenty v Tekhnologicheskih Sistemah 97, pp. 113–123, 2022. **22.** *Grzesik, W., Zak, K., Kiszka, P.:* Comparison of surface textures generated in hard turning and grinding operations, Procedia CIRP 13, pp. 84–89, 2014. **23.** *Korzynski, M., Dudek, K., Palczak, A., Kruczek, B., Kocurek, P.:* Experimental models and correlations between surface parameters after slide diamond burnishing, Measurement Science Review 18, pp. 123–129, 2018. **24.** *Deltombe, R., Kubiak, K.J., Bigerelle, M.:* How to select the most relevant *3D* roughness parameters of a surface?, Scanning 36, pp. 150–160, 2014. **25.** *Molnar, V.:* Tribological properties and *3D* topographic parameters of hard turned and ground surfaces, Materials 15(7), paper 2505, 2022. **26.** *Struzikiewicz, G., Sioma, A.:* Evaluation of Surface Roughness and Defect Formation after The Machining of Sintered Aluminum Alloy AlSi10Mg, Materials 13, paper 1662, 2020. **27.** *Elbah, M., Laouici, H., Benlahmidi, S., Nouioua, M., Yallese, M.*: Comparative assessment of machining environments (dry, wet and MQL) in hard turning of AISI 4140 steel with CC6050 tools, International Journal of Advanced Manufacturing Technology 105, pp. 2581–2597, 2019. **28.** *Vishwanatha, J.S., Srinivasa Pai, P.:* Application of Edge Detection Technique for Surface Roughness Estimation of Ti-6Al-4V Turned Surfaces, Manufacturing Technology 21, pp. 269–277, 2021. **29.** *Li, S., Chen, T., Qiu, C., Wang, D., Liu, X.:* Experimental investigation of high-speed hard turning by PCBN tooling with strengthened edge, International Journal of Advanced Manufacturing Technology 92, pp. 3785–3793, 2017. **30.** *Molnar, V.:* Tribology and Topography of Hard Machined Surfaces, Rezanie i Instrumenty v Tekhnologicheskih Sistemah 94, pp. 49–59, 2021.

Нора Надь, Мішкольц, Угорщина

ЕКСПЕРИМЕНТАЛЬНЕ ДОСЛІДЖЕННЯ ПАРАМЕТРІВ ТОПОГРАФІЇ ПОВЕРХНІ ТА ТВЕРДОСТІ ЦЕМЕНТОВАНОЇ СТАЛІ 16MNCR5, НА ОСНОВІ ТРИБОЛОГІЇ

Анотація. *Трибологічні властивості є визначальними у функціональності контактних поверхонь елементів машин. Зносостійкість або несуча здатність впливають на термін служби цих деталей. У цьому дослідженні були проаналізовані параметри тривимірної топографії поверхні (S_{sk}; S_{bi}), пов'язані з трибологією (головним чином зносостійкість) і твердість за Віккерсом жорстко точених загартованих поверхонь. Експерименти проводилися на різних рівнях подачі та швидкості різання, а також на двох пластинах КНБ з різною геометрією. Для чисельних результатів розраховано кореляційні зв'язки. В експерименті з жорстким токарним обробленням змінювалися два параметри різання: швидкість подачі (f = 0,04; 0,12; 0,2 мм/об) і швидкість різання (v_c = 120; 180; 240 м/хв). Глибина різання була фіксованою (a_p = 0,2 мм). Випробування на твердість проводили на універсальному твердомірі (Reicherter UH250). Навантаження становило 10 кПа, а час перебування 10 с. Для вимірювання застосовувався стандарт DIN EN ISO 18265. Тверді точені поверхні аналізували з точки зору зносостійкості та несучої здатності. Параметри топографії S_z, S_a, S_{sk} і S_{bi} і значення твердості HV10 були проаналізовані та порівняні один з одним. Параметри S_z, S_a, S_{bi} і HV10 збільшуються з ростом швидкості подачі. Це справедливо для параметра S_{sk} у випадку вставки A (NP-CNGA 120408 TA4; α = 35°). Значення S_z, S_a, S_{bi} та HV10 нижчі у випадку вставки B (4NC-CNGA 120408; α = 25°). Зв'язок між значеннями твердості та значеннями S_{sk} слабкий, тоді як значення S_{bi} мають середньо-сильний зв'язок зі значеннями твердості. Коли параметри рельєфу покращуються, отримують менш сприятливі значення значень твердості. Наведені вище висновки справедливі в проаналізованих діапазонах параметрів жорсткого точіння (a_p = 0,2 мм; v_c = 120–240 м/хв; f = 0,04–0,2 мм/об). Аналіз можна розширити до аналізу більшої кількості рівнів глибини різання, більшої кількості інструментів і більшої цілісності поверхні або властивостей, пов'язаних з трибологією.*

Ключові слова: *твердість HV; шорсткість поверхні; S_{sk}; S_{bi}; жорстка механічна обробка.*

UDC 620.179.118 **doi: 10.20998/2078-7405.2023.98.08**

J. Sultana, I. Sztankovics, Miskolc, Hungry

ROUNDNESS ERROR AND TOPOGRAPHY OF HARD TURNED SURFACES

Abstract. *Accuracy and topography are significant indicators of precision machined high-quality surfaces. Case hardened steel (16MnCr5) was analyzed to obtain information about the effects of technological data and the connections between the analyzed accuracy (roundness) and roughness parameters (S_a, S_z, S_{sk}, S_{ku}). It was found that the feed rate has a significant influence on the roundness and the roughness parameters, and there are strong relationships between the roundness and these roughness parameter values: the correlation coefficients varied between 0.78 and 0.85.*
Keywords: *roundness; 3D surface topography; hard turning; precision machining.*

1. INTRODUCTION

Several types of machined components are built into units or products where they must fulfill numerous requirements concerning the functionality and lifetime. The purpose of precision machining is ensuring the accuracy of these components and the quality of their surfaces [1]. Although additive manufacturing has been in the focus of research in recent years by endeavoring to increase accuracy, also conventional technologies face challenges due to the new materials [2], cutting tool materials [3] and special technologies [4, 5].

Accuracy is an important characteristic of a machined component, because it affects the durability and assembly of the parts [6, 7]. At the same time, surface quality, such as surface layer characteristics [8], texture, roughness or stress state, also play an important role in the lifetime of a component [9].

Numerous studies have been published in the topic of machined part accuracy; among others they focus on the optimization of machining parameters [7], the effect of coolant material [10], the simulation of uncertainties [11, 12] or the application of artificial intelligence [13, 14]. Concerning surface roughness topics, the most focused-on topics are the cutting data selection for optimizing the roughness parameter values [15, 16], roughness prediction [17, 18], comparison of machining technologies [19, 20], tribological effects of surface quality [21, 22], cutting conditions [23, 24] or the analysis of measurement methods [25, 26].

In precision machining not only abrasive but also single-point-tools are applied to ensure the same surface quality. However, from a surface functional point of view it has to be considered whether a periodic or a random topography is needed [27]. Several studies report about the applicability of one or the other procedure [28, 29] or about comparative results for hard turning and grinding [30] based on surface quality considerations.

In this study hard turned surfaces are analyzed from an accuracy and surface quality point of view based on some widely applied qualification parameters. Roundness and topography measurements were carried out and compared to obtain information about the effects of cutting parameters. In the experiment 16MnCr5 case hardened steel was applied, which is widely used in the automotive industry. 3*D* topography analysis was applied to obtain exact information about the surface quality [31]. The experiment was carried out based on factorial experiment design and basic statistical indicators were calculated to understand the relationship between the roundness and the analyzed roughness parameters in detailed manner.

2. EXPERIMENTAL METHODS

The hard turning experiment was carried out on the machine tool EMAG VSC400 DDS. The applied tool holder and the CBN insert were PCLNR 2020-K12 and CNGA 120408, respectively. The cutting parameters were:

- a_p (depth-of-cut): 0.05 and 0.35 mm;
- v_c (cutting speed): 120 and 240 m/min;
- f (feed rate): 0.04 and 0.2 mm/rev.

The machining was carried out in all combinations of the parameter values (two values per parameter), which resulted in eight different setups. The machined material was 16MnCr5, and Ø60 mm surfaces were hard turned. The hardness of the material was between 60 and 63 HRC.

The roughness measurement was carried out on a 3*D* topography tester equipment Altisurf 520. For the topography scanning (CL2) an optical sensor was used. The resolution of the sensor in *x*, *y* and *z* directions was 1, 1, and 0.012 µm, respectively. The squared evaluation areas of the surfaces were 4 mm^2. Two cut-off lengths were applied because of the periodicity differences of the machined surfaces: 0.08 and 0.8 mm. The preparation of scanned surfaces included form removal, Gauss filtering and thresholding of the extreme peaks and valleys. In Eqs 1–4 the analyzed roughness parameters are defined: S_a – arithmetical mean height; S_z – maximum height; S_{sk} – skewness; S_{ku} – kurtosis.

$$Sa = \frac{1}{\mathrm{A}} \iint_{\mathrm{A}} |Z(x,y)|\, dx\, dy \tag{1}$$

$$Sz = \max_{\mathrm{A}} Z(x,y) + \left|\min_{\mathrm{A}} Z(x,y)\right| \tag{2}$$

$$Ssk = \frac{1}{Sq^3}\left[\frac{1}{\mathrm{A}} \iint_{\mathrm{A}} Z^3(x,y)\, dx\, dy\right] \tag{3}$$

$$Sku = \frac{1}{Sq^4}\left[\frac{1}{A}\iint_A Z^4(x,y)\,dx\,dy\right] \quad (4)$$

The roundness error measurement was carried out on the shape and position accuracy measuring equipment Talyrond 365. The scanning speed was 6 mm/s, the scaling was 1 μm/div. For the analysis the minimum zone type reference circle method was applied. The applied filter was Gauss filter, and the filtering range was 1–500 upr.

3. RESULTS AND DISCUSSION

The machined surfaces were analyzed based on widely used roughness data. The roundness error has high importance in qualifying the accuracy of cylindrical surfaces. In Table 1 the cutting and the measurement data of the analyzed surfaces are summarized.

Table 1 – Cutting data and measurement data of the machined surfaces

Surface	a_p	v_c	f	S_a	S_z	S_{sk}	S_{ku}	RONt
A	0.05	120	0.04	0.11	0.81	-0.05	3.27	0.99
B			0.2	1.21	5.16	0.64	2.22	1.63
C		240	0.04	0.15	1.04	-0.01	3.15	0.57
D			0.2	1.22	5.17	0.64	2.16	1.63
E	0.35	120	0.04	0.25	1.87	-0.05	3.27	1.5
F			0.2	1.18	5.17	0.71	2.35	1.76
G		240	0.04	0.24	1.73	0.02	3.17	0.6
H			0.2	1.18	5.23	0.63	2.22	1.96

3.1. Analysis of the roughness values

In Fig. 1 the roughness values of the surfaces are presented. Analyzing the effects of the cutting data on the roughness values, the following can be stated.

The A, C, E, G surfaces are machined at the lower feed rate, and the values of S_a and S_z are significantly lower than those belonging to the surfaces machined at the higher feed rate. The cutting speed and the depth-of-cut do not influence these values. The same can be observed in the skewness values: the height distribution of the A, C, E and G surfaces indicate normal distribution by their S_{sk} values around 0. The B, D, F and H surfaces are asymmetric, they are less filled in the peak zone,

which means that their wear resistance and load-bearing capacity are lower. Concerning the kurtosis values, those of the surfaces machined at the lower feed rate indicate normal distribution by their S_{ku} values around 3. The surfaces machined at the higher feed rate incorporate fewer sharp peaks and valleys, therefore, e.g. their fluid-retention abilities are worse. Neither the cutting speed nor the depth-of-cut have an influence on these two topography parameters.

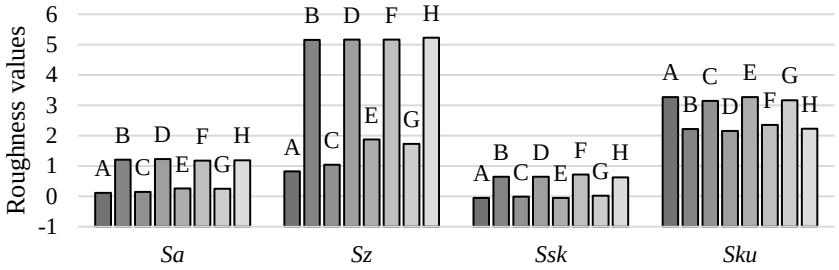

Figure 1 – Roundness values of the machined surfaces

3.2. Analysis of the roundness values

Analyzing the effects of cutting data on the roundness, the following observations can be made (Fig. 2): at the low feed rate the roundness error decreased by 40–58% when the cutting speed was increased. This connection was not observed at the higher feed rate. When the depth-of-cut increased, all the roundness data increased by 5–52%.

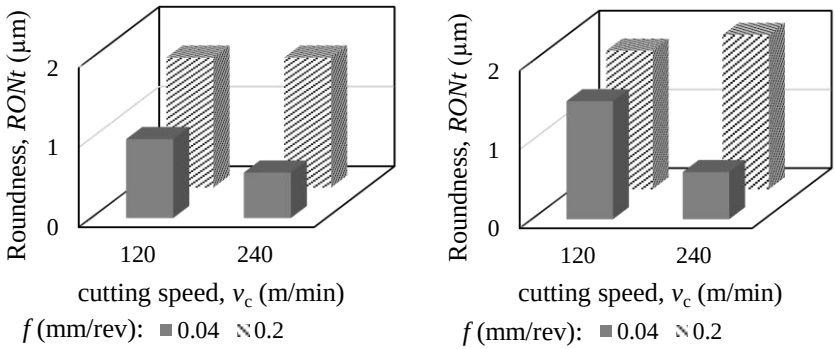

Figure 2 – Roundness values of the different setups

In Figs. 3–6 the roundness diagrams are demonstrated. At low depth-of-cut (a_p = 0.05 mm), cutting speed (v_c = 120 m/min) and feed rate (f = 0.04 mm/rev) the roundness error is relatively low and the surface (A) includes no unmeasured points or ranges that result from extreme peaks (Fig 3a). At the higher feed rate (f = 0.2 mm/rev), the number of these outliers of the surface points (B) increased and a certain level of roundness was obtained (Fig 3b), which increased the roundness value by 65%.

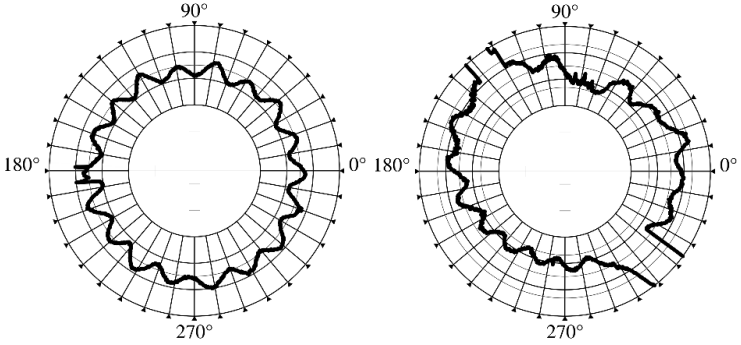

a) b)

Figure 3 – Roundness of surface A (a) and B (b)

At the higher cutting speed (v_c = 240 m/min) and low depth-of-cut the irregularities of the surface (C and D) increased (Fig 4) and ovality was obtained at the surface (D) machined by the higher feed rate (Fig 4b). These resulted in the increase of roundness by 186%.

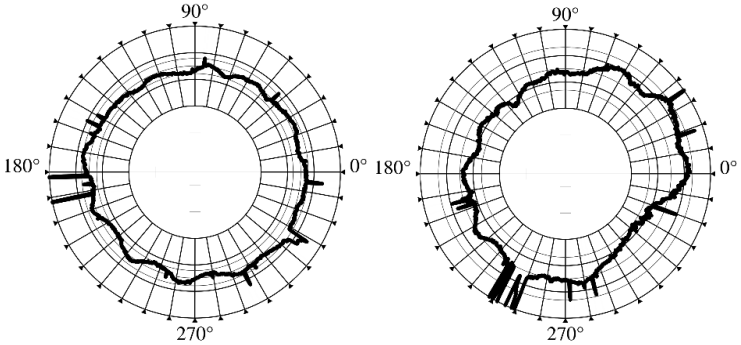

a) b)

Figure 4 – Roundness of surface C (a) and D (b)

At the higher depth-of-cut (a_p = 0.35 mm) and lower cutting speed more outliers were obtained for the surface (E) machined by lower feed rate (Fig 5a). However, the ovality can be observed on the surface (F) machined by the higher feed rate, which resulted in a 17% increase in the roundness (Fig 5b).

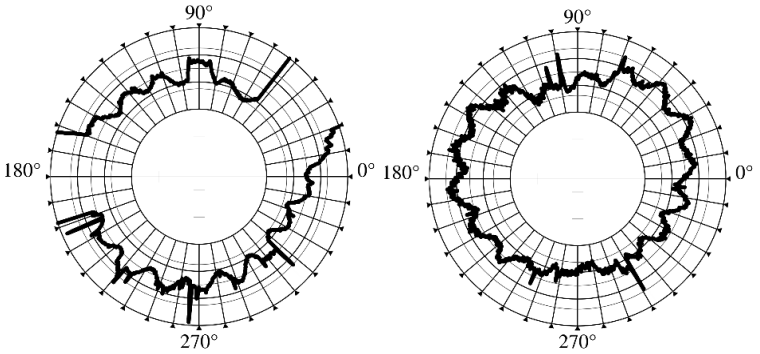

a) b)

Figure 5 – Roundness of surface E (a) and F (b)

Similar phenomena can be observed at the surfaces machined at the higher depth-of-cut and cutting speed. The surface machined at the lower feed rate (G) has more outliers (Fig 6a), and the one (H) machined at the higher feed rate has a higher ovality (Fig 6b), which resulted in 227% higher roundness.

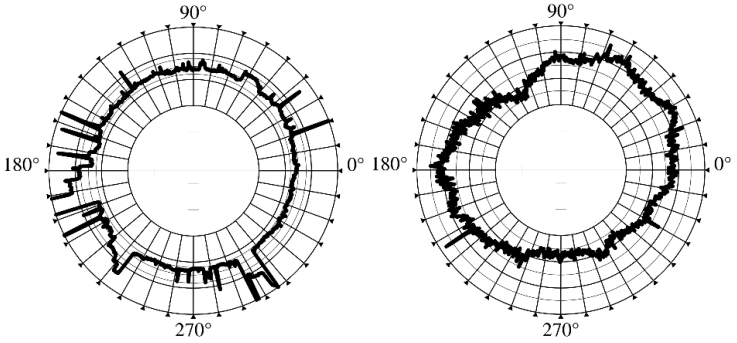

a) b)

Figure 6 – Roundness of surface G (a) and H (b)

3.3. Connections between the roughness and roundness values

In Figs. 7 and 8 the connections between the measured roundness values and each roughness parameter are demonstrated and the separated groups of the results at different feed rates can be observed clearly.

The mean values of the S_a parameter at the lower and higher feed rates are 0.19 and 1.20 μm, respectively (Fig. 7a). The standard deviation values are 0.07 and 0.02 μm, the former can be considered high (relative deviation is 38%). The mean values of the S_z parameter are 1.36 and 5.18 μm at the lower and the higher feed rates, respectively (Fig. 7b). Here, the standard deviations are 0.52 and 0.03 μm, and the former can be considered high (relative deviation is 38%).

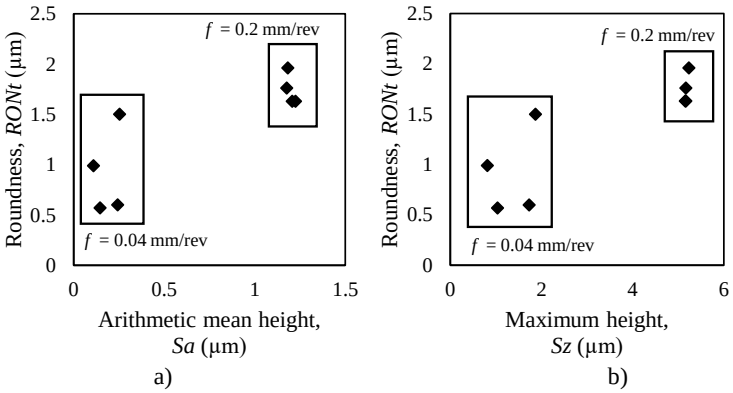

Figure 7 – The roundness and the S_a (a) and S_z (b) values

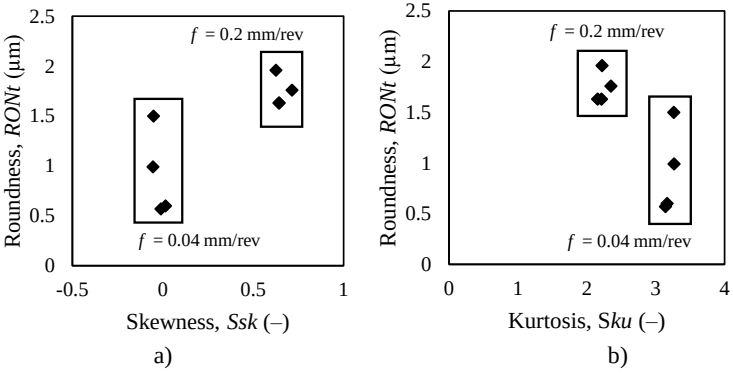

Figure 8 – The roundness and the S_{sk} (a) and S_{ku} (b) values

The mean values of the skewness are -0.03 and 0.66, and the standard deviations are 0.03 and 0.04 at the lower and the higher feed rates, respectively (Fig. 8a). The mean values of the kurtosis are 3.21 and 2.24, and the standard deviations are 0.06 and 0.08 at the lower and higher feed rates, respectively (Fig. 8b). The deviations can be considered low in the case of these two parameters.

The mean values of the roundness are 0.92 and 1.75 μm, and the standard deviations are 0.43 and 0.16 at the lower and higher feed rates, respectively. In the former case the relative deviation is relatively high: 47%.

The correlation (r) between the corresponding parameter pairs were analyzed. The correlation between S_a and the roundness is 0.83 and between S_z and the roundness is 0.85. These indicate not extremely, but strong relationships. These values for the skewness and kurtosis are 0.80 and 0.78, respectively. These indicate slightly weaker but still strong relationships.

The reason for the obtained connections between the roughness and roundness parameters is that at higher feed rate the analyzed roughness parameter values can be separated from each other, and meanwhile the higher feed rate results in higher cutting forces, which cause the deformation of the surface (ovality) or extremely outlying peaks or areas in the surface texture.

4. SUMMARY

Based on a machining experiment (hard turning) and roundness and roughness (S_a, S_z, S_{sk}, S_{ku}) measurements, the effects of the cutting data on the measured parameters were analyzed, and the connections between the roughness and the roundness data were compared. The findings can be interpreted for hard turning and in the analyzed parameter range (a_p = 0.05–0.35 mm; v_c = 120–240 m/min; f = 0.04–02. mm/rev). The main findings are the following:

- The measured S_a and S_z values obtained at the 0.04 mm/rev feed rate are lower than those obtained at 0.2 mm/rev, which strengths the findings of several earlier studies.
- The roundness error of hard turned surfaces is higher if higher feed rate or depth-of cut is applied. The increased error results from the ovality and/or the extreme outliers of the machined surface.
- There are strong relationships (high correlation coefficient) between the analyzed roughness and the roundness values: r = 0.78–0.85.

The limitation of the study is that the machining was carried out in only 8 parameter combinations. More refined results can be obtained by applying more (3 or 4) levels of the cutting data.

References: 1. *Kundrak, J., Mamalis, A.G., Molnar, V.:* The efficiency of hard machining processes, Nanotechnology Perceptions 15, pp. 131–142, 2019. **2.** *Turmanidze, R., Popkhadze, G., Inasharidze, K.:* Improving the performance characteristics of human hip-joint implants by increasing the quality of

processing and geometric accuracy of their spherical surfaces, Cutting and Tools in Technological System 93, pp. 103–113, 2020. **3.** *Kovalev, V., Klymenko, G., Vasylchenko, Y., Shapovalov, M., Antsiferova, O., Maiskykh, I.:* Results of industrial testing of carbide cutting tools by pulsed magnetic field treatment and the effect on the increase of the cutting process efficiency, Cutting and Tools in Technological System 95, pp. 3–12, 2021. **4.** *Bartarya, G., Choudhury, S.K.:* State of the art in hard turning, International Journal of Machine Tools and Manufacture 53(1), pp. 1–14, 2012. **5.** *Kvasnova, P., Kucerka, M., Hruby, D., Novak, D., Novak, V.:* Hardness tests and dimensional and shape precision analysis of construction and agricultural machinery components, Manufacturing Technology 18(6), pp. 943–949, 2018. **6.** *Fedorovich,V., Pyzhov, I., Ostroverkh, Y., Pupan, L., Garachenko, Y.:* Methodology for developing an expert system for the grinding of superhard materials, Cutting and Tools in Technological System 96, pp. 82–88, 2022. **7.** *Sumesh, C.S., Akbar, D.S., Purandharadass, H.S., Chandrasekaran, R.J.:* Optimization of dimensional tolerances and material removal rate in the orthogonal turning of AISI 4340 **steel**, Periodica Polytechnica Mechanical Engineering, 65(3), pp. 205–216, 2021. **8.** *Alok, A., Das, M.:* White layer analysis of hard turned AISI 52100 steel with the fresh tip of newly developed HSN2 coated insert, Journal of Manufacturing Processes 46, pp. 16–25, 2019. **9.** *Chen, L., Tai, B. L., Chaudhari, R. G., Song, X., Shih, A. J.:* Machined surface temperature in hard turning, International Journal of Machine Tools and Manufacture 121, pp. 10–21, 2017. **10.** *Jirapattarasilp, K., Kuptanawin, C.:* Effect of turning parameters on roundness and hardness of stainless steel: SUS 303, AASRI Procedia 3, pp. 160–165, 2012. **11.** *Binali, R., Kuntoglu, M., Pimenov, D.Y., Usca, U.A., Gupta, M.K., Korkmaz, M.E.:* Advance monitoring of hole machining operations via intelligent measurement systems: A critical review and future trends, Measurement 201, art no 111757, 2022. **12.** *Varatharajulu, M., Duraiselvam, M., Kumar, M.B., Jayaprakash, G., Baskar, N.:* Multi criteria decision making through TOPSIS and COPRAS on drilling parameters of magnesium AZ91, Journal of Magnesium Alloys 10, pp. 2857–2874, 2021. **13.** *Du, C., Ho, C.L., Kaminski, J.:* Prediction of product roughness, profile, and roundness using machine learning techniques for a hard turning process, Advances in Manufacturing 9, pp. 206–215, 2021. **14.** *Zolpakar, N.A., Yasak, M.F., Pathak, S.:* A review: use of evolutionary algorithm for optimisation of machining parameters, The International Journal of Advanced Manufacturing Technology 115, pp. 31–47, 2021. **15.** *Cardoso, L.G., Madeira, D.S., Ricomini, T.E., Miranda, R.A., Brito, T.G., Paiva, E.J.:* Optimization of machining parameters using response surface methodology with desirability function in turning duplex stainless steel UNS S32760, The International Journal of Advanced Manufacturing Technology 117, pp. 1633–1644, 2021. **16.** *Bartarya, G., Choudhury, S. K.:* Effect of cutting parameters on cutting force and surface roughness during finish hard turning AISI52100 grade steel, Procedia CIRP 1, pp. 651–656, 2012. **17.** *Ozel, T., Karpat, Y.:* Predictive modeling of surface roughness and tool wear in hard turning using regression and neural networks, International Journal of Machine Tools and Manufacture 45, pp. 467–479, 2005. **18.** *Rehor, J., Fulemova, J., Kutlwaser, J., Gombar, M., Harnicarova, M., Kusnerova, M., Vagaska, A., Povolny, M., Valicek, J., Zatloukal, T.:* ANOVA analysis for estimating the accuracy and surface roughness of precisely drilled holes of steel 42CrMo4 QT, The International Journal of Advanced Manufacturing Technology 126, pp. 675–695, 2023. **19.** *Kundrak, J., Molnar, V., Deszpoth, I.:* Comparative analysis of machining procedures, Machines 6(2), art no 13, 2018. **20.** *Grzesik, W., Zak, K., Kiszka, P.:* Comparison of surface textures generated in hard turning and grinding operations, Procedia CIRP 13, pp. 84–89, 2014. **21.** *Molnar V.:* Tribological properties and 3D topographic parameters of hard turned and ground surfaces, Materials 15(7), art no 2505, 2022. **22.** *Molnar V.:* Asymmetric height distribution of surfaces machined by hard turning and grinding, Symmetry 14(8), art no 1591, 2022. **23.** *Poulachon, G., Moisan, A. L.:* Hard turning: chip formation mechanisms and metallurgical aspects, Journal of Manufacturing Science and Engineering 122(3), pp. 406–412, 2000. **24.** *Farsky, J., Baksa, T., Zetek, M.:* Grinding of maraging steel 1.2709 with SiC grinding wheels and effect of grinding conditions on the surface roughness and wear of the wheels, Manufacturing Technology 20(1), pp. 18–22, 2020. **25.** *Pytlak, B.:* The roughness parameters 2D and 3D and some characteristics of the machined surface topography after hard turning and grinding of hardened 18CrMo4 steel, Archives of Mechanical Technology and Automation 31(4), pp. 53–62, 2011.

26. *Linins, O., Krizbergs, J., Boiko, I.:* Surface texture metrology gives a better understanding of the surface in its functional state, Key Engineering Materials 527, pp. 167–172, 2013. **27.** *Kundrak J., Deszpoth I., Molnar V.:* Decision support method for the applicability of hard turning, Cutting and Tools in Technological System 96, pp. 110–120, 2022. **28.** *Zawada-Tomkiewicz, A.:* Analysis of surface roughness parameters achieved by hard turning with the use of PCBN tools, Estonian Journal of Engineering 17, art no 88, 2011. **29.** *Novak, M.:* Surface quality of hardened steels after grinding, Manufacturing Technology 11(1), pp. 55–59, 2011. **30.** *Kundrak, J., Molnar, V., Markopoulos, A.P.*: Joint machining: Hard turning and grinding, Cutting and Tools in Technological System 90, pp. 36–43, 2019. **31.** *Molnar, V., Szabo, G.:* Designation of minimum measurement area for the evaluation of 3D surface texture, Journal of Manufacturing Processes 83, pp. 40–48, 2022.

Якія Султана, Іштван Станкович, Мішкольц, Угорщина

ПОХИБКА ОКРУГЛОСТІ ТА ТОПОГРАФІЇ ЖОРСТКО ТОЧЕНИХ ПОВЕРХОНЬ

Анотація. *Точність і рельєф є важливими показниками прецизійно оброблених високоякісних поверхонь. Загартована сталь (16MnCr5) була проаналізована для отримання інформації про вплив технологічних даних і зв'язку між проаналізованою точністю (округлість) і параметрами шорсткості (S_a, S_z, S_{sk}, S_{ku}). Було виявлено, що швидкість подачі має значний вплив на параметри округлості та шорсткості, і існують сильні зв'язки між округлістю та цими значеннями параметрів шорсткості: коефіцієнти кореляції коливалися між 0,78 та 0,85. У цьому дослідженні тверді точені поверхні аналізуються з точки зору точності та якості поверхні на основі деяких широко застосовуваних параметрів кваліфікації. Вимірювання округлості та топографії були проведені та порівняні для отримання інформації про вплив параметрів різання. В експерименті використовувалася загартована сталь 16MnCr5, яка широко використовується в автомобільній промисловості. Для отримання точної інформації про якість поверхні було застосовано 3D аналіз топографії. Експеримент проводився на основі факторного плану експерименту та були розраховані основні статистичні показники для детального розуміння зв'язку між округлістю та проаналізованими параметрами шорсткості. На основі експерименту з механічної обробки (жорстке точіння) та вимірювань округлості та шорсткості (S_a, S_z, S_{sk}, S_{ku}) було проаналізовано вплив параметрів різання на виміряні параметри та порівняно зв'язок між даними шорсткості та округлості. Результати можна інтерпретувати для жорсткого точіння та в аналізованому діапазоні параметрів (a_p = 0,05–0,35 мм; v_c = 120–240 м/хв; f = 0,04–0,2 мм/об). Виміряні значення S_a та S_z, отримані при швидкості подачі 0,04 мм/об, нижчі, ніж отримані при 0,2 мм/об, що підтверджує висновки кількох попередніх досліджень. Похибка круглості жорстко точених поверхонь вища, якщо використовується більша величина подачі або глибина різання. Підвищена похибка виникає внаслідок овальності та/або крайніх викидів обробленої поверхні. Існують сильні зв'язки (високий коефіцієнт кореляції) між аналізованими значеннями шорсткості та округлості: r = 0,78–0,85. Обмеження дослідження полягає в тому, що обробку проводили лише за 8 комбінаціями параметрів. Більш точні результати можна отримати, застосовуючи більше (3 або 4) рівнів даних режимів різання.*

Ключові слова: *округлість; 3D рельєф поверхні; жорстке точіння; прецизійна обробка*

UDC 658.511 **doi: 10.20998/2078-7405.2023.98.09**

M. Hermans, P. Tamás, Miskolc, Hungary

IMPROVING THE EFFICIENCY OF MAINTENANCE PROCESS IN MANUFACTURING SYSTEMS USING INDUSTRY 4.0 TOOLS

Abstract. *In ever bigger quest to maximal efficiency, this article wants to show a route for Total Production Maintenance (TPM) at maximal efficiency. By bringing the digital twin into the real world, this essay wants to show how a digital twin can be used as a reliable basis for controlling the running line. But before the digital twin can be used at its maximal potential, a common ground must be defined not only in calculating Overall Equipment Effectiveness (OEE), but also in categorizing TPM tasks according to 3 factors of OEE. The paper outlines the foundations of a new concept that has not been applied in practice.*
Keywords: *TPM; predictive maintenance; executable Digital Twin; OEE.*

6. INTRODUCTION

Not only energy crisis due to the Russian Ukrainian war, but especially the vastly unfolding climate crisis, will force each and every company, independent of its profile and its activities to search for solutions to maximize efficiency and sustainability (1, 2). Maintenance will not be spared from this quest and maintenance teams will be forced to improve the use of their resources to maximal efficiency.

This paper presents a possible road for increasing maintenance efficiency for serial production lines, using industry 4.0 solutions. The chosen concept is however a concept that should be applicable not only to the latest and newest lines but should also find use in older production lines without the hassle of a full-scale renovation, needed to use most recent technologies and so-called smart sensors.

7. TO TPM OR NOT, SHOULD NOT BE THE QUESTION

The seeds of this concept can be found in short book from Mr. Arno Koch, OEE for the production team (4). In this book Mr. Koch mentioned TPM or the time needed for maintenance as a time loss. For him this interval can be defined as an interval where machines are available for production but are not used for the purpose of production. On the other hand, in numerous thesis, papers and works (9-11), as well as in personal experience, TPM can be seen as a way of making unplannable events or at least the loss due to unplannable events, more or almost fully plannable.

Out of the perspective of efficiency, these two ideas are fully contradictive. If one tries to minimize maintenance and reach maximum production efficiency, one

risks unexpected losses. Even the idea of preventive maintenance, especially for serial production with low and very low cycle times, poses a potential risk, because although breakdown is prevented, the standstills can only be predicted on relative short notice.

The idea surveyed in this thesis, is to try and find a break even between on the one side the possibility of reducing maintenance activity and on the other side minimizing losses due to unplannable events by fixed maintenance activities.

8. STRUCTURE OF THE CONCEPT AND PREVIEW OF MAIN ARGUMENTS

The following figure presents the concept of this thesis. The main three pillars, discussed in this order are:

1. a general OEE-Calculator,
2. a graph mapping maintenance task against the 3 factors of OEE
3. an executable Digital Twin, for advice on maintenance tasks.

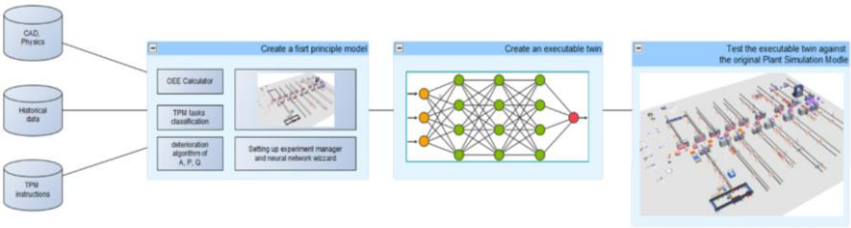

Figure 1 – Proposed solution

8.1. A GENERAL OEE-CALCULATOR

Definition of OEE by Nakajima, S. (1988, Introduction to total productive maintenance, Productivity Press, Inc.): Probability that the machine is producing without any loss (5). If we define the different losses of a production system or unit in the following way:

- $\overline{A_G}$: Planned Losses,
- $\overline{A_U}$: Unplanned Losses,
- $\bar{A}$: Availability Losses, where $\bar{A} = (\overline{A_G} \cup \overline{A_U})$,
- $\bar{P}$: Speed Losses,
- $\bar{Q}$: Quality Losses.

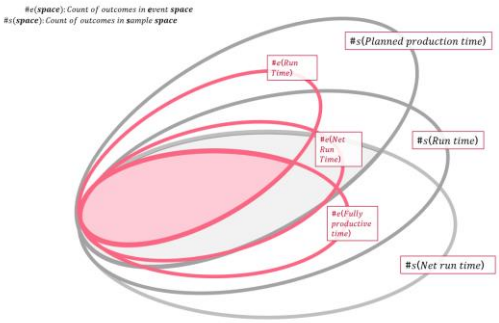

Figure 2 – Explanation on correlation and statistical independence of the 3 factors of OEE (own editing)

OEE can be written as:

$$OEE = 1 - P(\bar{A} \cup \bar{P} \cup \bar{Q})$$

or

$$OEE = P(A \cap P \cap Q)$$

Using the Bayes' theorem, under the condition that the 3 factors are statistical independent, this expression can be rewritten as the general formula for OEE:

$$OEE = P(A) \times P(P) \times P(Q)$$

Formula for OEE, as defined by its inventor (6):

$$OEE = \frac{\#e(Run\ time)}{\#s(Planned\ production\ time)} \times \frac{\#e(Net\ run\ time)}{\#s(Run\ time)} \times \frac{\#e(Fully\ productive\ time)}{\#s(Net\ run\ time)}$$

where:

$$\#e(space): Count\ of\ outcomes\ in\ the\ event\ space$$
$$\#s(space): Count\ of\ outcomes\ in\ the\ sample\ space$$

The decay of OEE and its three factors in time will be used to arrange TPM tasks in order of their importance. To make certain that the results of the simulation can be carried to the real system, a common way of calculating OEE must be defined. This general calculator should respect the following topics:

- the model as well as the real line, should use the same signals and structures to calculate OEE.
- the calculating algorithm should respect the correlation of the three factors as well as their statistical independence of each other.
- the algorithm should not use any predefined or "subjective" parameters, all parameters must be calculated based on the data available.

Plotting the change of throughput against the 3 factors of OEE, each factor has a very distinct signature. And it is this signature, that gives further direction in defining the OEE calculator. During production without loss and during the interval of quality loss, an arithmetic average can be used to describe central tendency, unfortunately this average is not capable of describing the loss during speed loss. In case of performance there is no loss if the production units produce at average throughput. But any deviation from this ideal throughput, will act as punishment and reduce performance and so OEE.

A better indicator would be the median. If we look at the bottleneck of the system, all predecessors and successors will clearly follow the bottleneck, the faster units before the bottleneck will be partly blocked, all faster successors will show an amount of waiting time. The changes in speed are induced on one side by the availability of the different units and here more specific the MTTR (Mean Time To Repair) of the units, on the other side by the buffers between the bottleneck and the faster machines. If we define performance by all cycle times between 0 and 2 times the median, the availability interval is then defined by the sum of the remaining cycle times over 2 times the median. The count of these cycle times is a good indicator for the number of failures and so a good indicator for MTBF (Mean Time Between Failures).

Last but not least remains Quality loss. In this case we have the following possibilities:

1. We have no detection after the unit. In this case we will assume that all parts are passed as iO-parts and the factor is neglected
2. We have post process measurements and parts out of specification will be taken from the system immediately. In this case the loss of this part can cause small performance loss at the successor units.
3. We have in process measurement and tooling is corrected during machining. In this case there is some performance loss at the unit itself as well as with the predecessor and successor units.

In the best case Quality loss can be neglected, in the worst case Quality loss will clutter the measurements and create some error on the observations.

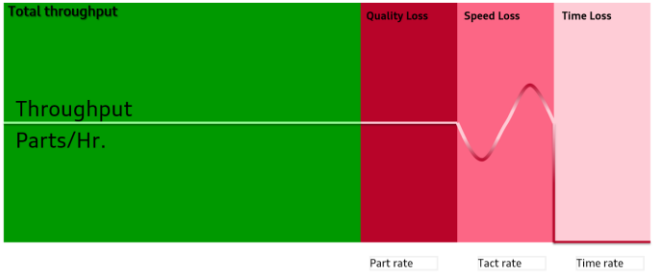

Figure 3 – OEE heartbeat visualizing the loss signatures (own editing)

3.2. MAPPING MAINTENANCE TASK AGAINST THE 3 FACTORS OF OEE

Before we can map each maintenance task against OEE, one first has to position the proposed strategy within existing maintenance strategies. TPM is a basically a form of preventive maintenance. In this type of strategy, the trend is to ensure safety and service maintenance by over-maintaining the asset, thus causing a high economic cost. (Digital Twin for Maintenance: a literature review, 2020)

Within the Industry 4.0 movement, one of the most investigated topics, is the topic of predictive maintenance. In predictive maintenance, we see two different approaches (8). A first approach is a data driven approach, where fast amounts of data are collected and analyzed. The hassle with this approach is not only developing the algorithm for analyzing the data, but also an immense deployment of appropriate sensors for collecting the data needed.

A second approach is a model-driven approach, where a model is developed that describes the asset in a mathematical way. Besides the need of specialized personal to operate the model, another big disadvantage of this approach is the very high cost computationally speaking. The idea of this assay is to use model-driven approach to minimize the economic cost of preventive maintenance, without the need for special trained personnel for operating the model. The executable digital twin will be used to anticipate and to advice on maintenance tasks, based on evidence of degradation and deviation from the normal behavior of the line modeled.

A first step in classifying maintenance tasks, can be found within the eight pillars of TPM. Each task can be classified as either autonomous maintenance or maintenance done by the operators or on the other hand as planned maintenance or maintenance done by the maintenance team. The main difference lays in interval

length. Autonomous maintenance tasks are tasks that will return every hour, every shift, every day. The cycle is relatively short, and the loss of time is minimal and can be expressed in minutes. On the other hand, planned maintenance tasks have a relative long interval, every week, every month, every 6 months or year. Their duration or time loss is also more elaborated and may range from 15 minutes to half a day or even a full day.

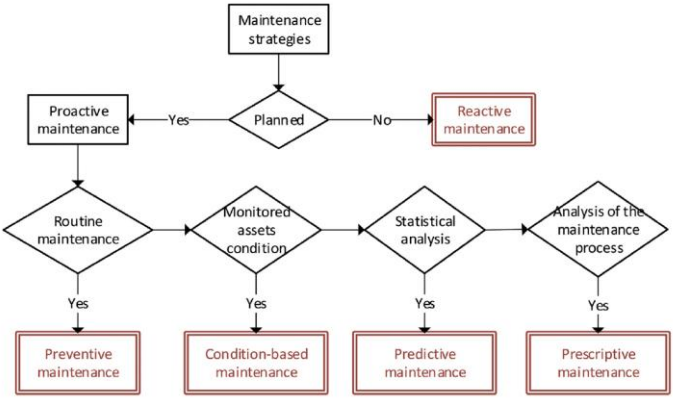

Figure 4 – Maintenance strategies diagram (7)

A second classification, also supported in literature, can be made on the their influence on MTTR and/or MTBF . Expected is that each task will influence MTTR (Mean Time To Repair) and MTBF (Mean Time Between Failure) at the same time. The idea is to combine interval length, duration, influence on MTTR and influence on MTBF by means of fuzzy logics techniques. Over the fuzzifier and the defuzzifier the four factors will be condensed into 1 factor which expresses the decay of OEE, Availability and/or Performance.

Although each maintenance task will probably get its own unique decay factor, it is not the idea to run the model for each unique factor several times. The values will be grouped in buckets and for each bucket several runs will be made to find a breakeven between loss of time and not doing certain group of activities. It is the historic data that these models will produce, which are of importance to the next phase.

3.3. THE EXECUTABLE DIGITAL TWIN, XDT

Although the previous steps do find support in literature, this last step makes the study unique. In this step we will harvest the full power of the digital twin, by integrating the digital representation of the production system with the operational environment in which it operates. In other words, we will use the digital twin as a

tool of real-time monitoring, rather than just a simulation or planning tool (8). By extracting a dedicated encapsulation from the digital twin, which models the decay of OEE and the 3 factors, we can create an executable representation that can be integrated into the operational execution environment of the physical asset it represents.

An executable digital twin should comply with following expectations:

- The response time of the digital twin should be minimal, preferred within seconds, eventually minutes,
- The digital twin is restricted to one certain element of interest, in this case the decay of OEE,
- The digital twin should be easily accessible from any controller,

Within industry 4.0 tools, neural networks offer themselves as a good solution. Furthermore, the Plant Simulation framework offers besides the experiment manager also a neural network wizard, simplifying the work of building and training a neural network. By use of the available wizards, all efforts can be shifted onto positioning the neural network outside plant simulation. And also, here Siemens offers with Mendix and the Mendix ML Kit a good solution to implement the idea at high speed.

9. SUMMARY

In the essay, we have discussed the concept of improving the efficiency of maintenance processes in manufacturing systems using Industry 4.0 tools. Several important aspects of the concept were touched, including categorizing TPM tasks in availability, performance, and quality; creating a standard algorithm for calculating OEE; building a model to mimic the decay of OEE based on changes in TPM task frequency; using historic data to train a neural network to prioritize TPM tasks based on continuous OEE monitoring; and the differences between TPM and predictive maintenance.

The main object of this essay is to highlight the importance of TPM in promoting sustainability and improving the efficiency of maintenance processes in manufacturing systems. By using Industry 4.0 tools like neural networks and simulation models, companies can prioritize TPM tasks and reduce the amount of maintenance resources needed, ultimately leading to increased productivity and profitability.

References: 1. *Chiara F., Benoit I., Salvatore M., Stefano R. (2018):* Maintenance for Sustainability in the Industry 4.0 context: a Scoping Literature Review 903-908. IFAC-PapersOnLine, 51 (11) https://doi.org/10.1016/j.ifacol.2018.08.459 **2.** *Molnár V., Szabo G., Kundrak J. (2018):* Waste reduction possibilities in a manufacturing process Rezanie i Instrumenty v Tekhnologicheskih Sistemah 89, pp. 109–116. **3.** *Krupitzer C., Wagenhals, T., Züfle M. Lesch, V., Schäfel D., Mozaffarin A., Edinger J., Becker C. Kounev, S. (2020).:* A Survey on Predictive Maintenance for Industry 4.0. ResearchGate, https://www.researchgate.net/publication/339374836_A_Survey_on_Predictive_Maintenance_for_Industry_4

0. **4.** *Koch, A. (2008).:* OEE für das Produktionsteam: Das vollständige OEE-Benutzerhandbuch oder wie Sie die verborgene Maschine entdecken. CETPM Publishing. ISBN 9-783940-775-04-7. **5.** *Nakajima, S. (1988).:* Introduction to TPM: total productive maintenance.(Translation). Productivity Press, Inc., 1988, 129. **6.** *E. Kreyszig (2006).:* Advanced engineering mathematics, 9th edition. John Wiley & Sons. **7.** *Itxaro E., Sergio B., Saioa A. (2020).:* Digital Twin for maintenance: A literature review. Computers in Industry Volume 123, December 2020, 103316, https://doi.org/10.1016/j.compind.2020.103316 **8.** *D. Hartmann and H. Van der Auweraar (2022).* The executable Digital Twin: merging the digital and the physics worlds. ResearchGate. https://www.researchgate.net/publication/364953428_The_Executable_Digital_Twin_merging_the_digital_and_the_physics_worlds. **9.** *Budai-Balke, G., Dekker, R., & Nicolai, R. P. (2006).:* A review of planning models for maintenance and production. Report/Econometric Institute, Erasmus University Rotterdam, (EI 2006-44). https://repub.eur.nl/pub/8022/ei2006-44.pdf. **10.** *Kobbacy, K. A., Murthy, D. P., Budai, G., Dekker, R., Nicolai, R. P. (2008).* :Maintenance and production: a review of planning models. Complex system maintenance handbook, pp. 321–344. Springer-Verlag London Limited. ISBN 978-1-84800-010-0. **11.** *Aghezzaf, E. H., Jamali, M. A., Ait-Kadi, D. (2007).:* An integrated production and preventive maintenance planning model. European journal of operational research, 181(2), pp. 679–685. https://doi.org/10.1016/j.ejor.2006.06.032.

Марк Германс, Петер Тамаш, Мішкольц, Угорщина

ПІДВИЩЕННЯ ЕФЕКТИВНОСТІ ПРОЦЕСУ ТЕХНІЧНОГО ОБСЛУГОВУВАННЯ У ВИРОБНИЧИХ СИСТЕМАХ ЗА ДОПОМОГОЮ ІНСТРУМЕНТІВ ІНДУСТРІЇ 4.0

Анотація. *У цій статті представлено можливий шлях підвищення ефективності технічного обслуговування серійних виробничих ліній за допомогою рішень індустрії 4.0. Повне виробниче обслуговування (ПВО) або час, необхідний для обслуговування, як втрату часу можна визначити як інтервал, коли машини доступні для виробництва, але не використовуються для цілей виробництва. З іншого боку, ПВО можна розглядати як спосіб зробити непланові події або, принаймні, втрати через непланові події, більш або майже повністю. плановий. З точки зору ефективності ці дві ідеї повністю суперечать один одному. Якщо хтось намагається мінімізувати технічне обслуговування та досягти максимальної ефективності виробництва, то ризикує отримати несподівані втрати. Навіть ідея профілактичного обслуговування, особливо для серійного виробництва з малим і дуже коротким часом циклу, становить потенційний ризик, тому що, хоча поломка запобігає, простої можна передбачити лише за відносно короткий термін. Ідея, розглянута в цій статті, полягає в тому, щоб спробувати знайти розбіжність між можливістю скорочення технічного обслуговування, з одного боку, і мінімізацією втрат через непланові події, з іншого боку, завдяки постійній технічній діяльності. Були обговорені кілька важливих аспектів концепції, включаючи класифікацію завдань ПВО за доступністю, продуктивністю та якістю; створення стандартного алгоритму розрахунку загальної ефективності обладнання (ЗЕО); створення моделі для імітації розпаду ЗЕО на основі змін у частоті завдань ПВО; використання історичних даних для навчання нейронної мережі визначати пріоритетність завдань ПВО на основі постійного моніторингу ЗЕО; і відмінності між ПВО і прогнозним обслуговуванням. Використовуючи такі інструменти Industry 4.0, як нейронні мережі та симуляційні моделі, компанії можуть визначати пріоритетність завдань ПВО і зменшувати кількість необхідних ресурсів для обслуговування, що в кінцевому підсумку призводить до підвищення продуктивності та прибутковості.*

Ключові слова: *ПВО; прогнозне обслуговування; виконуваний Digital Twin; ЗЕО.*

UDC 621.791.389 **doi: 10.20998/2078-7405.2023.98.10**

V. Tonkonogyi, O. Stanovskyi, M. Holofieieva,
O. Levynskyi, S. Klimov, Odesa, Ukraine

INCREASING THE ACCURACY OF DEFECTOSCOPY BY THE METHOD OF ACTIVE THERMOGRAPHY OF PRODUCTS MADE OF NON-METALLIC HETEROGENEOUS MATERIALS AND USED IN ENGINEERING

Abstract. *Nowadays, non-metallic heterogeneous materials are widely used in mechanical engineering, which is primarily due to their unique properties, such as strength, light weight, corrosion resistance, and high vibration, sound, and heat insulation characteristics. At the same time, non-destructive control methods that would allow to obtain the most complete picture of the defective state of products made of such materials are of great importance. The main task of the work is the development of optimal algorithms for determining each defect of a product made of non-metallic heterogeneous material with the establishment of its exact location, including the depth of occurrence, as well as its geometric parameters. The method of thermal non-destructive testing is considered promising. Studies of the accuracy of determining the parameters of defects in non-metallic heterogeneous materials by the specified method have been carried out.*
Keywords: *non-metallic heterogeneous materials; thermal control method; flaw detection; infrared equipment.*

1. INTRODUCTION

Nowadays, non-metallic heterogeneous materials are widely used in mechanical engineering, aerospace engineering, and other sectors of the economy, which is primarily due to their unique properties, such as strength, light weight, corrosion resistance, and high vibration and sound, thermal insulation characteristics. At the same time, such materials are characterized by specific technological and operational defects. First of all, this applies to delaminations that are visually imperceptible, but can lead to a serious weakening of the structure and, as a result, cause the failure of a product made of non-metallic heterogeneous material [1]. Taking into account the responsibility of the assignment of nodes and aggregates, especially in aircraft structures, non-destructive control methods that would allow obtaining the most complete picture of the defective state of products made of non-metallic heterogeneous materials are of great importance.

The main task of the work is the development of optimal algorithms for determining each defect of a product made of non-metallic heterogeneous material with the establishment of its exact location, including the depth of occurrence, as well as its geometric parameters. To date, the method of thermal non-destructive

testing is considered to be one of the most promising for flaw detection of products from the specified class of materials [2]. This type of flaw detection is based on visualization of the thermal field of the surface of the research object using infrared equipment and analysis of anomalies of this field.

2. LITERATURE REVIEW

As a rule, temperature fields arise as a result of thermal stimulation of the material (active thermal control). However, sometimes they are formed as a result of the operation of the product being diagnosed (passive thermal control). The work considers active thermal control, in which thermal energy is excited by heating the surface with a single thermal pulse or their sequence. In this case, the amplitude and time parameters of the thermal field at each point of the surface of the control object carry information about the presence and geometric characteristics of defects [3].

There are several methods of stimulating thermal energy in objects during real research. The most convenient and closest to the conditions of measuring products in mechanical engineering and aviation engineering is the so-called one-sided control mode, in which heating and registration of a thermal image in the form of a thermogram is carried out from the same side of the defectoscopy object [4]. Figure 1 shows a diagram of the location of the research object and the means by which flaw detection is carried out.

With this approach, temperature changes on the surface of the sample under study are analyzed in the defect-free zone $T_{fl} = f(x, y, t)$ and in the projection of the defect $T_f = f(x, y, t)$ after heating the surface with a single thermal pulse of finite length t. Figure 2 [4] schematically shows the change in the temperature of the surface of the tested sample in the defective and defect-free zones during the implementation of one-sided excitation of thermal energy during

It is clear that during heating, the excess temperature of the investigated surface increases and reaches its maximum value at the moment of time t, which, according to Figure 2, corresponds to the end of the thermal pulse. During the cooling of the surface of the object, in the process of propagation of the heat wave through the volume of the material and heat exchange with the environment, the excess temperature decreases to zero. At the same time, there is a difference in excess temperatures and the speed of their change in defect-free and defective zones [2].

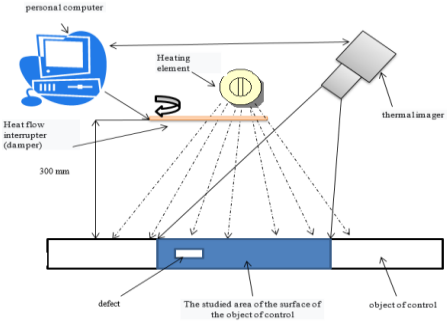

Figure 1 – The scheme of conducting active thermal imaging control

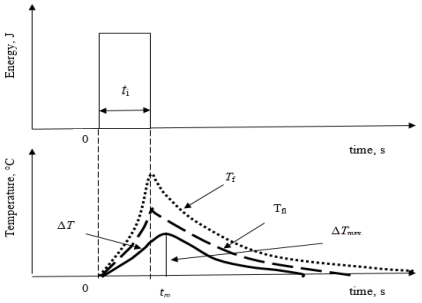

Figure 2 – Changes in the temperature of the surface of the research object over the defective and defect-free zones during unilateral thermal imaging control

This is due to the difference in thermophysical properties in the specified zones and, as a result, different conditions of heat wave propagation. In the zone above the defect, the regular nature of the thermal field changes, and so-called temperature anomalies appear, which are characterized by an absolute temperature contrast, i.e., the temperature difference in the defective and defect-free zones $\Delta T = f(x, y, t)$, which can be defined as follows:

$$\Delta T(x,y,t) = T_f(x,y,t) - T_{fl}(x,y,t), \quad (1)$$

It should be noted that depending on the ratio of thermal conductivities in the defective and defect-free zones, $\Delta T = f(x, y, t)$ can have both a positive and a negative value. With this definition, $\Delta T > 0$ for defects whose thermal conductivity is lower than the thermal conductivity of the main non-metallic heterogeneous

material. Accordingly, if the defects are more thermally conductive than the main material, then $\Delta T < 0$. It is even possible to invert the sign of ΔT during cooling [4].

The dependence of the temperature contrast on time has an extremum ΔT_{max} at the moment of time t_m, which is the optimal time for observing the defect. Both of these parameters are the main parameters of the amplitude method of thermal control and depend not only on the thermophysical characteristics of the studied non-metallic heterogeneous material, but also on the depth of embedment and the size of the defect itself [5].

In [4] it is shown that for a semi-infinite object that is heated by a Dirac pulse, the optimal time for observing an internal defect in the form of a material discontinuity can be determined as the time it takes for the heat wave to reach the defect, reflect from it, and return back, that is:

$$t_m = \frac{l^2}{a} = \frac{l^2 \cdot c \cdot \rho}{\lambda}, \tag{2}$$

where l – the depth of the defect;
a – coefficient of thermal conductivity;
c – heat capacity;
ρ – density;
λ – thermal conductivity coefficient.

Expression (2) can be used for a very short thermal pulse, i.e. $t_m >> t_i$, which is quite difficult to implement in practice ($t_i \approx 10$ μs). If the pulse length is commensurate with the optimal defect observation time, then the estimation formula [2] can be used:

$$l^2 = a \cdot (t_m - t_i) \tag{3}$$

3. MAIN MATERIAL PRESENTATION

In the work, carbon fiber samples with a thickness of 4 mm were studied, in which defects in the form of layers were specially formed at various depths (air gaps up to 0.2 mm thick and with an area of more than 1.5 cm^2), which are the most common types of defects for the class of materials that is considered The minimum depth of defects is $l \approx 1$ mm. Taking into account the passport data of the coefficient of thermal conductivity for carbon-plastics in the transverse direction of the layers $a \approx 4.5 \cdot 10^7$ m^2/s, the maximum length of thermal pulses, which is necessary for thermal stimulation of the defect in the structure of such a material $t_i \leq 1$ s. This makes it possible not to use expensive xenon flash lamps, which are traditional for generating a heat wave during active thermal control of metals and metal composite materials. In the experiment, for this purpose, an electric heater

with a mechanical interrupter of the heat flow in the form of a movable flap (Fig. 1) was used, which allowed the formation of heat pulses with a length of (0.5...20) s. thermal radiation power density $P \approx 10^4$ W/m^2.

It should be noted that the studied surfaces are characterized by relatively low relaxation rates of excess temperature fields. This made it possible to use infrared devices without special requirements for their speed. In the experiment, a thermal imager with a frame rate of ≈ 1 Hz was used.

Among the advantages of infrared technology devices used in thermal control, in addition to non-contact and fast operation, it is also necessary to include high resolution, which ensures the detection of local temporary temperature contrasts on the surface of the investigated objects [6]. Given that the accuracy of flaw detection of products made of non-metallic heterogeneous materials by the amplitude thermal method (measurement of maximum temperature contrasts) is determined by the accuracy of the used thermal imagers, it is necessary to pay attention to instrumental and methodical measurement errors.

A significant drawback of non-contact methods of measuring temperature using infrared devices is the lack of data on the emissivity of the surface of the research object under experimental conditions. The object's ability to emit infrared radiation can vary, as it depends not only on the material itself, but also on the properties of the surface (for example, roughness, the presence of dirt, oil films, etc.) and the direction of observation of this surface [7, 8]. It is the uncertainty in setting the coefficient of emissivity of the surface of the research object that is the main difficulty in temperature calculations based on the results of thermal imaging measurements. And, therefore, this introduces an additional methodical error into the results of determining the depth of defects in non-metallic heterogeneous materials.

Therefore, before conducting studies of thermal processes on the surfaces of samples for the purpose of their defectoscopy, the coefficient of surface emissivity was determined at reference points. The latter necessarily included surface points with a surface condition different from the basic one. For example, with a different roughness, the presence of scratches, coatings, films and the like, which could be perceived as defects according to the thermogram. This operation must be carried out during defect inspection of products that were in use, since the state of the surface at different points can be significantly different from each other.

Determination of the emissivity coefficient was carried out in the following order. In the characteristic zone of the studied surface without temperature anomalies, reference points were chosen, the temperatures of which were measured by a contact thermometer (thermocouple). At these same points, the temperature was measured with a thermal imager with preset shooting parameters (reflected background temperature, ambient temperature and humidity, distance to the research object). In the event that a difference in the results of temperature

measurement by the contact and non-contact method was recorded, such 9a value of the emissivity coefficient was selected from the panel of the thermal imager, which reduced this difference to zero. The value of the emissivity coefficient obtained in this way was taken as a characteristic of the surface at the investigated reference point and used in further thermal imaging control.

There is one more factor that significantly affects the result of temperature measurement by infrared devices. In work [7], studies the influence of the observation angle on the coefficient of emissivity perceived by measuring equipment were carried out. It can be seen from Figure 1 that during flaw detection of products by amplitude thermal imaging control with one-sided access to the research surface, it is practically impossible to ensure the normality of the location of the thermal imager in relation to the investigated area.

Therefore, to increase the accuracy of determining the depth of occurrence and parameters of defects of products made of non-metallic heterogeneous materials, the influence of the angle at which the measuring device is located to the surface of the object under investigation should be taken into account.

For metals, the emissivity coefficient is constant in the range of viewing angles 0...40º, for dielectrics (which in most cases include non-metallic heterogeneous materials) - in the range of angles 0...60º. Beyond these ranges, the emissivity coefficient changes significantly when observing tangentially [9].

The calculation of the actual surface temperature, in which the influence of the observation angle on the measurement accuracy is taken into account, was carried out according to the expression [10]:

$$T_{fact} = \frac{T_{rad}}{\sqrt[4]{\frac{\varepsilon_{mea}}{K_{ang}}}} \tag{4}$$

where T_{fact} – the actual temperature of the surface of the control object;
T_{rad} – radiant temperature perceived by a thermal imager;
ε_{mea} – the measured value of the emissivity coefficient;
K_{ang} – coefficient of influence of the observation angle.

For dielectrics, the dependence of K_{ang} on the observation angle is most accurately described by the expression [10]:

$$K_{ang} = -0{,}0014 \cdot \varphi^3 + 0{,}022 \cdot \varphi^2 - 0{,}1 \cdot \varphi + 1{,}1 \ , \tag{5}$$

where φ – the angle of observation of the studied area of the surface of the control object.

With the help of the described method, thermal imaging studies of control carbon-plastic samples were carried out; in this study, the peculiarities of

temperature distribution in the defective zone were studied. An analysis of the texture of the temperature field in the delamination type defect zone and defect-free zones was carried out. Figure 3 shows the thermogram of the investigated surface and graphs of changes in temperature contrasts at the specified points of the surface over time.

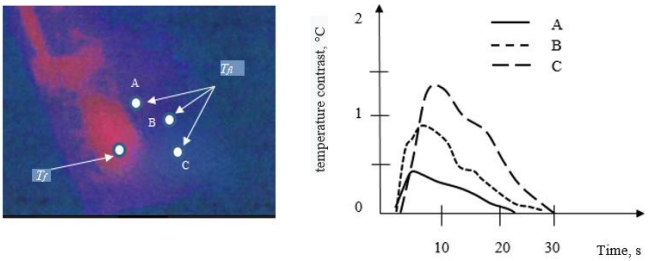

Figure 3 – Thermogram of the studied surface and graphs of changes in temperature contrasts at the specified points of the surface over time

It can be seen from the figure 3 that the change in the contrast amplitudes at the time t_m of optimal observation of the defect depends on the position of the defect-free zone relative to the temperature anomaly (defect area). Accordingly, the calculated value of the depth of the defect is changed. Obviously, given that the conditions of heat removal in zones A, B, and C are the same, it can be concluded that such a difference in the readings is caused by the presence of a methodical error from not taking into account the difference in the coefficients of the emissivity of the surface at the reference points.

4. CONCLUSIONS

As a result of the conducted studies of thermal processes on the surface of control carbon-plastic samples, it was possible to detect the majority of defects (the equipment used did not allow detecting 7% of embedded defects). At the same time, thanks to the use of the proposed method of eliminating the methodical error caused by the difference in the emissivity coefficient at the investigated points of the surface, it was possible to increase the accuracy of determining the depth of the defects.

References: 1. *Bezimyanniy Yu.G.* Acoustic control of materials with a developed mesostructure *Physico-chemical mechanics of materials* - 2007. – No. 4. – pp. 53–65. **2.** *E.Yu. Gordienko, N.I. Glushchak, Yu.V. Fomenko, G.V. Shustakova, I.I. Dzeshulskaya, Yu.F. Ivanko* Diagnostics of composite materials of aircraft elements by active thermography *Nauka innov*: 2018, 14(2). – pp. 39–50. **3.** *Vavilov*

V.P. Thermal control of aerospace products *In the world of non-destructive testing*. 2003. T20, No. 2. pp. 4–10. **4.** *Vavilov V.P.* Infrared thermography and thermal control. Moscow: Spectrum. 2009. 544 p. **5.** *Maldague X.P.* Theory and Practice of Infrared Technology for Nondestructive Testing. *New-York: John Willey & sons*, 2001. 682 p. **6.** *Oborskyi G.O., Levynskyi O.S., Holofieieva M.O.* Study of the influence of the emissivity of materials on the accuracy of the thermal imaging control method *Technological audit and reserves of production*. – No. 2/3(28), 2016 – pp. 4–7. **7.** *Oborskyi G., Levynskyi O., Holofieieva M.* The effect of surface observation angle on accuracy of non-contact temperature measurement method // *Technological audit and reserves of production*. – №1/2(33), 2017 – pp. 19–23. **8**. *Molnar, V., Sztankovics, I.*: Analysis of Roughness Parameters Determining Tribological Properties in Hard Turned Surfaces, Hungarian Journal of Industry and Chemistry 49(2), pp. 77–84, 2021. **9.** *Gossorg, J.* Infrared thermography. Basics. Technique. Application – M. : Mir, 1988 – 416 p. **10.** *Levynskyi O.S., Holofieieva M.O., Babich Yu.I.* The influence of the observation angle on the accuracy of the thermal imaging method of measurement *Measuring and computing equipment in technological processes*, – No. 2(55), 2016. – pp. 51–54.

Володимир Тонконогий, Олександр Становський, Марина Голофєєва,
Олександр Левинський, Сергій Клімов, Одеса, Україна

ПІДВИЩЕННЯ ТОЧНОСТІ ДЕФЕКТОСКОПІЇ МЕТОДОМ АКТИВНОЇ ТЕРМОГРАФІЇ ВИРОБІВ З НЕМЕТАЛЕВИХ ГЕТЕРОГЕННИХ МАТЕРІАЛІВ, / ЩО ВИКОРИСТОВУЮТЬСЯ В ТЕХНІЦІ

Анотація. *Нині неметалеві гетерогенні матеріали широко використовуються в машинобудуванні, що пов'язано, перш за все, з їх унікальними властивостями, такими як міцність, мала вага, корозійна стійкість, високі вібро-, звуко- і теплоізоляційні характеристики. При цьому неабиякого значення набувають методи неруйнівного контролю, що дозволяють отримати найбільш повну картину дефектного стану виробів із таких матеріалів. Основною задачею роботи є розробка оптимальних алгоритмів визначення кожного дефекту виробу з неметалевого гетерогенного матеріалу з встановленням точного його розташування, в тому числі, глибини залягання, а також його геометричних параметрів. На сьогоднішній день одним з найбільш перспективних для дефектоскопії виробів із зазначеного класу матеріалів вважається метод теплового неруйнівного контролю. Цей вид дефектоскопії базується на візуалізації теплового поля поверхні об'єкта дослідження за допомогою приладів інфрачервоної техніки та аналізу аномалій цього поля. В роботі досліджувалися вуглепластикові зразки товщиною 4 мм, в яких на різноманітній глибині були спеціально сформовані дефекти у вигляді розшарувань (повітряні зазори товщиною до 0,2 мм та площею більше 1,5 см^2), які є одними з найбільш поширених видів дефектів для класу матеріалів, що розглядається. Вивчені особливості розподілення температури в дефектній зоні. Проведено аналіз текстури температурного поля в зоні дефекту типу розшарування та в бездефектній зоні. Проведено дослідження точності визначення параметрів дефектності неметалевих гетерогенних матеріалів зазначеним методом. В результаті проведених досліджень теплових процесів на поверхні контрольних вуглепластикових зразків вдалося виявити більшість дефектів (використовувана апаратура не дозволила виявити 15 % закладних дефектів). При цьому, завдяки використанню запропонованої методики виключення методичної похибки, що викликана відмінністю коефіцієнту випромінювальної здатності в досліджуваних точках поверхні, вдалося підвищити точність встановленні глибини залягання дефектів.*

Ключові слова: *неметалічні різнорідні матеріали; метод теплового контролю; дефектоскопія; інфрачервоне обладнання.*

UDC 620.179.118 **doi: 10.20998/2078-7405.2023.98.11**

I. Sztankovics, Miskolc, Hungary

ANALYSIS OF SELECTED FUNCTION-DEFINING 2*D* SURFACE ROUGHNESS PARAMETERS IN TANGENTIAL TURNING

Abstract. *Among other, more frequently analysed surface topography parameters, the function-defining parameters must be analysed in different machining procedures to outline their application possibilities. These values are the core roughness, the reduced peak height, the reduced valley depth, the skewness, and the kurtosis of the roughness profiles. Tangential turning is a promising machining procedure, which can produce ground-like surfaces with twist-free properties by defined cutting edged tools. The achievable productivity is also very high. Therefore, in this paper, these roughness parameters were analysed from 2D roughness profiles measured on surfaces machined by tangential turning.*
Keywords: *functional parameters; kurtosis; skewness; tangential turning.*

1. Introduction

Machining with tangential turning [1] is analysed in this paper in the point of view of the functional parameters of the surface. Among others Molnár also proved [2,3], that between the frequently analysed surface topography parameters, the extent of the R_k parameters is equally significant. This cutting procedure has many advantageous properties. It can be an alternative to rotational turning in machining of outer cylindrical surfaces [4,5] because twist-free surfaces are achievable [6]. Leichner et al. proved in their study that oil leakage, wear of the tool and machining costs can be reduced, when tangential turning is applied on sealing surfaces [7]. The combined procedure, where turning and grinding is done in one clamping, can be a good alternative [8], however MQL technique can be applied in tangential turning. Better tool life can be achieved than in traditional turning due to the different insert and feed motion [9]. The application of tangential turning is widely developed by machine tool manufacturers as well (e. g. EMAG [10]).

In this paper, the function defining parameters of the roughness profile are studied in tangential turning by changing the cutting speed, feed, and depth of cut. The core roughness, the reduced peak height, the reduced valley depth, the skewness, and the kurtosis of the roughness profiles were measured and analysed. During the measurement, the recommended adjustment values are set [11,12].

2. Experimental conditions and methods

The aim of this study was the analysis of the function defining surface parameters in tangential turning. Cutting experiments were carried out to achieve this goal. The tools used during the experiments was the following. A tangential

tool with 45° inclination angle was used. The indexable turning tool is made by HORN Cutting Tools Ltd. and consisted of two parts S117.0032.00 insert and H117.2530.4132 holder. The working part of the tool was an uncoated carbide insert (MG12 grade). In the experiments, a cylindrical workpiece is machined, which outer diameter was 70 mm. The chosen material was 42CrMo4 grade alloyed steel, which processed by hardening heat treatment to 60 HRC hardness before the experiments. The tangentially turned surfaces was prepared before the experiments by turning with a standard CNMG 12 04 12-PM 4314 cutting insert made by SANDVIK Coromant, which was put into a PCLNR 25 25 M12 tool holder. An EMAG VSC 400 DS hard machining centre was applied for the study.

I aimed to analyse the alteration effect of the setup parameters of tangential turning, therefore the cutting speed (v_c), the feed per workpiece revolutions (f) and the depth of cut (a) were changed during the experiments. A lower and an upper limit value were chosen for each studied parameter. The lower value range of the parameters are aimed in this study in the initial research of the topic. Therefore, the cutting speed was chosen to be 100 m/min and 200 m/min, the feed was set to 0.3 mm and 0.6 mm. Two kinds of depth of cut were also chosen: 0.1 mm and 0.2 mm. This limit values resulted in 8 different setups, which can be seen in Table 1.

Table 1 – Experimental setups

Setup	1	2	3	4	5	6	7	8
v_c [m/min]	100	200	100	200	100	200	100	200
f [mm]	0.3	0.3	0.6	0.6	0.3	0.3	0.6	0.6
a [mm]	0.1	0.1	0.1	0.1	0.2	0.2	0.2	0.2

The necessary measurements were carried out after the experiments with an AltiSurf 520 three-dimensional topography measuring instrument using a confocal chromatic probe. The measurement variables were chosen according to ISO 4288:1996 standard. In this paper, the 2*D* roughness parameters describing the functional properties of the surfaces were evaluated.

The analysed parameters were (ISO 13565-2:1996 and ISO 4287:1997):

- R_k – Core Roughness, is a measure of the core (peak to valley) roughness of the surface [μm]
- R_{pk} – Reduced Peak Height, is a measure of the peak height above the core roughness [μm]
- R_{vk} – Reduced Valley Depths, is found from a measure of the valley depths below the core roughness [μm]

- R_{sk} – Skewness of the assessed profile [-]
- R_{ku} – Kurtosis of the assessed profile [-]

3. Experimental results

The experiments were carried out with the planned setups. Figure 1 shows an example of the measured roughness profile and the assessment of the R_k parameters in case of Setup 8. The Bearing Area Curve based on the ISO 13565-2:1996 standard, and the core roughness, reduced peak height and valley depths are calculated for each measurement. The skewness and kurtosis parameters are calculated from the profiles according to ISO 4287:1997. Each machined workpiece was measured three times and the average values of the registered values were calculated. These results are shown in Table 2.

Table 2 – Measurement results

Setup	1	2	3	4	5	6	7	8
R_k [µm]	7.00	4.48	4.07	9.75	1.09	0.91	1.29	1.26
R_{pk} [µm]	1.33	0.98	0.89	1.83	0.60	0.36	0.69	0.55
R_{vk} [µm]	3.75	2.16	1.58	2.63	1.12	0.40	0.36	0.35
R_{sk} [-]	-0.45	-0.50	-0.38	-0.18	-0.23	-0.99	0.49	0.26
R_{ku} [-]	2.98	2.66	2.90	2.40	2.33	5.82	2.81	2.90

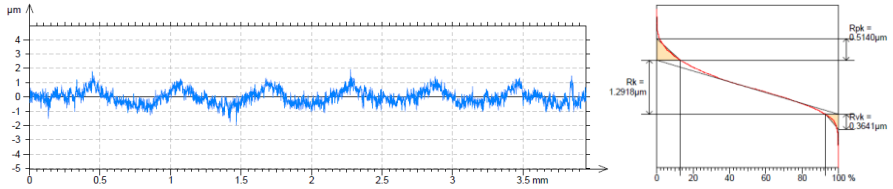

Figure 1 – Example of the measured 2*D* profile and the evaluation of the R_k parameters

4. Discussion

The three R_k parameters were analysed based on the graphs shown in Figure 2. Here the green points represent the 100 m/min cutting speeds while the red points show the values measured after the machining with 200 m/min. The four directions represent four different parameter combination. The feed increases in the bottom

left direction while the depth of cut increases in the bottom right direction. Based on these graphs, a complex analysis can be done on these parameters.

Increasing the cutting speed results in lower values of these three parameters. This conclusion shows, that in the viewpoint of the R_k parameters, the material removal is better in 200 m/min cutting speed. This is caused by the increased rate of plastic strain, which results a more favourable plastic deformation.

As the analysis of the other two setup parameters, it can be seen, that the increase of the depth of cut results in lower values of the studied roughness parameters. Higher depth of cut means higher chip width, which also improves the material removal in the chip root. The increase of the feed resulted in a more different effect. The reduced valley depth decreases while the core roughness and the reduced peak height increases, if we increase the feed from 0.3 mm to 0.6 mm.

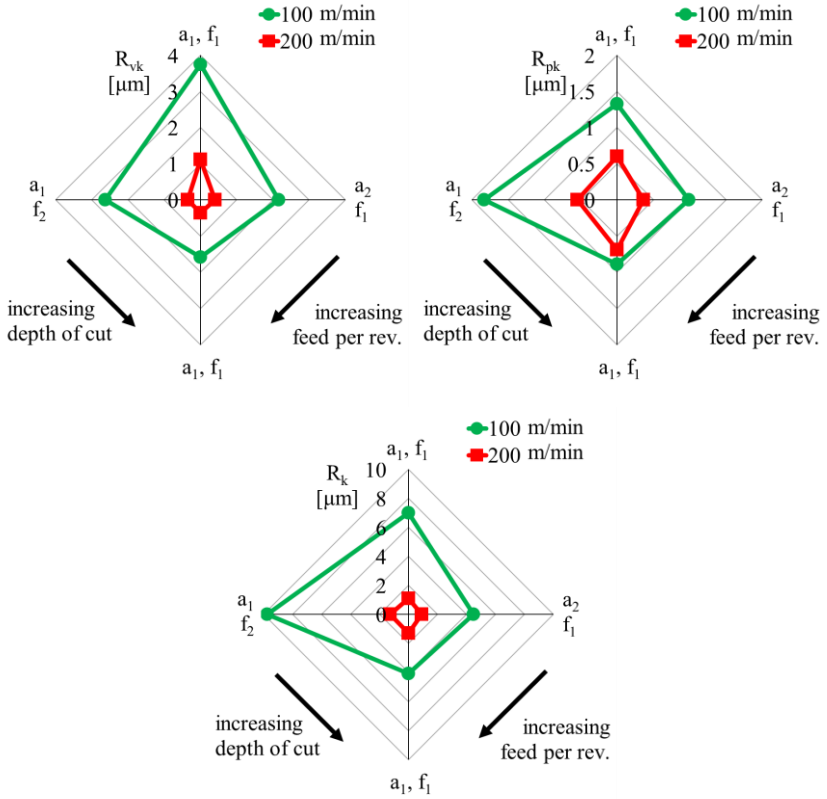

Figure 2 – Alteration of the R_{sk}, R_{vk}, R_k parameters

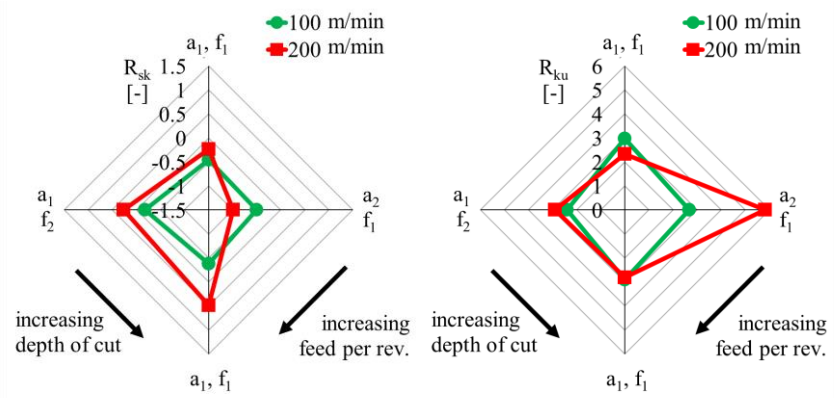

Figure 3 – Alteration of the skewness and kurtosis of the roughness profile

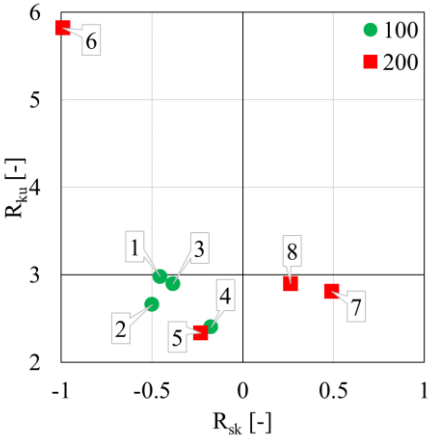

Figure 4 – Topological map of the studied setups

The skewness and the kurtosis of the roughness profiles are shown in Figure 3. Machining with lower cutting speed resulted in a lower value of the skewness, which means a flatter surface with some small valleys. As the cutting speed increased, this attribute of the surface is reversed. Increasing the feed per rev. decreases the flatness of the surface, while increasing the depth of cut had almost no effect. These mean that to achieve a machined surface with a better bearing capability, the cutting speed must be decreased while the feed should be increased in tangential turning. The reason for this phenomenon is the higher than usual contact length of the cutting tool, which helps to achieve a smoother surface. The

kurtosis of the roughness is in the region of 2.3 – 3.0 in 7 cases and showed no clear correlation with the setup parameters in the studied region. This represents that the tangentially turned surfaces has a higher periodicity, and the peaks and valleys on the surface are wider, which means better functional attributes and longer life-time of the machined parts.

The topological map (R_{sk}–R_{ku} graph) is presented in Figure 4 based on the measured results. In the viewpoint of the functionality of the machined surface, the lower left quadrant of the map is preferred to be achieved, because these surfaces show the better bearing capability and life-time. The lower cutting speed has a clear advantage over the higher cutting speed because all the results with 100 m/min cutting speed remained in the desired quadrant. Increasing the feed and depth of cut resulted in worse skewness or kurtosis, which should be avoided.

5. Conclusions

Cutting experiments were carried out to study the functional attributes of tangentially turned outer cylindrical surfaces. In this work the cutting speed, the feed and depth of cut were adjusted to analyse the alteration effect of these parameters. After the cutting experiments the core roughness, the reduced peak height, the reduced valley depth, the skewness, and the kurtosis of the roughness profiles were measured. In the evaluation of the resulted data the following conclusions were drawn:

- Higher cutting speed is favourable to achieve better R_k parameters.
- The skewness of the profile is better on lower cutting speed.
- The kurtosis showed no clear correlation with the studied technological parameters.
- Surfaces with good functional attributes can be achieved with tangential turning.

References: **1.** *Schreiber, L., Trott, K.:* Verfahren zur drallfreien spanenden Bearbeitung von rotationssymmetrischen Flächen. Patent DE19963897A1, 1999. **2.** *Molnar, V.:* Tribological properties and 3D topographic parameters of hard turned and ground surfaces, Materials 15(7), art. no. 2505, 2022. **3.** *Molnar, V.:* Asymmetric height distribution of surfaces machined by hard turning and grinding, Symmetry 14(8), art. no. 1591, 2022. **4.** *Kundrák, J., Gyáni, K., Deszpoth, I.:* Precision Hard Turning of External Cylindrical Surfaces by Rotation Procedure. Rezanie I Instrumenty V Tekhnologicheskih Sistemah 79 pp. 108–117., 2011. **5.** *Kundrák, J.; Fedorovich, V.; Pyzhov, I.; Markopoulos, A. P.:* Improving the effectiveness of combined grinding processes for processing superhard materials. Journal of Manufacturing Processes 43 pp. 270–275, 2019. **6.** *Schubert, A., Zhang, R., Steinert, P.:* Manufacturing of Twist-Free Surfaces by Hard Turning, Procedia CIRP, vol. 7, pp. 294–298, 2013. **7.** *Leichner, T., Franke, V., Sauer, B., Aurich, J. C.:* Investigation of the tribological behavior of radial shaft rings and soft turned shafts under the influence of abrasive particles. Production Engineering, vol. 5, no. 5, pp. 531–538, 2011. **8.** *Kundrak, J., Molnar, V., Markopoulos, A.P.:* Joint Machining: Hard turning and Grinding. Rezanie I Instrumenty V Tekhnologicheskih Sistemah 2019 : 90. pp. 36–43. 2019. **9.** *Schneider, J., Schreiber, L.:* Mit dem Tangentialdrehen zu drallfreien Oberflächen. Werkstatt

und Betrieb, vol. 6, pp. 40–45, 2002. **10.** *EMAG*: "Scroll-Free Turning from EMAG: Fast, Precise, Reliable. EMAG GmbH & Co. KG, [Online]. Available: https://www.emag.com/technologies/scroll-free-turning.html. [Accessed 16. 02. 2021.]. **11.** *Molnar, V.:* Minimization method for 3D surface roughness evaluation area, Machines 9(9), art. no. 192, 2021. **12.** *Molnar, V., Szabo, G.:* Designation of minimum measurement area for the evaluation of 3D surface texture, Journal of Manufacturing Processes 83, pp. 40–48, 2022.

Іштван Станкович, Мішкольц, Угорщина

АНАЛІЗ ВИБРАНИХ ФУНКЦІЙНО-ВИЗНАЧАЛЬНИХ 2*D* ПАРАМЕТРІВ ШОРСТОСТІ ПОВЕРХНІ ПРИ ТАНГЕНЦІАЛЬНОМУ ТОЧІННІ

Анотація. *Серед інших, часто аналізованих параметрів топографії поверхні, параметри, що визначають функції, повинні бути проаналізовані в різних процедурах обробки, щоб окреслити можливості їх застосування. Це такі значення як: основна шорсткість, зменшена висота піку, зменшена глибина западини, асимметрія і ексцес профілів шорсткості. Тангенціальне точіння є багатообіцяючою процедурою обробки, за допомогою якої можуть вироблятися поверхні аналогічні шліфованим з безскручувальними властивостями за допомогою інструментів із певними ріжучими крайками. Досяжна продуктивність також дуже висока. Тому в цій статті ці параметри шорсткості були проаналізовані на основі 2D профілів шорсткості, виміряних на поверхнях, оброблених тангенціальним точінням. У роботі досліджено функції, що визначають параметри профілю шорсткості при тангенціальному точінні шляхом зміни швидкості різання, подачі та глибини різання. Було виміряно та проаналізовано шорсткість серцевини, зменшену висоту піку, зменшену глибину западини, перекос і ексцес профілів шорсткості. Експерименти з різанням проводилися для вивчення функціональних властивостей тангенціально обточених зовнішніх циліндричних поверхонь. Швидкість різання, подача та глибина різання були скориговані для аналізу ефекту зміни цих параметрів. Після експериментів з різанням були виміряні шорсткість серцевини, зменшена висота піку, зменшена глибина западини, перекос і ексцес профілів шорсткості. В результаті оцінки отриманих даних було зроблено наступні висновки: вища швидкість різання сприятлива для досягнення кращих параметрів R_k, асиметрія профілю краща при меншій швидкості різання, ексцес не показав чіткої кореляції з досліджуваними технологічними параметрами, поверхні з хорошими функціональними характеристиками можна отримати за допомогою тангенціального точіння.*

Ключові слова: *функціональні параметри; ексцес; перекос; тангенціальний поворот.*

UDC 621.9.048 **doi: 10.20998/2078-7405.2023.98.12**

A. Nagy, J. Kundrak, Miskolc, Hungary

INVESTIGATION OF FACE MILLED SURFACE TOPOGRAPHY ON C45 WORKPIECE ASSUMING MOVEMENT AT 30° AND 60° TO FEED DIRECTION

Abstract. *When surfaces with anisotropic texture are moved in different directions related to their assembled counterpart during operation, the friction conditions change, as they are determined by the lay of the topographies. In the article, contributing to the exploration of this characteristic, we analyze the inhomogeneity of the topography on a face milled plane surface with a symmetrical setting in sections at an angle of 30° or 60° to the feed direction. Roughness profiles are recorded at 13 points located equidistantly from each other in each measurement plane, and the degree and distribution of the roughness deviations are determined on the surface.*
Keywords: *face milling; surface roughness; distribution of roughness; direction-dependent characterization of topography.*

1. Introduction

The aim of machining is to product parts of the required shape, dimensions, condition, etc., while achieving their prescribed accuracy. These are important factors, so that machines can fulfill their specified functions during the planned lifetime. Such expectations can be fatigue life [1], wear [2] and corrosion resistance, lubrication [3] and sealing ability, etc. [4]. To guarantee these, the specifications on the part drawings (tolerances, surface quality, condition) must be followed during production. One of the most common methods of production is cutting. During the process, the tool penetrates the material of the workpiece and creates a new machined surface while removing chips [5]. The surface is formed by impressions left on it by the edge(s) of the tool, which can be characterized as periodic or random.

A periodic topography is typically created with machining methods using a tool having defined edge(s), which form regularly repeated grooves. This has been investigated in different processes, mainly characterized by the values of profile roughness parameters. When examining the effect of tool coating and cutting data (cutting speed v_c, feed f, depth of cut a_p) on roughness and tool wear in the hard turning of corrosion-resistant steel, it was found that the maximum profile height R_z was significantly reduced, the friction and flank and crater wear rates were notably decreased, and the service life was increased with PVD coating [6]. The roughness value further decreased for increasing v_c and decreasing f and a_p. When turning hard-to-cut austempered ductile iron, the reduction of average roughness R_a value was achieved by increasing values of v_c and a_p in the studied ranges [7]. In rotational turning, the theoretical roughness profile in the reference plane was determined, and

it was stated that half to one-sixth of values of R_a and R_z can be achieved with this process compared to roughness values measured on a surface peripheral turned with a traditional CNMG insert [8]. In drilling of a titanium alloy the value of R_a was also significantly affected by v_c, f and the helix angle [9]. There was a large increase in roughness due to the high rotation speed, thus the appearance of diffusion wear, as well as thermal softening and the increase in forming resistance. On burnished cylindrical surfaces, up to a third of R_a, R_q and R_z values were measured compared to the previous, turned topography if set to the appropriate values of burnishing force, feed and number of passes [10].

In addition to traditional profile roughness analysis, the 3*D* topographic parameters are increasingly used during the examination of surfaces machined with a defined edge tool due to their higher accuracy [11]. The topography of a hard turned hole in a hardened steel gear is anisotropic (the level of isotropy was below 5%), and by increasing the feed from 0.2 mm/rev to 0.3 mm/rev the wear resistance (based on values of S_p, S_{pk}, V_{mp} parameters) and the lubricant retention capacity (determined by Ssk and Svi indices) of the surface deteriorated [12]. In the comparative study of this process and grinding, where the relationships between the cutting parameters, the tribological characteristics of the surfaces, and the topographical parameters were analyzed, a significant correlation was found between S_p and V_{mp} indicating the wear resistance, between S_v and V_{vv} indicating the ability to keep the lubricant [3], and between V_{mp}, V_{vv} and S_{sk} parameters [13] that characterize both functions. In the case of burnishing after turning, it was further found that better wear resistance of the surfaces can be achieved based on the values of S_{sk} and S_{ku} parameters [14]. Topographies created by the methods discussed so far have the same feature that their roughness can be properly specified when measured in the feed direction (perpendicular to the cutting marks), and in this case the theoretical roughness profile is the same at any location on the surface.

The topography created with a rotating tool – milling – is one of the most commonly used process in industry, due to the productivity of its multi-point tool. Thus, face milling (where the tool axis is perpendicular to the machined plane surface) is also a frequently investigated research topic. The conditions that create a favorable topography of machined surfaces are often analyzed. Compared to machining methods discussed above, processes working with a rotated tool are characterized by the fact that the texture is more complicated, with the profile height of the topography changing in different parts of the surface. This can also be observed on the theoretical topography, which is determined only by the kinematic conditions, the tool edge geometry and the feed in the reference plane [15]. The nature of the texture is further complicated by the fact that the tool edges can scratch the already cut surface when turning back during their rotating movement. As a result of all this, there are large differences between profiles measured in several parallel

planes in the feed direction and measured in different directions (Figure 1) [16]. This variability is supported by research results so far.

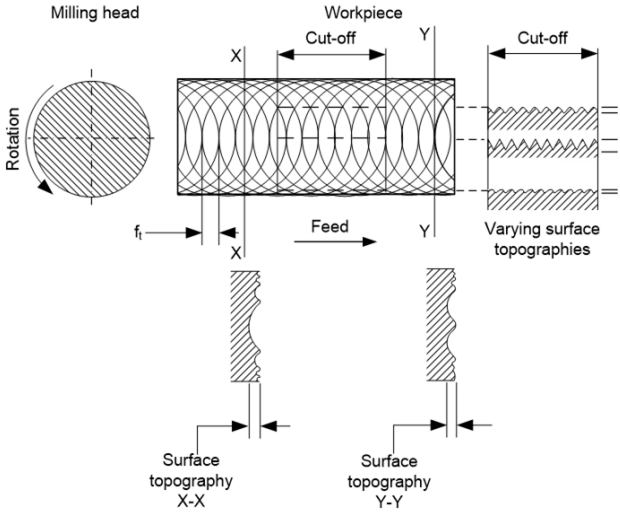

Figure 1 – Change in surface roughness with measurement direction in face milling [15]

During the examination of a developed face milled topography model, its great variability was pointed out, with profiles taken in different directions and locations [17]. An investigation of the depth of cut effect on roughness measured 5 surface elements on the finished face milled topography, one in the symmetry plane and the others in places mirrored to it [18]. The roughness of the surface parts were compared for the up-milled and down-milled part and the symmetry plane determined by the tool and workpiece movement conditions. Other researchers also considered the kinematic conditions, i.e. the different topographical parts formed by the path of the tool edge on the milled surface, for the analysis of which measurements were made at 5×5 locations [19]. It was found that the maximum roughness values can be measured in the plane of symmetry, and the values decrease in other parallel planes further away from it. The heights of the roughness profile curves in each plane changed accordingly. Furthermore, while on the theoretical topography the amplitude parameter values are the same on both sides of the symmetry plane at the same distance from it, on the real surface, larger values were observed on the side where the tool edge enters the workpiece. Theoretical and real roughness of surfaces face milled with increasing

feed was investigated in three parallel measurement planes (in the symmetry plane and on both sides at equal distances from it) [20]. It was found that, the model showed good agreement with the real results; furthermore, the researchers pointed out the differences in roughness values in different parts of the topography, which are significant at larger feeds.

In summary, we conclude that the degree and characteristics of change in roughness on face milled surface have not been comprehensively analyzed, although they can significantly influence the functional properties of fitted surfaces. Therefore, the aim of the research described in the article is to contribute to the exploration of face milled topography characteristics; in this case specifying the degree and nature of the roughness deviations measured in different directions than the feed vector. For this, we assume that the milled surface of a part moves in relation to a connecting surface during operation, in the given direction(s) according to its function, where the characteristics of the surface texture in this direction are decisive. The presented study is a continuation of our previous analysis [21], where profiles measured in parallel and perpendicular directions to the feed were performed at different locations on the surface.

2. Experimental conditions

For the investigation we carried out an experiment. Conditions are summarized in Table 1.

Table 1 – Experimental conditions

Machining	
Machine tool	PerfectJet MCV-M8 vertical milling center
Workpiece material	normalized C45 unalloyed steel
Machined surface geometry	58 mm width, 50 mm length
Cutting tool	ATORN 10612120 (D_t = 80 mm, κ_r=43°)
Cutting insert	one ATORN OCKX 0606-AD-TR, HC4640 (γ_o=25°; α_o=7°; r_ε=0.5 mm)
Cooling-lubrication	No
Cutting strategy	Symmetrical tool-workpiece setting, only front-cutting traces on the surface
Cutting data	v_c=300 m/min, f_z=0.4 mm/rev/tooth, a_p=0.4 mm
Roughness measurement	
Measuring equipment	AltiSurf 520 3*D* topography measuring instrument
Measuring sensor	CL2 confocal chromatic probe
Evaluation length	4 mm
Section (cut-off) length	0.8 mm
Evaluation software	AltiMap Premium

First, we milled the plane surface in its full width, where the tool axis moved in its symmetry plane. The edge only formed front-cutting marks on the surface by setting the tool axis perpendicular to the surface during machining, and the workpiece was feed moved from the edge of the tool to the center.

This was followed by the roughness measurement. During this, two planar sections with a common center, rotated by 30° and 60° from the feed direction, were defined on the surface (α and β), on which 7 profiles each were measured equidistantly (Figure 2). The middle points of the profiles recorded in the measurement planes are shown with dots and their coordinates are given in Figure 2. Their base (the origin of the coordinate system) is point α4 = β4. The parameter values set during the measurement and evaluation were given according to the requirements of the ISO 21920:2021 standard.

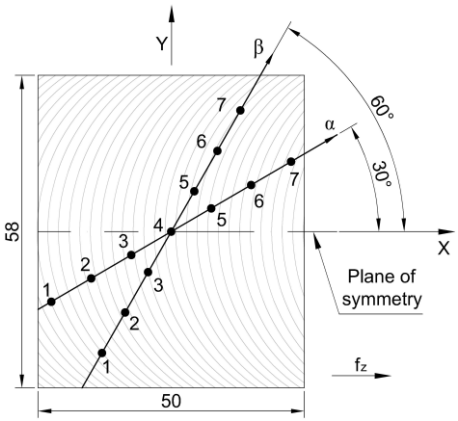

Profile point	Section α		Section β	
	X [mm]	*Y*	*X* [mm]	*Y*
1	-22.5	-13	-13	-22.5
2	-15	-8.67	-8.67	-15
3	-7.5	-4.33	-4.33	-7.5
4	0	0	0	0
5	7.5	4.33	4.33	7.5
6	15	8.67	8.67	15
7	22.5	13	13	22.5

Figure 2 – Measurement points and planes on the milled surface

3. Results and Discussion

The arithmetic mean roughness R_a and maximum profile height R_z values measured at the examined points are summarized in Table 2, which are the arithmetic averages of the results of three measurements. Furthermore, the roughness and waviness profile curves measured at points 1, 3, 5 and 7 of the two sections are shown in Figure 3.

Based on the results presented in Table 2 and Figure 3, we analyze the roughness measured in different parts of the topography and its inhomogeneity along the measurement directions. For this we assume that the milled surface moves in certain directions relative to its counterpart during operation. In this case,

a greater part or the whole of the surface determines the friction characteristic. Because of this, we measured and analyzed the roughness at several points of the topography in the measurement directions, then we specify the arithmetic mean ($\overline{R_x}$)in Table 2 and the degree of deviation ($^{\Delta R_x}$) in Table 3 for each direction and parameter according to the formulas below, where *x = a, z* means the parameter, and *i* is the number of the measurement point. The latter is expressed by the extent and its percentage compared to the average.

$$\overline{R_x} = \frac{\sum_{i=1}^{7} R_{x,i}}{7}$$

$$\Delta R_x = R_{x,i} - \overline{R_x}\ [\mu m]$$

$$\Delta R_x = \frac{R_{x,i} - \overline{R_x}}{\overline{R_x}}\ [\%]$$

The changes in values of the two examined roughness parameters are almost identical (Figure 4), which means that the measured profiles and the repetition of milling marks is also regular; the ratio of average peak-to-valley height of the profiles and the size of areas below and above the center line are almost the same.

Table 2 – Roughness values in measurement planes

Profile point:		**1**	**2**	**3**	**4**	**5**	**6**	**7**	$\bar{R}$
Section α	Ra [μm]	1.32	1.37	1.40	1.40	1.38	1.33	1.27	1.35
	Rz [μm]	6.31	6.67	6.85	6.99	6.97	6.79	6.86	6.78
Section β	Ra [μm]	1.21	1.27	1.30	1.26	0.98	0.54	0.79	1.05
	Rz [μm]	6.03	6.32	7.02	6.86	6.77	4.28	6.38	6.24

Based on the data in Table 3, the degree of roughness deviations in plane α is ΔR_a = 0.14 μm (10.2%) and ΔR_z = 0.68 μm (10%), while in plane β it is ΔR_a = 0.76 μm (72.2%) and ΔR_z = 2.74 μm (43.9%). In previous studies, the change in values of the same roughness parameters was minimal (4%) in the symmetry plane (in the feed

direction) [22] and was enormous (up to 154%) in the perpendicular direction [23]. It follows that when the angle of the measurement plane (and direction) from the feed vector is increased to 90°, the extent of the differences increases. The degree of deviation shows that the inhomogeneity is still small in the measurement direction at an angle of 30° to the feed, where similar R_a and R_z values can be measured along the studied length. However, at the larger angle of 60° it has become significant.

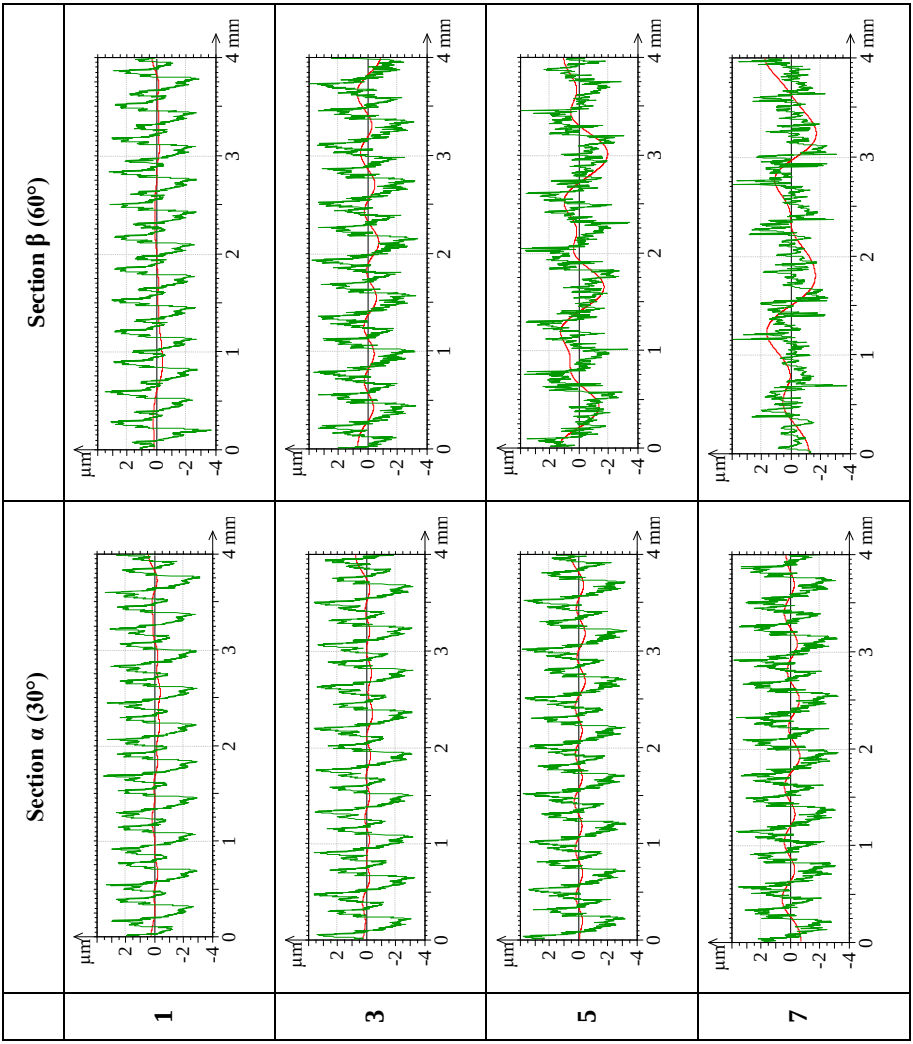

Figure 3 – Roughness and waviness profile curves at several measurement points

Table 3 – Deviations in roughness values in measurement planes

Profile point:		**1**	**2**	**3**	**4**	**5**	**6**	**7**	**Δ*R***	
Section α	ΔR_a [μm]	-0.037	0.019	0.050	0.051	0.031	-0.027	-0.088	0.138	10.2%
	ΔR_z [μm]	-0.464	-0.110	0.074	0.214	0.195	0.012	0.079	0.678	10.0%
Section β	ΔR_a [μm]	0.157	0.224	0.247	0.209	-0.067	-0.510	-0.261	0.757	72.2%
	ΔR_z [μm]	-0.203	0.079	0.781	0.621	0.534	-1.958	0.146	2.739	43.9%

In plane α, maximum values are found at point 4 (in the vicinity of the symmetry plane), and from this location they decrease in two directions with distance. This feature is in agreement with our previous statement that the roughness values are basically determined by the distance and position of the measurement location from the symmetry plane [23], and also with the observation described by Varga and Kundrak [19]; by moving away from the symmetry plane in two directions, the values of amplitude parameters decrease, if profiles are measured in the feed direction.

Values of points 1–4 show the same character in both planes. However, in plane β significant changes can be observed in other parts (Figure 4). Minimum values measured at point 6 are lower by 49% for R_a and by 31% for R_z than the arithmetic averages given in this section. This is due to the characteristics of the milled topography created by the looped cycloid tool edge path. The milling marks are repeated at the same distance on a profile measured in the feed direction; at any position on the topography, however, the angle between a measurement plane taken in a different direction from the feed and successive cutting marks (see illustration of these in Figure 2) varies, and therefore the width of milling marks measured in the plane also changes. In plane β, the distance between adjacent milling marks increases from point 1 to 6, and at point 6 the measurement plane is almost tangential to the milling edge traces (for this reason, a much smaller profile height can be measured at the set evaluation length), then the width decreases to point 7. The same can be observed in plane α, but in this measurement direction and studied width, its value-changing effect is minimal. By further rotating the measurement plane, e.g. in a direction perpendicular to the feed, we also experienced a deviation of 154% for R_a and 124% for R_z compared to the average of values measured on the surface [23]. Based on the nature of changes in values, it

can be concluded that, while in the case of measurements parallel [24] or perpendicular [23] to the feed, the roughness changes in the same way when moving away from the symmetry plane in two directions, when measured in a direction and plane different from the feed, the change in values is not symmetrical to the middle.

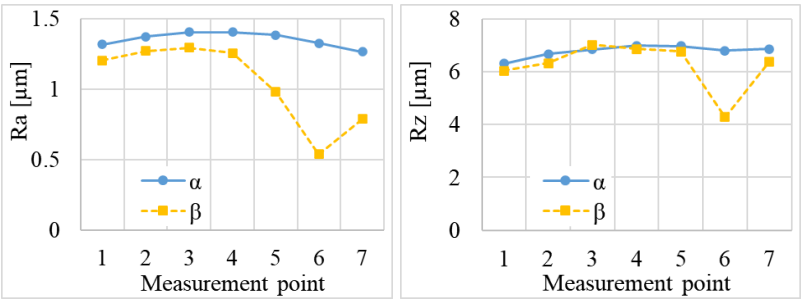

Figure 4 – Roughness values as a function of measurement direction and location

Roughness profile curves are basically determined by the impression of the tool edge on the surface depending on the edge geometry and the feed value. In order to evaluate this, to filter out waviness (e.g. tool, workpiece vibration traces) from the primary profile, it is necessary to choose the appropriate cut-off length value. According to ISO 21920, in case of periodic profiles its value should be taken according to the mean width of the profile elements (milling marks). However, applying the cut-off value for all measurements that is standard for the topography, due to the change in the width of profile elements, the waviness curve will be likely-periodic, its amplitude will increase, and in exchange the roughness peak-to-valley height will decrease on successive profiles along the measurement planes. This means an incorrect filtering method, where evaluated profile heights are displayed that are not accurate. Therefore, it would be useful to clarify the method for the choice of appropriate cut-off length value, taking into account such a case (e.g. in the direction-dependent analysis of face milled topography). This requires further investigations.

5. Conclusions

In this article we investigated the roughness and inhomogeneity of a surface topography face milled with a symmetrical setting in planar sections with an angle of 30° and 60° to the feed direction, assuming that the fitted surface can move relatively in these directions, where the texture is decisive in the friction conditions. During this, we recorded 7 equally spaced profiles in each

measurement direction, covering as much length as possible on the surface, in order to analyze the differences in roughness. Our findings are summarized below.

- Minimal deviations were observed in the measurement direction at an angle of 30° from the feed vector, and significant differences in the plane at an angle of 60°. Along with our previous observations, it can be predicted that when the angle of the measurement plane (and direction) from the feed direction is increased to 90°, the degree of deviation will increase.
- The results show that the movement of the fitted surface during operation in a direction different from the feed by 30° may not change the friction conditions remarkably; however, the increase of the angle to 60° may cause significant changes.
- In plane α, the nature of the change in values was mainly determined by the distance of measurement position from the symmetry plane, where the values of amplitude parameters decreased slightly with distance from it.
- In the direction with a larger angle, the size of the angle between the measurement plane and the direction of milling marks had a dominant effect on the high degree of inhomogeneity. The profile height was minimal in a position where the measuring plane was almost tangential to the cutting trace.
- In measurement directions other than the direction of feed, the width of milling marks always changes. As a result, when the same cut-off length value was set, the waviness curve became likely-periodic along the measurement directions and the evaluated profile curves were characterized by heights different from the real ones. In order to choose the appropriate evaluation conditions, further tests are required to refine the method.

References: 1. *Liu, G., Huang, C., Zhu, H., Liu, Z., Liu, Y., Li, C.* The modified surface properties and fatigue life of Incoloy A286 face-milled at different cutting parameters. *Materials Science and Engineering: A.* 2017. vol. 704. pp. 1 – 9. **2.** *Molnár, V.* Wear Resistance of Hard Turned Surfaces. *Cutting & Tools in Technological System.* 2022. vol. 96. pp. 65 – 72. **3.** *Molnár, V.* Tribological Properties and 3D Topographic Parameters of Hard Turned and Ground Surfaces. *Materials.* 2022. vol. 15. № 7. ArtNo. 2505. **4.** *Grzesik, W.* Prediction of the functional performance of machined components based on surface topography: State of the art. *Journal of Materials Engineering and Performance*. 2016. vol. 25. pp. 4460 – 4468. **5.** *Mitsyk, A., Fedorovich, V., Grabchenko, A.* Main technological factors determining the efficiency and quality of the vibration process**.** *Cutting & Tools in Technological System.* 2022. vol. 96. pp. 131 – 137. **6.** *Sharma, N., Gupta, K.* Influence of coated and uncoated carbide tools on tool wear and surface quality during dry machining of stainless steel 304. *Materials Research Express.* 2019. vol. 6. № 8. ArtNo. 086585. **7.** *Parhad, P., Likhite, A., Bhatt, J., Peshwe, D.* The effect of cutting speed and depth of cut on surface roughness during machining of austempered ductile iron. *Transactions of the Indian Institute of Metals*. 2015. vol. 68. № 1. pp. 99 – 108. **8.** *Sztankovics, I.* Analysis of Rotational Turning in Precision Finish Machining (in Hungarian). Miskolc, Hungary: István Sályi Doctoral School of Mechanical Engineering Sciences, 2022. 96 p. **9.** *Balaji, M., Venkata Rao, K., Mohan Rao, N., Murthy, B.* Optimization of drilling parameters for drilling of TI-6Al-4V based on surface roughness, flank wear and drill vibration. *Measurement.* 2018. vol. 114. pp. 332 – 339.

10. *Ferencsik, V., Varga, G.* The Influence of Diamond Burnishing Process Parameters on Surface Roughness of Low-Alloyed Aluminium Workpieces. *Machines.* 2022. vol. 10. ArtNo. 564. **11.** *Molnár, V., Szabó, G*. Designation of minimum measurement area for the evaluation of 3D surface texture. *Journal of Manufacturing Processes*. 2022. vol. 83. pp.40 – 48. **12.** *Molnár, V., Sztankovics, I.* Analysis of Roughness Parameters Determining Tribological Properties in Hard Turned Surfaces. *Hungarian Journal Of Industry And Chemistry*. 2021. vol. 49. № 2. pp.77 – 84. **13.** *Molnár, V.* Asymmetric Height Distribution of Surfaces Machined by Hard Turning and Grinding. *Symmetry*. 2022. vol. 14. ArtNo. 1591. **14.** *Ferencsik, V., Varga, G.* The Effect of Burnishing Process on Skewness and Kurtosis of the Scale Limited Surface. *Cutting & Tools in Technological System.* 2022. vol. 97. pp. 83 – 90. **15.** *Felhö, C.* Investigation of surface roughness in machining by single and multi-point tools. Aachen: Shaker Verlag, 2014. 188 p. **16.** *Smith, G.T.* Cutting Tool Technology: Industrial Handbook. London: Springer-Verlag, 2008. 559 p. **17.** *Arizmendi, M., Jiménez, A.* Modelling and analysis of surface topography generated in face milling operations. *International Journal of Mechanical Sciences.* 2019. vol. 163. ArtNo. 105061. **18.** *Chuchala, D., Dobrzynski, M., Pimenov, D., Orlowski, K., Krolczyk, G., Giasin, K.* Surface roughness evaluation in thin EN AW-6086-T6 alloy plates after face milling process with different strategies. *Materials.* 2021. vol. 14. № 11. ArtNo. 3036. **19.** *Varga, G., Kundrák, J.* Effects of Technological Parameters on Surface Characteristics in Face Milling. *Solid State Phenomena.* 2017. vol. 261. pp. 285 – 292. **20.** *Kundrak, J., Felho, C.* Topography of the machined surface in high performance face milling. *Procedia CIRP*. 2018. vol. 77. pp. 340 – 343. **21.** *Nagy, A., Kundrak, J.* Analysis of the change in roughness on a face-milled surface measured every 45° direction to the feed. *Cutting & Tools in Technological System.* 2021. vol. 95. pp. 29 – 36. **22.** *Nagy, A., Kundrak, J.* Analysis of inhomogeneity of surfaces milled with symmetrical, down-milling, and up-milling settings. Development in Machining Technology: Scientific – Research Reports vol.10. Cracow, Poland: Cracow University of Technology. 2022. pp. 51 – 62. **23.** *Nagy, A., Kundrak, J.* Changes in the values of roughness parameters on face-milled steel surface. *Cutting & Tools in Technological System.* 2020. vol. 92. pp. 85 – 95. **24.** *Kundrak, J., Nagy, A.* Investigation of Surface Roughness Characteristics of Face Milling. *Cutting & Tools in Technological System.* 2019. vol. 90. pp. 63 – 72.

Антал Надь, Янош Кундрак, Мішкольц, Угорщина

ДОСЛІДЖЕННЯ РЕЛЬФЕРУ ТОРЦЕВОГО ФРЕЗЕРУВАННЯ НА ЗАГОТІВЦІ С45 ПРИ ПЕРЕМІЩЕННІ НА 30° ТА 60° В НАПРЯМКУ ПОДАЧІ

Анотація. *У цій статті автори досліджували шорсткість і неоднорідність рельєфу поверхні, відфрезерованої з симетричною установкою в плоских перерізах під кутом 30° і 60° до напрямку подачі, припускаючи, що підігнана поверхня може рухатися відносно в цих напрямках, де текстура є вирішальною в умовах тертя. Під час цього автори записали 7 рівновіддалених профілів у кожному напрямку вимірювання, охоплюючи якомога більшу довжину поверхні, щоб проаналізувати різницю в шорсткості. Мінімальні відхилення спостерігалися авторами в напрямку вимірювання під кутом 30° від вектора подачі, а значні розбіжності в площині під кутом 60°. Поряд з попередніми спостереженнями, можна передбачити, що коли кут площини вимірювання (і напрямку) від напрямку подачі збільшується до 90°, ступінь відхилення збільшиться. Результати показують, що переміщення підігнаної поверхні під час роботи в напрямку, що відрізняється від подачі на 30°, може не значно змінити умови тертя; однак збільшення кута до 60° може викликати значні зміни. У площині α характер зміни значень визначався в основному віддаленістю місця вимірювання від площини симетрії, де значення амплітудних параметрів дещо зменшувалися з віддаленням від неї. У напрямку з більшим кутом величина кута між площиною вимірювання та напрямком сліду від фрезерування мала*

домінуючий вплив на високий ступінь неоднорідності. Висота профілю була мінімальною в положенні, де площина вимірювання була майже дотичною до сліду різання. У напрямках вимірювання, відмінних від напрямку подачі, ширина слідів фрезерування завжди змінюється. У результаті, коли було встановлено те саме значення граничної довжини, крива хвилястості стала ймовірно періодичною вздовж напрямків вимірювання, а оцінювані профільні криві характеризувались висотами, відмінними від реальних. Для того, щоб вибрати відповідні умови оцінки, необхідні додаткові дослідження для вдосконалення методу.

Ключові слова: *торцеве фрезерування; шорсткість поверхні; розподіл шорсткості; залежна від напрямку характеристика топографії*.

CONTENT

Наукове видання

РІЗАННЯ ТА ІНСТРУМЕНТИ
в технологічних системах

Міжнародний науково-технічний збірник

Випуск № 98

Укладач *д.т.н., проф. І.М. Пижов*
Оригинал-макет *А.М. Борзенко*
Відп. за випуск *к.т.н., проф. Є.В. Островерх*

В авторській редакції

Матеріали відтворено з авторських оригіналів

Підп. до друку 12.02.2019.Формат 60x84 1/16. ПапірСоруРарег.
Друк - ризографія. Гарнитура Таймс. Умов.друк.арк. 10,93. Облік.вид.арк. 11,0. Наклад 300 прим.
1-й завод 1-100. Зам. № 1149. Ціна договірна.

Видавничий центр НТУ «ХПІ»
Свідоцтво про державну реєстрацію ДК № 116 від 10.07.2000 р.
61002, Харків, вул. Кирпичова, 2